Mechanism of actin polymerization by adhesion and degranulation-promoting adaptor protein (ADAP)

Inaugural-Dissertation

to obtain the academic degree

Doctor rerum naturalium (Dr. rer. nat.)

submitted to the Department of Biology, Chemistry, Pharmacy

of Freie Universität Berlin

by

Nirdosh Dadwal

in 2021

The work presented in this thesis was conducted from October 2016 to June 2021 under the supervision of Prof. Dr. Christian Freund at the Institute of Chemistry and Biochemistry, Freie Universität Berlin, Germany.

First reviewer: Prof. Dr. Christian Freund

Freie Universität Berlin

Institute for Chemistry and Biochemistry

Thielallee 63, 14195 Berlin, Germany

Phone: +49 30 838 54389

(chfreund@zedat.fu-berlin.de)

Second reviewer: Dr. Sutapa Chakrabarti

Freie Universität Berlin

Institute for Chemistry and Biochemistry

Takustr. 6, 14195 Berlin, Germany

Phone: +49 30 838 75094

(chakraba@zedat.fu-berlin.de)

Date of defense: 26th January, 2022

Affidavit

I declare that my doctoral thesis "**Mechanism of actin polymerization by adhesion and degranulation-promoting adaptor protein (ADAP)**" has been written independently and with no other sources or aid than those cited.

Nirdosh Dadwal

Table of contents

1. Introduction

1.1 The immune system

Our environment is full of microorganisms, some of which are helpful to human beings (for example *Lactobacillus* spp. responsible for converting milk into curd or *E.coli* in the gut) while some can cause infections and diseases (such as parasites, viruses or gram-negative bacterial toxins) [1-3]. In order to protect our body from these pathogens or foreign microbes, higher mammals have developed a sophisticated network of defense mechanisms known as the immune system [4]. Based on its response mechanism, the immune system can be divided into two major parts: the non-specific or innate immunity and the specific or adaptive immunity. The majority of infections are cleared successfully by the innate immune system, while those that cannot be resolved by innate immunity trigger an adaptive immune response, followed by a long-lasting immunological memory [4, 5].

Innate immunity is the immune system's first line of active defense and has emerged to rapidly respond to invading pathogens. However, innate immunity is not specific, which means that the cells of innate immune system recognize factors which are common for many pathogens, commonly known as pathogen associated molecular patterns (PAMPs). These factors are recognized by specialized innate immune receptors called pattern-recognition receptors (PRRs). Humoral components (such as cytokines, chemokines or factors of the complement system) and cellular components (for example, natural killer cells, monocytes/macrophages, granulocytes (neutrophils, basophils and eosinophils) or dendritic cells) make up the innate immune responses [4, 5].

On the other hand, the adaptive immune response is triggered when the infection cannot be cleared by the innate immune system, and thus represents the second line of defense. Moreover, adaptive immunity is characterized by the presence of immunological memory (described in section 1.2) [6]. Like innate immunity, the adaptive immune system is also comprised of humoral and cellular components, with the humoral components including antibodies secreted by B cells, cytokines, and chemokines, and the cellular components including the highly specialized families of B cells and T cells [4, 5].

1.2 T cells and their development

The thymus is the lymphoid organ where T cells are generated [7, 8]. It is situated in the upper anterior mediastinum, just above the heart. Anatomically, the thymus can be divided into an outer cortex and an inner medulla. Despite the fact that the thymus belongs to the hematopoietic system, it does not contain self-renewing hematopoietic stem cells. In fact, T-cell precursors originate in the bone marrow and reach the thymus through the blood stream. They enter the cortex, where most of the differentiation steps take place, and subsequently migrate in the medulla where T-cell precursors undergo final maturation. Mature T cells leave the thymus and populate the secondary lymphoid organs. Thymocyte subpopulations present in the thymus can be distinguished according to the expression of CD4 and CD8. The most immature thymocytes do not express CD4 or CD8 and are termed double negative (DN) cells. Based on the expression of two additional markers (CD25 and CD44), DN cells can be further subdivided into 4 different subpopulations. DN cells have the potential to differentiate into αβ or γδ-TCR+ T cells [5, 7, 8].

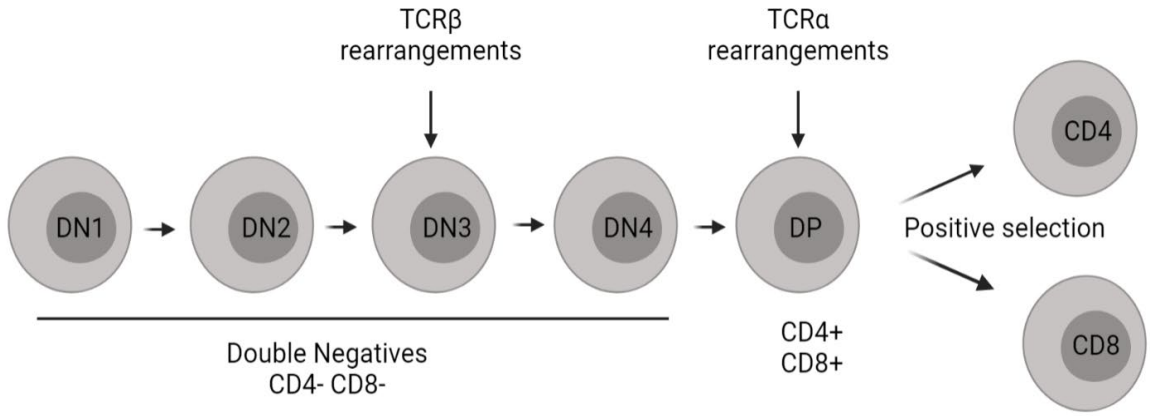

Fig. 1.1: Different developmental stages of T cell. DN (double negative) cells do not express CD4 and CD8. The double negative thymocytes are further subdivided in DN1, DN2, DN3 and DN4. At DN3 stage the pre-TCR is assembled and expressed. Cells expressing fully rearranged β-chain further matures to DN4 stage. DN4 cells develop into double positive (DP) thymocytes which undergo additional selection processes (i.e., death-by-neglect, positive and negative selection). Finally, positively selected DP cells mature into single positive (SP) thymocytes. (Adapted from [7, 8])

T cell precursors that differentiate into the αβ lineage undergo two key selection checkpoints. The first selection checkpoint occurs at the DN3 stage and is called β-selection **(Fig. 1.1)**. DN3 cells express the pre-TCR that is composed of the invariant pre-Tα chain, a rearranged TCR β-chain and the CD3 and TCR-ζ molecules. Signals induced by the pre-TCR inhibit further TCRβ rearrangement (allelic exclusion), rescue cells from apoptosis,

induce proliferation and differentiation into DN4 thymocytes. DN4 cells will ultimately differentiate in cells expressing CD4 and CD8. These cells are called double positive (DP) thymocytes. The β-selection checkpoint ensures that only thymocytes that have generated (rearranged) a functional TCR-β chain become selected. Mice lacking the recombination activating genes 1 or 2 (RAG1, RAG2) do not rearrange the TCR β-chain. Thymocytes from these mice do not express a pre-TCR and their development is arrested at the DN3 stage [9].

The second key selection step (TCR αβ selection) occurs at the DP stage **(Fig. 1.1)**. DP cells constitute approximately 90% of the lymphoid compartment in the thymus. From this large number of DP cells nearly 95% die and only 5% survive and will mature into single positive (SP) cells expressing either CD4 or CD8. This developmental step is characterized by three selection outcomes: death by neglect, positive selection, and negative selection. The fate of DP thymocytes is determined by the avidity/affinity of the αβ-TCR for MHC/self–peptides. DP thymocytes expressing TCRs that are not able to interact with MHC molecules or that possess extremely low avidity undergo “death by neglect”. Similarly, T cells that express TCRs strongly interacting with MHC/self-ligands are also eliminated (negative selection), as they are potentially dangerous and can cause autoimmunity. Conversely, only DP cells expressing TCRs with intermediate avidity (or proper avidity) initiate a multi-step process known as positive selection that allows the differentiation and maturation of DP thymocytes into $CD4^+$ or $CD8^+$ T cells **(Fig. 1.1)**. The last step of T-cell development is characterized by the downregulation of either CD4 or CD8 and the commitment to the helper or cytotoxic cell lineage. These selection steps ensure the generation of T cells that recognize foreign antigens but not self-peptides [5, 7, 8, 10-12]. Therefore, thymocyte selection contributes to the establishment of “central tolerance” [13].

Based on the expression of the surface markers CD4 or CD8, two major T cell subfamilies are defined. $CD4^+$ T cells are helper T cells (T_h), which assist in activating B cells, enhancing the response of $CD8^+$ T cells, and regulating macrophage functions by secreting cytokines. They detect foreign peptide antigens bound to MHC II molecules presented on antigen presenting cells (APCs). $CD4^+$ T cells can be further differentiated into various subtypes such as T_{h1}, T_{h2}, T_{h17} and T_{regs}, depending on the surrounding cytokine milieu. With regards to cytokine production, T_{h1} (T helper 1) cells secrete interferon gamma (IFNγ) and are involved in the activation of macrophages while T_{h2} cells produce a variety of interleukins (like IL-4, IL-5 and IL-13) to enhance the antibody production in B cells [14]. T_{h17} cells secrete IL-17 and provide an anti-microbial defense mechanism, while T_{regs} (regulatory T cells) are mainly required to maintain self-tolerance and produce IL-10 and TGF-β to suppress immune responses [14]. On the other hand, $CD8^+$ T cells are cytotoxic effector

cells and recognize antigenic peptides presented on MHC class I molecules. Their main function is to kill virus-infected cells and tumor cells by the release of soluble factors like perforin, granzymes, and granulysin [5, 10, 14, 15].

The $CD4^+$ or $CD8^+$ T cells eventually die after clearing up an infection leaving a small set of effector cells which further differentiate into long-living memory cells that are antigen-experienced and respond faster to the reoccurring infections [8, 14, 15] [16].

1.3 The Immunological Synapse and T cell activation

Naive T cells leave the thymus after maturation, enter the bloodstream, and circulate continuously from the bloodstream to the secondary lymphoid organs (such as spleen) until they encounter an antigen presenting cell (APC), such as a dendritic cell. In the first eight hours of entering the lymph nodes, T cells initially engage in transient (less than 10 min) contacts with dendritic cells. These contacts induce a change in T cell behavior, leading to reduced motility and a prolonged T cell-APC interaction. These interactions result in a series of molecular rearrangements, culminating in the formation of a distinct structure at the contact site between the two cells known as immunological synapse (IS) **(Figure 1.2)** [17, 18]. At the IS, the TCR and associated signaling molecules are localized in the center region

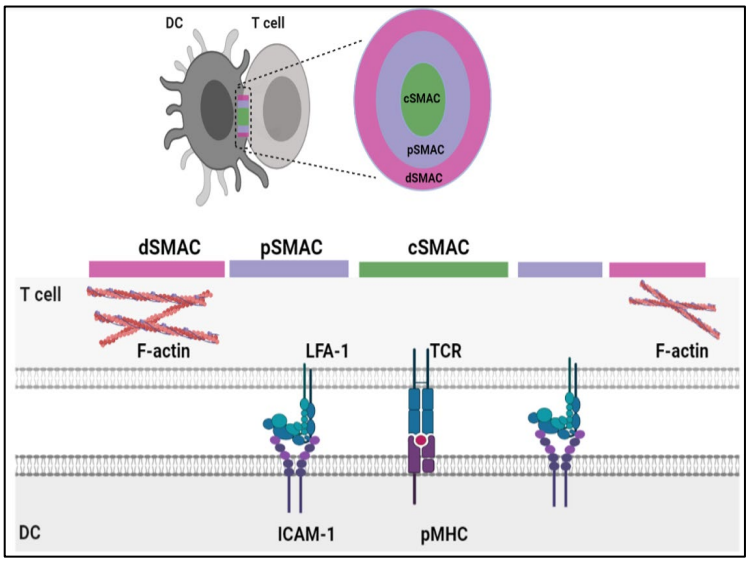

Fig 1.2: Schematic of a T cell interaction with an APC and the formation of the immunological synapse. Circular rings show the spatial pattern of different SMACs (supramolecular activation clusters), with the cSMAC (central) in green, the pSMAC (peripheral) in blue and the dSMAC (distal) in purple. In the lower part of the image the key components of each cluster involved in T cell activation are depicted: the TCR/MHC complex is a part of cSMAC, LFA-1 is the critical component of pSMAC, and actin is mainly found in the dSMAC. (adapted from [18])

called the cSMAC (central supramolecular activation cluster), whereas integrins are enriched in the middle ring known as pSMAC (peripheral SMAC) of the IS [19]. A third distal region called dSMAC (distal SMAC) possesses a circular array of filamentous actin **(Figure 1.2)** [17, 18, 20]. Thus, T cell activation relies on the formation of the IS with defined central and peripheral signaling platforms, which is also linked to adhesion and interaction with APCs [17, 19, 21-23].

However, the formation of the IS is not sufficient to fully activate a T cell. It also requires various secondary signals, with the primary binding of TCR to the foreign peptide-MHC complex is defined as signal 1. Further, a co-stimulatory signal (also referred as signal 2) **(Figure 1.3)** is essential which initiates clonal expansion [24] and, if absent, can lead to a permanent non-responsive state of T cell called anergy. This signal is generated by the CD28 molecule on the T cell, which binds to CD80(B7-1) or CD86(B7-2) expressed on mature APCs **(Figure 1.3)** [24]. In addition to TCR- and CD28- mediated signals, instructive cytokines (signal 3) are also required for T cell to differentiate into a distinct subtype [24, 25] [5] (explained in LAT signalosome in section 1.4).

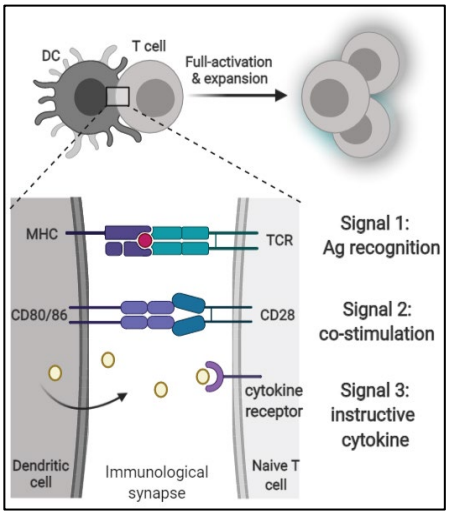

Fig 1.3: Graphic representation of signals required for a full activation of T cell after the formation of the IS. Signal 1 includes binding of TCR to a peptide-MHC complex present on the APC (here a DC). The Signal 2 comes from the binding of the co-stimulatory molecule CD28 displayed on the T cell surface to CD80 or CD86 expressed on APCs. The cytokine milieu released from APC are necessary for the full activation and differentiation of a T cell. Absence of the co-stimulatory signal can lead to T cell anergy (a non-responsive state of T cell).

1.4 Initiation of TCR mediated signaling (events in cSMAC)

The downstream events of the TCR signaling cascade have been extensively studied [5, 25-30] [31]. The full TCR/CD3 complex **(shown in fig 1.4)** consists of a TCRαβ heterodimer, CD3εδ and CD3εγ heterodimers, and a TCRζζ homodimer. The TCR-induced downstream signaling is dependent on the phosphorylation of tyrosine motifs located within the CD3 and TCRζ chains called ITAMs (immunoreceptor tyrosine-based activation motifs). Once the TCR binds to an antigenic peptide presented on MHC molecule, an Src family kinase such as Lck (lymphocyte-specific protein tyrosine kinase) phosphorylates the ITAMs. However, the process of Lck activation upon TCR triggering is still not well understood. Following ITAM phosphorylation, a member of the Syk (spleen tyrosine kinase) family, ZAP70 (zeta-chain-associated protein kinase 70 kDa) gets recruited to the phosphorylated ITAMs, which subsequently gets phosphorylated by Lck at position Y^{315} and Y^{319}, then undergoes auto-phosphorylation for full activation. Active Zap70 is required for the phosphorylation of LAT (linker of activated T cells) and SLP-76 (SH2 domain-containing leukocyte of 76 kDa), which facilitates the formation of a signaling hub called the LAT signalosome, consequently leading to gene expression, cytoskeleton re-organization and T cell activation **(as shown in figure 1.4)** [25].

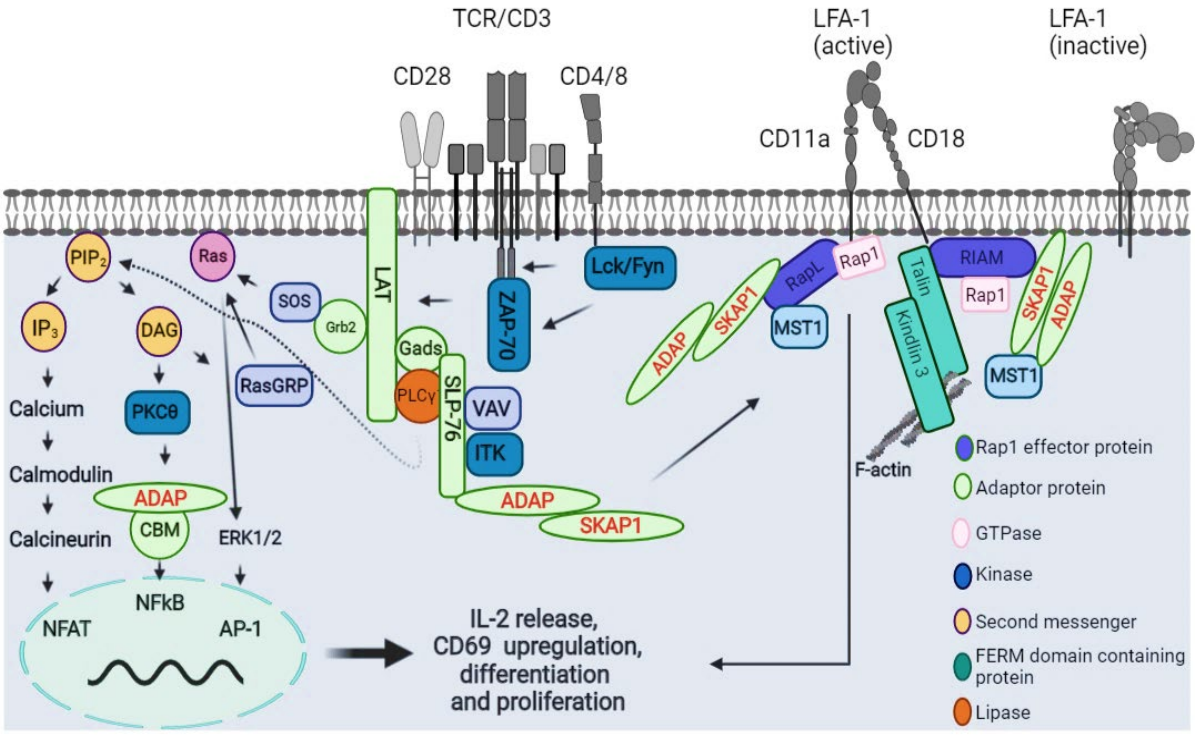

Fig 1.4: Schematic overview showing the TCR-signalling cascade involving various regulators, leading to integrin activation and gene regulation. Upon TCR stimulation, LCK phosphorylates the ITAMs allowing the recruitment and activation of ZAP70. Active ZAP70

phosphorylates LAT and SLP76 adaptor proteins, thus facilitating the formation of the LAT signalosome (which includes LAT, SLP76, GADS, PLCγ1, ITK and ADAP). ITK phosphorylates PLCγ1 which subsequently hydrolyses PIP2 into DAG and IP3. IP3 activates transcription factor NFAT whereas DAG activates two different transcription factors, NFkB (via CBM/ADAP complex formation) and AP1. The activation of these transcription factors results in synthesis of IL-2 to further support T cell activation and proliferation. At the same time, different modules containing ADAP/SKAP55 get recruited at the cytoplasmic tail of LFA-1, consequently leading to its activation and binding to ICAM-1. The module which binds to the CD11a chain consists of RapL/Rap1/ADAP/SKAP55/Mst1 while the other complex binding to CD18 chain is a complex of Talin/Kindlin3/RIAM/ADAP/SKAP55/actin pool (adapted from [30] [25, 27, 32])

The LAT signalosome includes SLP-76, PLCγ1 (phospholipase C gamma 1), GADS (grb2-related adaptor downstream of shc) and ITK (interleukin T cell kinase). Upon binding with LAT, PLCγ1 gets phosphorylated at Y^{783} and activated by ITK. Activation of PLCγ1 is of particular importance during the process of T cell activation, as it hydrolyzes the membrane lipid PIP2 (phosphoinositole-4,5bisphosphate) into IP3 (inositol-1,4,5-triphosphate) and DAG (diacylglycerol), which initiate the signaling pathways leading to the activation of three transcription factors – NFAT (nuclear activated T cells), NFκB (nuclear factor kappa light chain enhancer of activated B cells), and AP1 (activator protein 1). These transcription factors are required for IL-2 production, crucial for T cell activation and proliferation **(figure 1.4)** [25].

For the activation of NFAT, IP3 plays an important role where it gives rise to calcium release from the ER and later influx via Ca^{2+} channels which is sensed by calmodulin (CaM). Calmodulin activates calcineurin, which further activates NFAT and allows for its translocation into the nucleus. On the other hand, DAG production leads to activation of two major pathways, PKCθ (protein kinase C) and Ras. PKCθ phosphorylates CARMA1 (CARD-containing MAGUK protein 1). Phosphorylated CARMA1 makes a complex with Bcl (B-cell lymphoma 10), and MALT1 (mucosa-associated lymphoid tissue lymphoma translocation protein 1) known as CBM complex (CARMA-1/Bcl10/MALT1). This complex unlocks the IKK (IkB kinase) catalytic site which phosphorylates IkB (inhibitor of kappa B). This phosphorylation leads to its degradation and releases NFkB, which then enters the nucleus and regulates gene transcription leading to full T cell activation and proliferation **(figure 1.4)** [25] [33]. In the other signaling cascade, DAG activates Ras, a guanine nucleotide-binding protein, via RasGRP (Ras guanyl nucleotide releasing proteins). Ras further activates ERK (extracellular signal-regulated kinase) cascade which is involved in activating AP-1 transcription complex and upregulation of CD69 expression, a marker of activating T cells [25, 34]. Thus, these signaling events in the cSMAC are tightly linked to the signaling cascade in pSMAC.

1.5 TCR mediated Integrin activation (events in pSMAC)

As mentioned in section 1.3, the pSMAC (peripheral supramolecular activation cluster) contains a ring of integrins, which are heterodimeric transmembrane receptors known to be crucial for cell-cell and cell-to-extracellular matrix adhesion and motility. They are comprised of one alpha and one beta chain. Each αβ subunit contains an extracellular domain, a transmembrane domain, and an unstructured cytoplasmic tail **(figure 1.5)**. In mammals, 18 α subunits and 8 β subunits have been identified which give rise to 24 different αβ pairs of integrins with different ligand specificities. Although, the two major integrins expressed on T cells are β2 integrin LFA-1 (αLβ2 also known as CD11a/CD18) and β1 integrin VLA-4 (α4β1 also known as CD49d/CD29) [5, 19, 35-46] [47].

Binding of LFA-1 to its ligand ICAM-1 (intercellular adhesion molecule 1), which is expressed on APCs is important for T cell-APC attachment whereas the interaction of VLA-4 to its ligand VCAM-1 (vascular cell-adhesion molecule 1) (found on the extracellular matrix) plays a role in adhesion to the extracellular matrix and lymphocyte migration to the mucosal lymphoid organs and to the sites of inflammation [40, 42, 44] [48]. T cells are substantially motile in the peripheral lymph node in search of APCs, which is probably mediated through chemokine regulated adhesive interactions with the extracellular matrix.

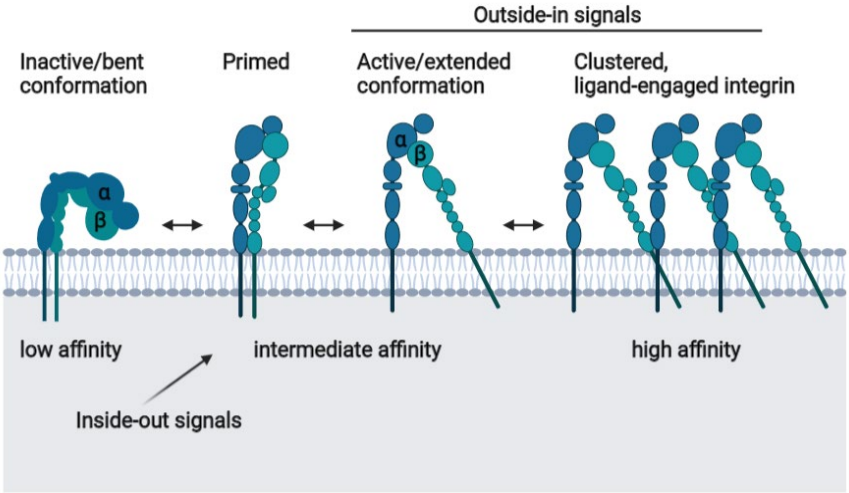

Fig 1.5: Three different conformations of LFA-1 affinity. In its inactive state, LFA-1 is expressed in closed/bent conformation and has low affinity towards its ligand ICAM-1. Upon T-cell receptor stimulation, a signaling cascade known as inside-out-signaling triggers where two different protein complexes bind to the cytoplasmic tail of α- and β- chains lead to the conformational change of LFA-1 and increase its affinity towards ICAM-1. Binding of intermediate affinity LFA-1 to its ligand induces full activation of LFA-1 which further forms clusters (avidity regulation) and increases adhesion. High affinity ligand binding permits co-stimulatory signals to the T cell which leads to T cell activation, proliferation, and differentiation referred as outside-in signaling.

Integrins exist in three different conformations, from the bent or resting form to an extended conformation which either have no or different affinities towards their ligands **(as shown in figure 1.5)** [42]. Unstimulated T cells or resting T cells are non-adherent, as the integrins present on their surface are in an inactive conformation or bend conformation. However, when a TCR ligates to a peptide-MHC complex or a chemokine receptor gets stimulated in response to encountering a chemokine, a conformational change occurs in integrins, increasing their affinity towards their ligands (affinity modulation). The intracellular signaling pathway that facilitates the clustering of integrins (avidity regulation) is referred to as 'inside-out signaling'. Once the integrin is bound to its ligand, it permits a co-stimulatory signal to the cell which leads to T cell activation, proliferation, and cytokine secretion (for example IL-2), a process called 'outside-in signaling' [40, 49]. On a stimulated T cell, active integrins are initially shown to form microclusters which then get redistributed and accumulated on one side of the cell [40] [35, 36, 38, 42, 44, 48, 50].

The human LFA-1 α and β subunit genes are located on chromosomes 16 and 21, respectively. The relevance of LFA-1 is illustrated by a disease called leukocyte adhesion deficiency. This disease results from a condition where the person lacks LFA-1 surface expression on cells, a deficiency in the β-subunit on chromosome 21, to be precise. The LFA-1 deficiency leads to life-threatening infections and display defects in adhesion or rolling dependent lymphocyte functions [51] [52]. The activity of integrins depend on many molecules which are discussed further.

1.6 Key regulators of 'inside-out' signaling

T cell activation is strongly linked to inside-out signaling [43] [53] [54]. Filamin has recently been shown to be a negative regulator of inside-out signaling, where its binding to the cytoplasmic tail of the β-chain of LFA-1 keeps integrins in inactive or bend confirmation in unstimulated T cells. Stimulation of the TCR prompts the phosphorylation of filamin A by serine threonine kinase Ndr2 (nuclear Dbf2-related kinase) at S^{2152} and results in its dissociation from the β-chain, which then allows recruitment of talin and kindlin3 via their FERM domains, leading to a conformational change in integrins and subsequently stabilizing LFA-1/ICAM-1 binding [55] [56]. Another key regulator, RIAM, binds to talin via its N-terminus domain and facilitates its localization to the plasma membrane as well as recruits Rap1 to integrins **(figure 1.4)** [57, 58]. In addition to β-chain, RapL binds directly to the cytoplasmic side of α-chain of LFA-1, allowing the recruitment of its binding partners Rap1 and Mst1. These molecules along with the cytosolic adaptor proteins such as ADAP

and SKAP55, are responsible for the assembly of an LFA-1 activating complex [49, 59] [37] [60]. SKAP55 bound constitutively to ADAP binds to the SARAH domain of RapL, and thus is recruited to the integrin α-chain as a larger RapL/Rap1/ADAP/SKAP55/Mst1 complex **(as shown in figure1.4)**. SKAP55 also interacts with the Rap1 effector molecule RIAM via its N-terminus, thus participating in the formation of another module consisting of Talin/Kindlin3/RIAM/ADAP/SKAP55 and the β-chain of LFA-1, thereby stabilizing the active conformation **(Fig. 1.4)**. Knock-out or knockdown of any of these molecules leads to severe negative consequences for T cell functioning such as impaired adhesion, proliferation or activation [49, 57, 58, 61, 62] [63] [64] [65]. This also illustrates the relevance of the involved adaptor proteins. There are two groups of adaptor proteins: transmembrane adaptor proteins and cytosolic adaptor proteins [66, 67].

1.7 Cytosolic adaptor proteins involved in T cell activation

Adaptor proteins are molecules deficient in enzymatic or transcriptional activity and often consist of several tyrosine motifs available for phosphorylation, proline rich regions, or domains that interact with other proteins/lipids in order to form larger multiprotein signaling complexes [66]. The two cytosolic adaptor proteins ADAP and SKAP55 play an important role in the inside-out signaling and T cell activation [27, 30, 49, 67, 68].

1.7.1 ADAP

Adhesion and Degranulation-promoting Adaptor Protein (ADAP) also called FYB [69] (Fyn Binding Protein) or SLAP130 [70] (SLP-76 associated protein of 130kDa) is expressed in thymocytes, peripheral T cells, myeloid cells, NK cells, platelets and dendritic cells and has also recently been shown to be expressed in neuronal cells in the hippocampus [46, 69-71] [72] [73] [74]. ADAP is mostly unfolded and consists of a proline rich region (PRR), two folded hSH3 domains ($hSH3^N$ and $hSH3^C$) separated with a linker, the linker contains an EVH1 (Ena/VASP homology 1) binding domain and multiple tyrosine residues that get phosphorylated upon TCR or chemokine-receptor stimulation **(Fig. 1.6)** [69, 70, 75]. It is expressed in two isoforms, one of which has an insertion of 46 amino acids on the linker between the two domains and is preferentially expressed in mature T cells [71]. In T cells, ADAP has been shown to be involved in different pools or subpopulations downstream of TCR stimulation. Approximately 70% of ADAP forms a complex with SKAP55

(ADAP/SKAP55 module), which participates in the LAT signalosome as well as integrin activation, while the remaining 30% (not bound to SKAP55) regulate NFκB activation via ADAP/CBM complex formation **(shown in figure 1.4)** [27, 44, 61].

The N-terminus of ADAP (residues 1-381) is predicted to be disordered **(appendix figure 4)** and has been shown to be important for the full phosphorylation of tyrosine residues present on the C-terminus which are required for binding to various SH2 domain containing proteins involved in the LAT signalosome [76]. Disordered proteins are generated when it fails to fold into a defined three-dimensional structure or have a compositionally biased amino-acid sequence such as presence of many proline residues as in the case of the N-terminus of ADAP which contains 64 prolines [77]. Interestingly, IDPs (intrinsically disordered proteins) or IDRs (intrinsically disordered regions) of protein are shown to mediate crucial signaling processes and have the potential to bind to many partners or contain multiple binding motifs [78]. The disordered N-terminus of ADAP is shown to contain an important serine residue at position 235 (S^{235}), which gets phosphorylated by serine/threonine kinases and involves in the signaling (unpublished data from Freund lab).

The proline rich region (PRR), specifically the residues from position 340-364, interacts directly with the SH3 domain of SKAP55 and SKAP-HOM **(figure 1.6)**. This interaction protects the latter proteins from degradation [49, 61, 79]. This direct binding with SKAP55 recruits ADAP to the cytoplasmic tail of integrins by interacting with RapL and RIAM, thus encouraging the formation of modules required for integrin activation [68] [80]. Deletion of either the entire proline rich region or subsequences at positions 340-364 results in impaired LFA-1/ICAM-1 and T cell/APC interaction [49, 61].

hSH3 domains (helically extended SH3 domains) of ADAP have an N-terminal α-helix packed against the β-sheets of the SH3 domain structure **(appendix figure 1a and b)** [81]. Unlike canonical SH3 domains, the hSH3 domains of ADAP do not interact with the PRR. Rather, these domains have been shown to bind to lipids *in vitro* and have been hypothesized to be involved in recruitment of ADAP to the PM following TCR stimulation [82-84]. Deletion of the α-helix of both the hSH3 domains of ADAP results in impaired T cell adhesion and migration upon TCR stimulation [83].

The FPPPP domain (residues 616-624) is present on the linker which binds to EVH1 (Ena/VASP binding homology 1) domain of Ena/VASP proteins [85, 86]. Ena/VASP proteins are actin-elongating proteins which have been shown to form tetramers via their EVH2 domain. They possess a monomer actin binding domain and a filamentous actin-binding domain by which they modulate the actin cytoskeleton during T cell trafficking [87] [88].

The tyrosine motifs of ADAP (Y462, Y571, Y595, Y625, Y651) become phosphorylated by Src kinase Fyn upon TCR-pMHC ligation [76, 89-91]. These phosphorylated tyrosine motifs attract SH2 domain containing proteins, for example, the SH2 domain of Fyn directly binds to the YDGI site (residues 625-628) of ADAP, and the domain of SLP-76 and Nck binds to YDDV motif (found twice on ADAP at residues 595-598 and 651-654) **(figure 1.6)**. Nck and ADAP are known to be involved indirectly in regulating actin polymerization and rearrangement by interacting with the WASP (Wiskott-Aldrich syndrome protein) [90, 92] [93] [94]. Kuropko *et.al.,* in 2016 showed the importance of tyrosine motif YDSL (residues 571-574) present at the surface of the hSH3N domain of ADAP which binds to the SH2 domain of ZAP70, and this interaction is crucial for T cell migration upon chemokine stimulation [32, 91]. The binding of phosphorylated tyrosines with SH2 domain-containing proteins is an important part of signaling which mediates various cellular responses like transcriptional activation and actin cytoskeleton remodeling.

T cells lacking ADAP are shown to be triple knock-out (i.e., no SKAP55 and no SKAP-HOM expression) [61]. These T cells show defects in β1 and β2 integrin-mediated adhesion and migration, reduced LFA-1 clustering and impaired IL-2 production [59, 61, 89, 95]. The abnormal IL-2 production is associated with a lack of ADAP/CBM (CARAMA1/Bcl10/MALT1) complex formation. This complex is essential for the activation of NFkB transcription factor and thus impaired proliferation [25]. ADAP has been shown to play an important role in the development of TCRαβ T cells [89]. ADAP knock-out mice show impaired thymic development, which already suggests the importance of this protein [73]. Hence, ADAP deficiency leads to overall defective positive/negative selection of T cells [89], however this defect is mild. Pazmair *et. al.* in 2017 studied the impact of ADAP loss in T cell subsets, $CD4^+$ and $CD8^+$ T cells and observed that ADAP deficiency does not affect TCR-triggered activation, proliferation, and effector functions in $CD8^+$ T cells. On the other hand, $CD4^+$ T cell functioning relies profoundly on ADAP [95]. *Engelman et. al.* in 2013 has also demonstrated using mice model that EAE (experimental autoimmune encephalomyelitis) is strongly attenuated upon conventional knock-out of ADAP [96].

In humans, ADAP has been shown to regulate HIV-1 infection in complex with SLP-76 and the knockdown of ADAP or overexpression of a mutant defective in binding to SLP-76 in T cell lines or human primary T cells, inhibit the spreading of HIV-1 infection [97]. This effect could be due to the formation of impaired $CD4^+$ T cells in absence of ADAP, as HIV specifically infects $CD4^+$ T cells. Thus, ADAP could be considered as a putative therapeutic target for blocking HIV-1 infection. Additionally, ADAP and SKAP55 deficiency in $CD8^+$ T cells has been shown to augment lytic activity because of impaired PD-1 (programmed death) expression which resulted in enhanced tumor prevention in ADAP knockout mice

[98]. Another study showed that in humans, the condition small platelet thrombocytopenia, an increase in bleeding tendency, occurs due to a homozygous mutation in ADAP genes. In this case, the patients carry a non-sense mutation where the guanine at position 393 is

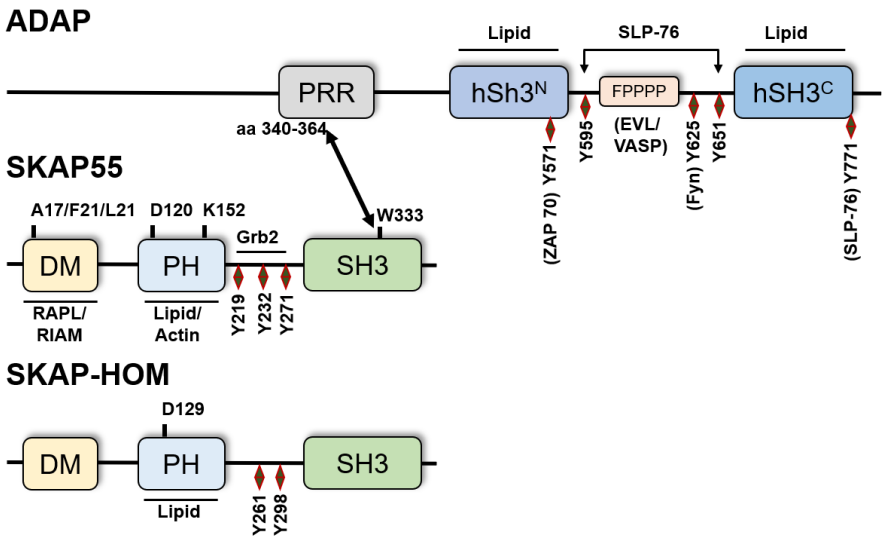

Fig 1.6: Structure of ADAP (short isoform), SKAP55, SKAP-HOM. ADAP has a proline rich region (PRR), two helical SH3 domains (hSH3), EVL/VASP binding site, multiple tyrosine motifs. Amino acids 340-364 of the PRR of ADAP binds to tryptophan at position 333 within the SH3 domain of SKAP55 and SKAP-HOM. SKAP55 has a Dimerization domain (DM, residues 1-60, crucial residues involved in dimerization are shown on structure), a Pleckstrin homology domain (PH, residues 106-205) and a C-terminal Src homology domain (SH3, residues 300-356) and three tyrosine motifs. SKAP-HOM has a similar structure but contains only two tyrosine motifs. Binding partners of tyrosine residues and different domains are indicated in the picture.

mutated to adenine (c.393G>A), which results in the occurrence of a stop codon (TGA) instead of a tryptophan (TGG) and leads to the premature termination of mRNA translation and formation of truncated ADAP protein [99] [100]. Since the truncated ADAP lacks the binding site for SKAP55, SLP-76, Fyn or all other SH2 domain containing proteins, the cells containing mutated ADAP should be functionally impaired in LFA-1 activation and proliferation. However more experiments need to be done to investigate the lymphocytes of these patients. ADAP deficient cells lack SKAP55 al well, so it is important to study the role of SKAP55 and its link to diseases.

1.7.2 SKAP Proteins

SKAP proteins include SKAP55 (also known as SKAP1 [101]) and its homolog SKAP-HOM [102] (also referred as SKAP55-related (SKAP55R) [75] or SKAP2) **(figure 1.6)**. These two proteins are quite conserved and share 40% of the sequence identity at protein level but differ mainly at the N-terminus [75].

The cytosolic adaptor protein SKAP1 selectively binds to the Src Kinase SH2 domain and therefore, it is also known as SKAP55 (Src Kinase Associated Phosphoprotein of 55Kda). It is preferentially expressed in T lymphocytes [103] and possesses a Dimerization domain (DM, residues 1-60) followed by a Pleckstrin Homology domain (PH, residues 106-205), an inter-domain that contains three tyrosine residues at position 219, 232, 271 and a C-terminal Src Homology 3 domain (SH3, residues 300-356) which interacts with ADAP **(shown in figure 1.6)** [79, 103-105]. Specifically, the tryptophan at position 333 (W333) on the SH3 domain of SKAP55 is important for binding to the proline-rich region (340-362) of ADAP [61, 79].

SKAP55 forms a complex with only 70% of the total pool of ADAP [79]. Many groups have independently demonstrated that the loss of ADAP in T cells destabilizes SKAP55 leading to its degradation at the protein level while the mRNA levels of SKAP55 remain normal [49, 61, 79]. Additionally, the re-expression of ADAP in ADAP-depleted cells simultaneously restores the expression of SKAP55. This suggests that the association between ADAP and SKAP55 is crucial for the stability of the SKAP55 protein [49, 61, 79]. However, it is still unclear how ADAP protects SKAP55 from degradation. In 2005, Huang *et. al.* [61] demonstrated that the half-life of SKAP55 is reduced from 90 mins to 18 mins in the absence of ADAP suggesting that either ADAP/SKAP55 complex formation stabilizes a protease-resistant conformation of SKAP55 or that ADAP causes SKAP55 to redistribute to subcellular compartments which are less accessible to proteases like the caspase machinery [61].

Furthermore, SKAP55 is known to localize primarily in the cytosol of un-stimulated T cells and relocalizes to the PM upon TCR stimulation where it plays a crucial role in 'inside-out signaling'(integrin activation/LFA-1 clustering/T-cell-APC conjugate formation) [106]. This has been investigated using $SKAP^{-/-}$ mice [58] as well as by downregulating SKAP55 expression using either retroviral gene transfer [68] or small interfering RNA [59] (siRNA). SKAP55-deficient T cells show normal expression of ADAP but defective LFA-1 clustering and T-cell/APC conjugate formation resulting in impaired adhesion [49].

The roles played by individual domains of SKAP55 in 'inside-out signaling' have also been a investigated [62, 105-107] [33]. In particular, the SH3 domain of SKAP55 containing tryptophan at position W333 has been shown to be essential for normal functioning of the protein [49].

PH domain of SKAP55 binds to phosphatidylinositol (3,4,5)- triphosphate (PIP3) and is also known to bind to filamentous actin [108] [106]. Witte *et. al*. [106] in 2017 demonstrated that the isolated PH domain of SKAP55 interacts with actin indirectly. Specifically, the lysine at

position 152 (K152) is one of the critical residues for the interaction with actin and is also shown to be important for targeting of the isolated PH domain to the plasma membrane upon TCR stimulation [106] [109]. Another critical residue discovered in the PH domain of SKAP55 is an aspartate at position 120 (D120). Mutating D120 to a positively charged amino acid (D120K) localizes SKAP55 to the PM and inducing T cell adhesion even when cells are not stimulated. However, cells expressing the double mutant D120K/K152E in SKAP55 show impaired TCR-induced LFA-1 to ICAM-1 association [106]. SKAP55 lacking the PH domain does not affect stable T cell adhesion [105], indicating that this domain is involved in an inhibitory process that can be bypassed by PH domain depletion.

The DM domain of SKAP55 is vital for dimer formation either with SKAP55 (homodimer) or SKAP-HOM (heterodimer), with residues A17/F20/L21 playing a pivotal role **(figure 1.6)** [107]. RapL and Rap1 (via its C-terminal SARAH domain) bind to the N-terminal region of SKAP55 and connect it to the cytoplasmic region of the α-chain of LFA-1 [62, 107]. It has also been proposed that DM-PH domains exist in an auto-inhibited conformation via an intramolecular switch mechanism that requires binding-induced release of the N-terminal DM domain, thereby allowing the PH domain of SKAP proteins to target the plasma membrane and initiate signaling [106, 110].

Similar to ADAP, SKAP55 has proven to be an attractive therapeutic target in various autoimmune, inflammatory diseases or lymphomas [98, 101, 111-115] [116]. SKAP55 is an important therapeutic candidate in HPV infected HNSCC (Head and Neck Squamous Cell Carcinoma), which is one of the most common tumors in humans. The over-expression of SKAP55 (together with eight other predicted genes involved in HNSCC) shows better response to immune check-point blockade (ICB) treatment/anti-tumor therapy as well as high sensitivity to chemotherapeutic agents like bleomycin [113]. The exact mechanism of SKAP55 involvement is still under investigation, but it seems that the protein is playing an important role not only in promoting adhesion of T cells but also in regulating inhibitory receptors in T cells. Importantly, SKAP55 was found to be not required for chemokine-induced migration, a finding that also sets its role clearly apart from its binding partner ADAP [101]. SKAP55 has further been investigated as a novel marker in several neoplastic lymphomas that could be used in diagnostic histopathology and thus become a useful tool to evaluate normal T cell differentiation [114].

SKAP2, a homologue of SKAP55 shares the domain arrangement of SKAP55 consisting of a DM domain, a PH domain, two tyrosine motifs, and a C-terminal SH3 domain, but is more widely expressed within the hematopoietic system [102] **(extended figure 1c)**. Similar to SKAP55, the conserved SH3 domain of SKAP-HOM binds to ADAP and is essential for its

stable expression in T cells [49, 75]. In addition to T cells, SKAP-HOM is also expressed in B cells [102]. Mice lacking SKAP-HOM survive and do not exhibit any evident abnormalities. The expression of SKAP55 and ADAP turns out to be normal in SKAP-HOM deficient T cells, indicating that SKAP-HOM does not interfere with their stability. To the contrary, SKAP-HOM deficient B cells, which do not express significant levels of SKAP55, show reduced proliferation in addition to defective β1/β2-mediated adhesion or cluster formation upon B cell receptor stimulation [49, 79, 102]. In this regard, Kyeong *et. al.* [59] showed that SKAP-HOM cannot substitute for the role of SKAP55 in TCR-mediated LFA-1 activation or clustering [59]. Thus, further experiments need to be performed to investigate the exact role of SKAP-HOM in B cells. However, it would be interesting if the regulators of inside-out signaling are also involved in actin remodeling upon T cell activation.

1.8 The actin cytoskeleton in T cell activation (events in the dSMAC)

TCR stimulation also triggers signaling pathways which induce cytoskeletal rearrangements leading to morphological changes in the cell, which are crucial for T cell adhesion, migration, and activation [20, 22, 23, 65, 117-128] [129]. Actin is the backbone and the basic building block of this highly dynamic cytoskeletal system. It is also one of the most abundant, as well as most conserved proteins in many cells [126]. It is a 42kDa globular protein which consists of four structural domains: domain 1 (residues 1-32, 70-144 and 338-375), domain 2 (residues 33-69), domain 3 (residues 145-180 and 270-337), and domain 4 (residues 181-269) **(figure 1.7 a)** [126]. The hydrophobic loop of actin (residues 262-274) has been shown to be important for filament growth and stability [130] [131, 132].

The monomeric form of actin is called Globular actin (G-actin) which undergoes a transformation from monomer to a long double-stranded polymer with a right handed helical twist (known as filamentous or F-actin) by a process named nucleation-elongation reaction **(figure 1.7 (right))** [133] [134] [135]. The actin involved in the process of polymerization is ATP bound (ATP binds in the deep cleft between subdomain 3 and 4) [126], and the whole process depends on three steps, the first one involving the formation of a stable actin nucleus where two or more actin monomers come together to form a stable nucleus (could be a dimer or a trimer) (Step1). The nucleus formation is the rate-limiting step in the polymerization process which uses proteins in the cell specialized to do this function, for example arp2/3, spire, formins, ciboulot [126, 136-139]. As soon as the actin-nucleus is formed, it elongates rapidly and the actin monomers start to attach to the nucleus from two ends, forming a long filament in a process called elongation (Step2). The third step which is called steady state, occurs when ATP on the longer filament gradually converts to ADP via ATP hydrolysis [140] [141]. This leads to the dissociation of ADP-actin by specialized proteins like cofilin from one end of the filament termed as the minus end or the pointed end, while the other end of the filament called the plus or barbed end [121, 126, 142]. On the barbed end, ATP-bound actin monomers continue to add-on to the filament assisted by

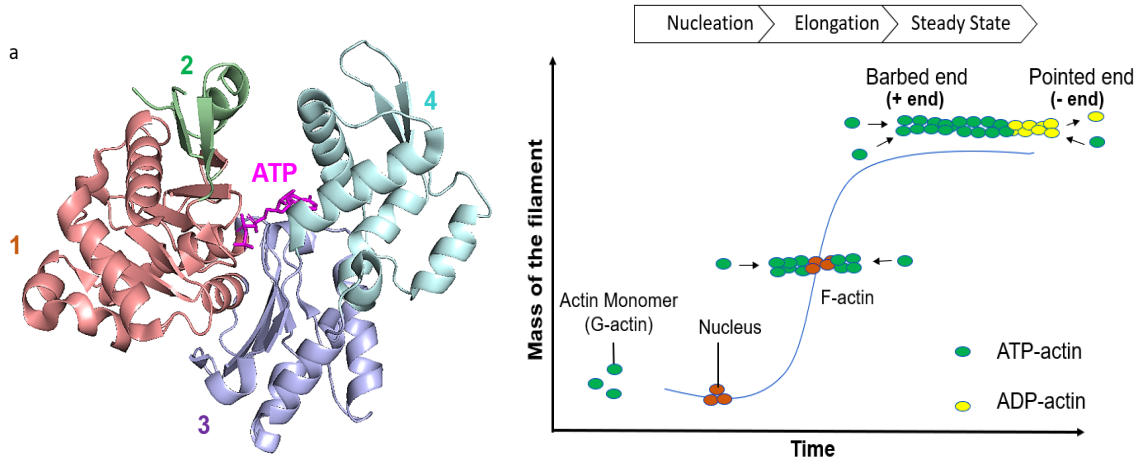

Fig 1.7: Structure of G-actin (PDB: 3HBT) and schematic representation of the basic process of polymerization. (a) G-actin has four subdomains (color code, domain 1: salmon, domain 2: green, domain 3: light-blue, domain 4: pale-cyan, ATP: magenta)**.** (b) Typical polymerization process: ATP bound monomeric actin also known as G-actin (green circles), first forms a stable nucleus consisting of two or three monomers in a process called nucleation. Polymerization starts from both the ends of the nucleus, elongating the filament by specialized proteins like Ena/VASP and profilin in a process called elongation. On the filament, ATP bound to actin hydrolyzes to ADP, attracting several proteins like cofilin which dissociate the ADP-actin from the filament. One end of the filament where the actin monomers keep on adding and the filament elongates faster from this end called barbed end or plus end. The other edge of the filament where actin starts to dissociate, and some actin monomers keep on adding at the same time. It is the slow growing end of the filament called pointed end or minus end.

various actin-elongating proteins like profilin and Ena/VASP **(figure 1.7)** [88, 126, 143]. The barbed end of the filament is more dynamic and elongates 10times faster than the minus end, at a rate of 11.6$\mu M^{-1}s^{-1}$ [121] [87, 126].

The newly discovered actin nucleators such as Spire, CobL, VopL and VopF contain clusters of WH2 domain which are 30-50 amino acid long conserved actin-binding motifs originally found in thymosin-beta proteins [126, 138, 139, 144] **(Fig. 1.8a)**. The WH2 domains bind actin via an amphipathic N-terminal alpha helix that binds between subdomain 1 and 3 of actin monomer [138, 139, 145-147]. However, the WH2 domain containing actin-nucleating proteins as well as formin proteins polymerize actin into linear filaments whereas ARP2/3 complex polymerizes actin in branched filaments [126] **(Fig. 1.8b and c)**.

The highly dynamic cytoskeleton system undergoes continuous change with either polymerization or depolymerization of actin filaments which can further assemble and form

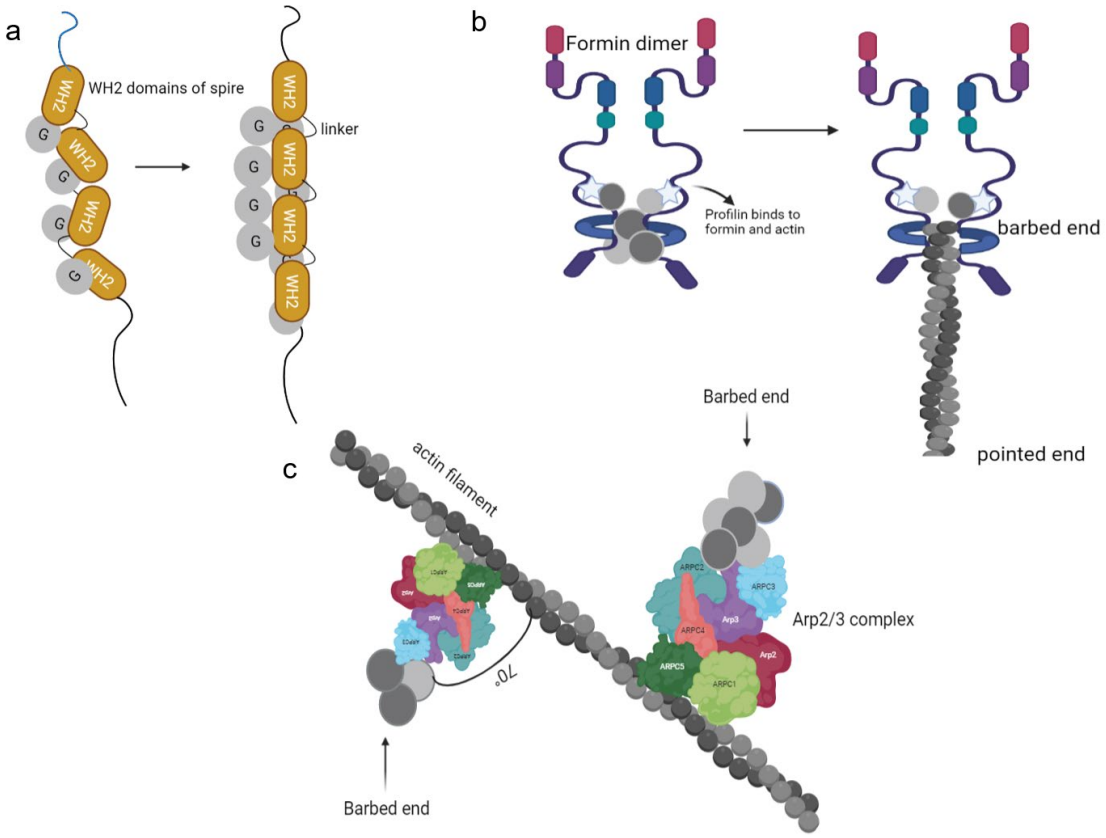

Fig. 1.8: Schematic representation of actin nucleation and polymerization by different mechanisms. (a) The four WH2 domains of spire protein bind to individual actin monomers, make a stable nucleus of four actin monomers and initiate polymerization. The other WH2 domain containing nucleators such as cobl, VopL and Lmod work similarly. (b) Formin proteins make a dimer and the FH2 domains of formin stabilize a nucleus of actin dimer. Profilin proteins bind to the proline rich region of formin, at the same time bind to the actin monomer and add it on the barbed end of the intermediate filament and continue polymerization together with formin. (c) Arp2/3 proteins bind on to the side of the mother filament and initiate nucleation at an angle of 70° and make branched filaments from the barbed end of the filament.

bundles with the help of the proteins such as α-actinin or fascine to carry out the bundling process [137, 138, 142, 146, 148-155] [156]. Polymerization has shown to be influenced in vitro by various factors like pH, temperature, salt, or cation concentrations. *Zimmerle et. al*. in 1988, has shown that actin polymerization is faster at lower pH (lower than pH 7) due to the conditions favoring actin dimer formation, such as the lower pH decreases the critical concentration (the minimum concentration required to initiate polymerization) of actin [157].

Yeasts express single isoform of actin whereas higher eukaryotes such as humans express three isoforms of actin (α-, β-, and γ-actin) [158] [159]. Despite the identical sequence, these isoforms reside into different parts of cells and incorporate into different actin cytoskeleton structures [158]. The isoform α-actin is expressed in muscle cells. The other two isoforms of actin, β-actin and γ-actin are expressed in non-muscle cells and differ at only 4 residues in the N-terminus [121, 126] [145].

T cells can adopt different morphologies by modulating their actin cytoskeleton [117, 121, 124]. A naïve T cell has circular shape due to the actin bundles arranged in parallel fashion [121]. Chemokine stimulation triggers the T cell to adhere and adopt a migratory phenotype, characterized by a leading edge at the front and a uropod at the rear. This shape has been described as a ‘hand mirror shape’ [117]. T cells show an amoeboid movement, where actin-rich protrusions in the front push forward while the contractile ring structure pulls forward. The interaction of the T cell with the APC causes the migration to halt and the cell begins to polarize towards the intercellular contact area [124]. It has been found that specialized actin microstructures known as actin foci form at the interface upon antigen encounter [20]. This relies on continuous nucleation of actin and a cell requires more than one mechanism for constructing the actin filaments, giving rise to the diverse functions performed by the actin cytoskeleton such as membrane trafficking, leading edge protrusion during cell migration, cell division and many more [139] [45]. Thus, the system needs to be tightly regulated and its exerted function depends on the action of various adaptor proteins assembling into different complexes.

1.9 Motivation of this work

The scaffolding protein ADAP has been characterized as an important regulator of inside-out signaling in T cells. Interestingly, it functions without directly binding to either of the stimulated receptors (TCR/ chemokine receptor) or the integrins. Such an intricate mechanism has kept the mode of action of ADAP elusive despite the fact that many studies have clearly annotated the ADAP C-terminal as a hub for tyrosine-phosphorylation

dependent interactions [32, 76, 90, 91]. Colocalization of ADAP with actin at the lamellipodia (where the F-actin polymerization initiates) (Stefanie Kliche, unpublished data) as well as direct physical interactions with the actin regulators Nck and Ena/VASP had been observed in T cells [92] [85, 93]. The ADAP deficient Jurkat T cells also showed significant reduction in total F-actin content upon chemokine receptor stimulation (unpublished data in collaboration with Stefanie Kliche). Thus, a direct role of ADAP on actin polymerization seemed conceivable and was therefore followed in this thesis.

Based on my initial observations that the unstructured N-terminal region of ADAP confers actin polymerization activity, several interesting questions could be posed that were subsequently followed during this work. The topics investigated are listed below:

1. Kinetics of polymerization induced by ADAP.
2. Impact of tyrosine phosphorylation on the polymerization activity of ADAP.
3. Molecular mechanism of actin polymerization by ADAP.
4. Can ADAP also bundle actin?
5. Does ADAP act independent or in concert with other actin regulatory proteins (such as arp2/3 or profilin)?

The results are presented in chapter 3.

2. Materials and methods

2.1 Materials

2.1.1 Chemicals

Most of the chemicals used in this research were purchased from Carl Roth (Karlsruhe, Germany), Sigma-Aldrich (St. Louis, USA) or Thermo Fisher Scientific Life Technologies GmbH.

2.1.2 Devices and Consumables

The Devices and Consumables used during this work are shown in table 2.1.

Table 2.1: List of Devices and Consumables

Device	Manufacturer
Mastercycler (PCR)	Eppendorf, Germany
Pipettes	Eppendorf Germany
Table centrifuge 5415D	Eppendorf, Germany
Table centrifuge 5804R	Eppendorf, Germany
Thermoblock MKR 13	HLC Biotech, Germany
Thermomixer comfort	Eppendorf, Germany
Vortex Genie 2	Scientific Industries, USA
Scale EW 1500-2M	KERN & SOHN gmbh, Germany
Scale ACJ 120-4M	KERN & SOHN gmbh, Germany
TruTemp DNA micro heating system	Robbins Scientific, USA
Profinia Protein purification system	Bio-Rad, Germany
NGC Quest	Bio-Rad, Germany
HiLoad 16/600 Superdex 75 pg	GE Healthcare, UK
HiLoad 26/600 Superdex 200 pg	GE Healthcare, UK
Superdex 200 Increase 5/150 GL	GE Healthcare, UK

Protino Nickel-NTA 5ml column	Macherey-Nagel, Germany
GSTrap FF 5ml column	GE Healthcare, UK
RCT basic stirrer	IKA, Germany
Seven easy pH meter S20	METTLER TOLEDA, Germany
Peristaltic Pump P1	GE Healthcare, UK
Avanti J-26 XP	Beckman Coulter, USA
Electrophoresis Power Supplies	Bio-Rad, Germany
MilliQ biocel	Merck Millipore, Germany
Gel stick gel imaging device	Intas Science Imaging gmbh, Germany
Safe-Lock tubes 1,5 ml / 2 ml	Eppendorf, Germany
SafeSeal micro tubes 1,5 ml / 2 ml	Sarstedt, Germany
Pipetus junior	Hirschmann, Germany
neoAccupette 3-9905	NeoLab, Germany
Incubation shaker	Infors HT, Switzerland
Branson Sonifier 250	Branson Ultrasonics, Germany
Glassware	DWK
Cylinders and beakers (plastic)	Vitlab, Germany
Nanodrop 2000 Spectrophotometer	Thermo Fisher Scientific, USA
Microsep Advance Centrifugal device	Pall Corporation, USA
Spectra/Por Dialysis membrane	Spectrum Laboratories, Inc., USA
Vivaspin 6 / 20	Sartorius AG
Millipore Express Plus Membrane Filter (0.22µm)	Merck Millipore, Germany
NMR tubes	Deutero, Germany
Microliter syringes	BBraun, Germany
Ultraspec 2100 pro	Amersham Bioscience, England
Bruker Avance III 700 Mhz spectrometer	Bruker, USA

Empore Octadecyl C18 47 mm Extraction Disks	Supelco Analytical (Sigma-Aldrich), Germany
TC20 Automated Cell Counter	Bio-Rad, Germany
Nikon Eclipse 5100	Nikon, Japan
Cell counting slides (Dual Chamber)	Bio-Rad, Germany
Amersham Protan 0.45 µm nitrocellulose blotting membrane	GE Healthcare, UK
ADVANCED fluorescence- and EPL-imager	Intas Science Imaging GMBH, Germany
TECAN multilabel plate reader	TECAN, Germany
384 well plates	Corning, USA
MonoQ GL 5/50	GE Healthcare, UK
6-well plates	Corning, USA
L-60 ultracentrifuge	Beckman Coulter, USA
Univapo 150	Uniequip, Germany

2.1.3 Enzymes and Antibodies

Commercial or self-produced enzymes were used for several purposes including molecular cloning, protein purification and modification during the work on this thesis are listed in table2.2.

Table2.2: List of Enzymes, proteins, antibodies

Enzyme, Antibody	Supplier
Benzonase (Nuclease)	Sigma-Aldrich
RNase A	Genaxxon bioscience, Germany
DNase I	Applichem gmbh, Germany
KOD Hot Start Polymerase	Merck Millipore, Germany
Restriction Enzymes (BamHI, NotI, MluI, XhoI, SacI)	New England Biolabs, USA
Thrombin	Merck
T4 Ligase	New England Biolabs, USA

Trypsin	Roche Diagnostics
Precission protease	GE Healthcare, UK
anti-actin HRP labelled (1:5000 dilution)	Miltenyi Biotec GmbH, Germany
goat anti-his HRP labelled (1:3000 dilution)	
anti- ADAP (1:1000 dilution)	Miltenyi Biotec GmbH, Germany
anti-SKAP55 (1:1000 dilution)	Miltenyi Biotec GmbH, Germany
anti-p-Tyr-100 (1:3000 dilution)	
Actin (rabbit skeletal muscle alpha actin)	Hypermol, Germany

2.1.4 Buffers and Stock solutions

The buffers and stock solutions used during this thesis work are listed in table 2.3. All the buffers and solutions that are involved in protein purification or protein storage have been prepared in deionized water and sterilized by either filtering through a Millipore Express Plus Membrane Filter (0.22µm) or autoclaving for 30 minutes at 120°C at 15 psi of pressure.

Table 2.3: List of buffers and solutions used during the work of this project.

Buffer / Solution	Composition
IMAC wash buffer 1 (2x)	600 mM KCl, 100 mM KH_2PO_4, 10 mM Imidazole, pH 8.0
IMAC wash buffer 2 (2x)	600 mM KCl, 100 mM KH_2PO_4, 10 mM Imidazole, pH 8.0
IMAC elution buffer (2x)	600 mM KCl, 100 mM KH_2PO_4, 500 mM Imidazole, pH 8.0
GST lysis / wash buffer (2x)	300 mM NaCl, 20 mM NaH_2PO4, 10 mM EDTA, pH 7.4
GST elution buffer	40 mM Glutathione, 200 mM Tris, 10 mM EDTA, pH 7.4
Cleaning Solution 1 (2x)	1000 mM NaCl, 100 mM Tris, pH 8.0
Cleaning Solution 2 (4x)	2000 mM NaCl, 400 mM NaOAc, pH 4.5
Storage solution (2x)	4% benzyl alcohol
SDS running buffer (10x)	250 mM Tris-HCl, pH 6.8, 1.92 M glycine, 1% SDS
Coomassie staining solution	0.25% Coomassie brilliant blue R-250, 50% methanol, 10 % acetic acid
Destaining solution (2x)	10% acetic acid
NaP phosphate buffer (10x)	200 mM NaH_2PO_4, 1 M NaCl, pH 6.5
M9 salt solution	80 g Na_2HPO_4 x H_2O, 20 g KH_2PO_4, 5 g NaCl (ad 1000 ml H_2O)

Trace element solution	2.5 g EDTA, 250 mg $FeSO_4$, 25 mg $ZnCl_2$, 5 mg $CuSO_4$ (ad 500 ml H_2O)
Buffer A (MS)	0.1% TFA, 5% ACN
Buffer B (MS)	80% ACN
Buffer C (MS)	50% methanol, 0.2% TFA
F-buffer (actin polymerization buffer)	10mM HEPES, 100mM KCl, 1mM $MgCl_2$, 10mM ATP, 1mM DTT, pH 7.6
G-buffer	2 mM Tris, 0.2 mM $CaCl_2$, 0.1 mM NaN_3, 0.1 mM DTT, pH 8
HEPES buffer	10 mM HEPES, 2 mM DTT, 50 mM NaCl, pH 7.5
Strep-tactin Elution buffer	100mM TRIS, 150mM NaCl, 1mM DTT, 20mMDesthiobiotin, pH 7.5
Sf9 Serum-Free/Protein-Free Medium, 1x glutamine	Corning, USA
RIPA buffer (no EDTA)	10 mM TRIS, 1% Triton X-100, 0.1% sodium deoxycholate, 0.1% SDS, 140 mM NaCl, 1 mM PMSF, pH 8.0
TBS buffer (10x)	200 mM TRIS, 1.5 M NaCl, pH 7.4
Actin mutant lysis buffer	10 mM imidazole, 10 mM HEPES, 300 mM NaCl, 2 mM $MgCl_2$, 1 Mm ATP, 1 mM DTT, 4% Triton X-100, 1 mg/ml Tween 20), pH 7.4
Actin mutant wash buffer	20 mM imidazole, 10 mM HEPES, 200 mM NaCl, 1 mM ATP, 1 mM DTT, pH 8.0
Actin mutant elution buffer	200 mM imidazole, 0.2 mM $CaCl_2$, 0.1 mM ATP, 1 mM DTT, pH 8.0

2.1.5 Growth Media

The following growth media were used to cultivate cells and express proteins.

Table2.4: Growth media used for cultivating bacteria, insect cells or Jurkat cells.

Medium	Composition
LB	10g/l tryptone, 5g/ yeast extract, 10g/l NaCl, pH 7.0
2xYT	16g/l tryptone, 10g/l yeast extract, 5g/l NaCl, pH 7.0
	16g/l Na_2PO_4, 4g/l KH_2PO_4, 1g/l NaCl, 2mM $MgSO_4$, 0.3mM $CaCl_2$, 7.5µM ZnCl, 0.8µM $CuSO_4$, 36µM $FeSO_4$, 1.5mg/l

M9	thiamine, 1.5mg/l biotin, 0.75g/l ^{15}N-NH_4Cl, 2g/l ^{13}C-D-glucose or 4g/l D-glucose, pH 7.0

2.1.6 Kits

The kits used during this thesis work are shown in table 2.5. In general, the enclosed protocols were followed very closely.

Table2.5: List of Kits

Kits	Supplier
Pierce BCA Protein Assay Kit	Thermo Fisher Scientific, USA
NucleoSpin Plasmid easy pure	Macherey-Nagel, Germany
NucleoSpin Xtra MiDi	Macherey-Nagel, Germany
NucleoSpin gel and PCR clean up	Macherey-Nagel, Germany

2.1.7 Constructs and Vectors

The constructs that have been created, were used as a template for PCR reactions or for protein expression are listed in table 2.6.

Table 2.6: List of constructs used in this work. Constructs that are labeled by (*) were not cloned by me but provided by Dr. Stefanie Kliche, from Magdeburg. The human actin constructs (**) were provided by Shimada group, University of Tokyo.

Construct	Vector	Antibiotic resistance
His6-ADAP^{120} (shorter isoform 1-783)	pET-28a modified	Kanamycin
His6-ADAP^{130} (longer isoform 1-829) (from origene)	pET-28a modified	Kanamycin
His6-ADAP$^{1-381}$	pET-28a	Kanamycin
His6-ADAP$^{1-100}$	pET-28a	Kanamycin
His6-ADAP$^{1-200}$	pET-28a	Kanamycin
His6-ADAP$^{240-340}$	pET-28a	Kanamycin
His6-ADAP$^{240-290}$	pET-28a	Kanamycin
His6-ADAP$^{290-340}$	pET-28a	Kanamycin
His6-ADAP$^{340-579}$	pET-28a	Kanamycin

His6-ADAP$^{340-486}$	pET-28a	Kanamycin
His6- SKAP55$^{full\ length}$ -linker-ADAP$^{340-450}$	pET28a	Kanamycin
His6-ADAP$^{1-381}$ Deletion1,2,3,4,5,6,7,8	pET28a	Kanamycin
His6-ADAP$^{1-783}$ /Strep-SKAP55$^{full\ length}$ (*)	pFastBacDual	Kanamycin, Gentamycin
His6-ADAP$^{340-783}$ /Strep-SKAP55$^{full\ length}$ (*)	pFastBacDual	Kanamycin, Gentamycin
His6-Fyn Kinase (*)	pFastBac-1	Kanamycin, Gentamycin
Actin-Linker-Tβ4-his8 (D56C) (**)	pFastBac-1	Kanamycin, Gentamycin
Actin-Linker-Tβ4-his8 (D292C) (**)	pFastBac-1	Kanamycin, Gentamycin
Actin-Linker-Tβ4-his8 (T201C) (**)	pFastBac-1	Kanamycin, Gentamycin
Actin-Linker-Tβ4-his8 (K215C) (**)	pFastBac-1	Kanamycin, Gentamycin
GFP-ADAP$^{1-783}$ (*)	pEGFP-C3	Kanamycin
GFP-ADAP$^{1-381}$	pEGFP-C3	Kanamycin
GFP-ADAP$^{1-340}$	pEGFP-C3	Kanamycin
GFP-ADAP$^{340-783}$	pEGFP-C3	Kanamycin
GFP-ADAP$^{381-783}$	pEGFP-C3	Kanamycin
GFP-ADAP$^{1-381\ deletion\ 8}$	pEGFP-C3	Kanamycin
Flag-ADAP$^{1-783}$ (*)	PCMS4	Ampicilin
Flag-ADAP$^{1-381}$	PCMS4	Ampicilin
Flag-ADAP$^{1-340}$	PCMS4	Ampicilin
Flag-ADAP$^{340-783}$	PCMS4	Ampicilin
Flag-ADAP$^{341-783}$	PCMS4	Ampicilin
GST-14-3-3-zeta (*)	pGEX-4T-2	Ampicilin

2.1.8 Primers

The primers used during this work are ordered from IDT technologies and Eurofin Scientific.

Table 2.7: List of primers

Primer	Sequence (5‘-3‘ direction)
ADAP_1_fw_NheI	cggctagcatggcgaaatataacac
ADAP_1_fw_BamHI	caggatccatggcgaaatataacacggg
FYB_1_fw_XhoI	cactcgagatggcgaaatataacacggg
FYB_1_fw_SacI	cagagctcatggcgaaatataacacgg
FYB_1_fw_MluI	caacgcgtatggcgaaatataacacgggggg
ADAP_50_fw_NheI	cggctagcggacccagcaat
ADAP_100_fw_NheI	cggctagcaccagagaccccg
FYB_240_fw_NheI	aggctagcccagcaagggaagac
FYB_290_fw_NheI	ctgctagcgctgctaagaacacctt
FYB_340_fw_NheI	cg gctagcaccccgaaacagaagcca
FYB_340_fw_XhoI	cactcgagaccccgaaacagaag
FYB_340_fw_SacI	cagagctcaccccgaaacagaag
FYB_340_fw_MluI	caacgcgtaccccgaaacagaag
FYB_381_fw_XhoI	cactcgagagcaaaggccagac
FYB_381_fw_SacI	cagagctcagcaaaggccagac
FYB_381_fw_MluI	caacgcgtagcaaaggccagac
FYB_50_rv_BamHI	caggatccttatcctgcaggaggg
FYB_100_rv_BamHI	ccggatccttaggtggtcaagctg
FYB_150_rv_BamHI	ccggatccttatggctttaagtcatgg
FYB_200_rv_BamHI	ccggatccttactggccaaaggc
FYB_290_rv_BamHI	cgggatccttaagcatctatcttcctatc
FYB_340_rv_BamHI	cgggatccttaggctgaattcttgtc
FYB_340_rv_NotI	cggcggccgcttaggctgaattcttgtc
FYB_381_rv_BamHI	cgggatccttagctagtactgtttccagaa
FYB_381_rv_NotI	tcgcggccgcttatgctagtactgtttcca

FYB_450_rv_XhoI	gactctcgagtcagatttccagcaccatcag
FYB_486_rv_BamHI	gaggatccttatttctccagctctaacctctt
FYB_579_rv_BamHI	cgggatccttagtctttttttcagtttcaaagaatcatag
FYB_783_rv_NotI	gggcggccgcttactagtcattgtcatagat
ADAP_783_rv_XhoI	ggctcgagttactagtcattgtcatagatg
SKAP55_1_fw_NheI	cttgctagcatgcaggccgccgc
SKAP55_rv_linkerAD340_450	gccagaacctccccctgatccaccgcctcctctttcttccacttcaa
ADAP_fw_340linker	tcaggggggaggttctggcggaggttcaaccccgaaacagaag

2.1.9 Bacterial Strains

Bacterial cells were used to amplify DNA as well as to over-express proteins. The *E. coli* strains used in this work are listed below.

Table 2.8: List of Constructs

Strain	Usage
XL1-Blue	Cloning
Top10	Cloning
BL21(DE3)	Protein expression
Rossetta	Protein expression
DH10Bac	Bacmid preparation (insect cells)

2.1.10 Programs and Tools

The programs used for data analysis and visualization are listed in table2.9.

Table 2.9: List of Programs and Tools

Program, Tool	Developer
ccpNMR Analysis	Laue Lab, Cambridge, England
Chemdraw Professional 16.0	PerkinElmer Informatics, USA
Igor Pro 6	WaveMetrics, Inc.
Microsoft Excel 2016	Microsoft Corporation, USA
Pymol 2.2.2	Schrödinger LLC, USA
SnapGene	GSL Biotech, USA
Origin	OriginLab corporation, USA
GarphPad Prism	GraphPad Software, San Diego

2.2 Methods

2.2.1 Molecular Cloning

All the ADAP constructs for bacterial expression were cloned using a full-length construct of ADAP in pET28a vector provided by Annika Manns from the lab of Prof. Eberhard Kraus as a template and using suitable oligonucleotides (**Table 2.7**) by means of a polymerase chain reaction (PCR).

2.2.1.1 PCR (Sticky end restriction cloning)

PCR was used for either generating the restriction sites that flanked the cDNA of interest or amplifying different fragments of ADAP using ADAP full length construct. The oligonucleotides that were used for PCR are listed in table2.7. The composition of PCR reaction mixture is shown below:

Table 2.10: Reaction mixture of the PCR to create different fragments of ADAP is shown below. The PCR reaction was divided into four PCR tubes before starting the amplification program in a Master cycler PCR machine.

Components	Volume $\sum 200\mu l$	Final concentration
Optitaq DNA polymerase (5 U/µl)	3 µl	0.075 U/µl
10x Optitaq buffer C	20 µl	1x
10 mM forward primer	4 µl	0.2 mM
10 mM reverse primer	4 µl	0.2 mM
20 ng DNA template	5 µl	0.5 ng/µl

20 mM dNTPs	4 µl	0.4 mM
Ad 200 µl ddH_2O	160 µl	-

The amplification program is illustrated below.

Table2.11: Protocol of the insert PCR for the cloning of different fragments of ADAP

Step	Temperature	Time	Cycles
Initial denaturation	92°C	2 min	1x
Denaturation	92°C	20 sec	
Annealing	59°C	30 sec	35x
Elongation	72°C	30 sec	
Final elongation	72°C	3 min	1x

The PCR product was analyzed on an agarose gel electrophoresis with a DNA marker on the side in another well to ensure the size of the amplified product. Once confirmed on agarose gel, the PCR product was purified using PCR clean-up kit and proceeded with restriction digestion.

2.2.1.2 Site-directed Mutagenesis

Quick change site directed mutagenesis or circle PCR was performed to generate the deletions or point mutations in the N-terminal part of ADAP specifically in ADAP_1-381 region. The classic method was chosen with two overlapping primers carrying the desired deletion or mutation.

Table 2.12: Reaction mixture of the mutagenesis PCR to create mutants of ADAP_1-381

Components	**Volume $\sum 50\mu l$**	**Final concentration**
Pfu plus polymerase (1 U/µl)	1 µl	0.02 U/µl
10x Pfu polymerase buffer	5 µl	1x
10 mM forward primer	1 µl	0.6 mM
10 mM reverse primer	1 µl	0.6 mM
50 ng DNA template (ADAP1-381))	1 µl	0.8 ng/µl
2 mM dNTPs	2.5 µl	0.2 mM
Ad 25 µl ddH_2O	35 µl	-

Table 2.13: Program of circle PCR

Step	Temperature	Time	Cycles
Initial denaturation	95°C	2 min	1x

Denaturation	95°C	50 sec	18x
Annealing	55°C/60°C	1 min	
Elongation	68°C	4 min	
Final elongation	68°C	7 min	1x

The amplified PCR product was confirmed on an agarose gel. If it was the correct product then the purification of the PCR product was performed using PCR clean-up kit (Macherey and Nagel). The purified PCR product was then digested with DpnI restriction enzyme for 1 hour at 37°C which was directly transformed into TOP 10 chemo-competent cells **(section 2.2.9**). DpnI cuts only the methylated template DNA and not the newly generated unmethylated DNA.

2.2.1.3 Restriction Digestion

For cloning a particular gene in a vector, the restriction sites were inserted in the gene of interest by PCR using appropriate primers. To cut at specific positions, restriction enzymes were used that recognize and cut specific palindromic sequences. For vectors, the double digestion was done by adding 2-10µg of DNA, 10x cut smart buffer, few units of enzyme I and II in final volume of 50-80µl solution and incubated at 37°C for 2 hours. The digested vector was then analyzed on agarose gel. After purifying the DNA using PCR cleanup kit (Nagel), the concentration was measured on nano-drop. The vector was re-digested for 20 more minutes using same. The vector was then phosphorylated at the overhangs to increase the chances of ligation using 1µl of rSAP (calve intestine phosphatase) enzyme in the solution and further incubated for 30mins at 37°C. The re-digested vector was directly cleaned using PCR clean up kit and the concentration was measured using Nano-Drop. In case of inserts, the inserts containing same restriction sites were digested the similar way and directly cleaned using PCR-cleanup without checking them on an agarose gel and measured the concentration.

2.2.1.4 Ligation

For Ligation, the vector DNA concentration was used as 100-300ng and the amount of insert was calculated using this formula:

X= (bp(insert)x 100ng (vector))/bp(vector)

The reaction mixture contained 10x T4 ligation buffer, 100ng of vector, X ng of insert, 1µl of T4 DNA ligase enzyme and nuclease free water add up to 10µl. The mixture was

incubated at RT for 30-60 mins then transferred to 16°C for overnight. The following day, ligation mixture was transformed into chemo-competent *E. coli* cells (Top10 or XL1blue) (**explained in section 2.2.1.6**).

2.2.1.5 DNA concentration Measurement

The concentration of DNA was measured using Nano-Drop. Before measuring the DNA concentration, clean water or elution buffer was used as a reference. Then, 2µl of DNA was put on the round surface of Nano-drop and the OD was measured at 260nm. For a pure and contamination free DNA, 260/280 ratio is considered to be between 1.8 and 2.0.

2.2.1.6 Transformation

The chemo-competent cells used for the transformation process are always stored at -80°C. The desired cells were thawed on ice before adding the DNA into it. During cloning, 10µl of overnight ligated sample was used or 50-100ng of plasmid DNA in case of already cloned DNA construct. The cells containing the DNA was incubated on ice for 20 mins and then heat shock was given at 42°C for 45 secs and again incubated on ice for 2 mins. The fresh LB medium was added followed by an incubation step at 37°C for 1 hour with constant shaking which allowed bacteria to multiply (except for DH10Bac cells which are grown for 3 hours). Then ~100-200µl of cells are plated on LB-agar plate containing appropriate antibiotic. The plates are further incubated overnight at 37°C for colonies to grow.

2.2.1.7 Sequencing

The LB-agar plate containing colonies obtained from ligation reaction were first checked using colony PCR along with appropriate negative and a positive control. The positive colonies were grown in 10ml LB medium overnight at 37°C with constant shaking at 120rpm. The next day, plasmids were isolated using plasmid isolation kit according to manufacturer's protocol. The plasmids were diluted to a concentration of 50-80ng/µl and were either premixed with the to-be sequenced primer or the desired primer was chosen from the Microsynth sequencing site before sending for sequencing and were sequenced at Microsynth.

2.2.1.8 DNA Agarose Gel Electrophoresis

DNAs were analyzed after DNA preparation, to confirm PCR products or after restriction digest on a 1% agarose gel. The gel was prepared by dissolving agarose powder in TAE buffer by boiling in microwave for few minutes. 5µl of ethidium bromide was added to 50ml of solution, once the agarose particles were fully dissolved which was loaded on the gel chamber (BioRad Mini DNA system). Samples were supplemented with 2µl of 5x loading dye and the electrophoresis was done at constant voltage of 80-120V for 15-30 mins depending on the gel size. 5µl of Marker was used to estimate the size of DNA fragment. The DNA was visualized and recorded under UV chambre (INTAS).

2.2.2 Protein Expression in Sf-9 insect cells

For protein expression in insect cells, the protocol from Thermo-Fischer Scientific was followed. The insect cells were used for the expression of larger proteins, especially the proteins that cannot be expressed in bacterial expression system.

To begin with, recombinant bacmid was generated by transforming the pFast-Bac-Dual vector containing the gene-of-interest (ADAP and SKAP55 in my case) into DH10Bac *E. coli* cells (as mentioned further).

2.2.2.1 Bacmid preparation

The required pFas-Bac-Dual vector containing ADAP/SKAP55 gene was already available for this project which was necessary for the insect cell Bac-to-Bac Baculovirus expression system. The vector was then transformed in DH10Bac *E. coli* cells (as mentioned in 2.2.1 6)) and plated on X-Gal plates which were then incubated at 37°C for 2 days. The white and blue colonies were distinctly visible after 2 days. 2-3 white colonies and 1 blue colony were re-streaked on a new X-Gal plate and again incubated at 37°C overnight. The recipe used for preparing the plates is shown below in Table 2.14

The white colony from the re-streaked plate was further used to start a bacterial culture for bacmid preparation. The 10ml bacterial culture was grown at 37°C overnight, containing appropriate amount of kanamycin, tetracycline, and gentamycin. The cells were centrifuged at 4000g for 5 mins. The bacmid DNA isolated and ethanol precipitated. The concentration of bacmid was measured on Nano-Drop.

Table2.14: Recipe for preparing X-Gal plates. The prepared plates were stored wrapped in aluminum cover protected from light.

Component in LB-Agar	Final Concentration
X-Gal	20 µg/ml
IPTG	1 mM
Tetracycline	10 µg/ml
Gentamycin	7 µg/ml
Kanamycin	35 µg/ml

2.2.2.2 Insect cell transfection

Insect cells were plated on a 6-well plate 0.5million cells in 2ml /well in insect cell medium containing AA (antimitotic and antibiotic) and incubated at 27°C overnight on a stable surface for cells to adhere to the surface.

For transfection, two different concentrations of DNA were used (1µg and 3µg), mixed in 100µl of aa-free SF9 medium. For lipid-base complex formation, 6µl (for low concentration of DNA) and 12µl (for higher concentration of DNA) of Cellfectin II Reagent were added to 100µl of aa-free SF9 medium in separate tubes. The content of two tubes was combined and incubated at room temperature for 30-45 minutes. In the meantime, the cells in the 6-wells plate were carefully washed with the aa-free sf9 medium. Then the ~200µl bacmid-cellfectin mixture was added to the wells and additional 500µl aa-free sf9 medium to each well. The plate was then incubated at 27°C for 5 hours, Then the medium was changed with 2ml of aa containing medium, which was further incubated at 27°C for 72 hours.

2.2.2.3 Virus amplification and insect cell infection

After incubating cells for 2 days at 27°C, cells were checked for infection signs for example increase in cell spreading, cell lysis, reduced cell growth and detachment of cells from the plate. Once the cells were showing such signs that implied infection, then the cells were harvested by centrifuging the medium containing cells at 500g for 5 mins to remove the cells or cell debris, and the supernatant was collected in a sterile falcon by filtering it through 0.20 or 0.45µm membrane filter. The ~3ml of collected supernatant was called P0 virus and was further used to infect 20ml of ~1x10^6/ml fresh insect cells in 100ml flask, incubated at 27°C with continuous shaking at 120 rpm. The cells were observed everyday under the microscope and the cell viability was measured by staining the cells with Trypon blue (which

stains the dead cells) on a dual chamber cell counting slide (BioRad) using TC20 cell counter (BioRad). Once the viability reaches ~80%, P1 virus was harvested by centrifuging the cells as described previously. Then the virus was used for infecting the bigger batch of fresh insect cells and so on.

2.2.2.4 Confirming transfection and protein expression in insect cells

The protein expression in insect cells was checked at different time points such as at P0 stage after the transfection then after harvesting P1 cells and so on using dot blot. Dot Blot is just like western bot but without the separation of protein bands on SDS PAGE. In this case, few micro liters of cells were centrifuged at 2000g at RT and pelleted cells were resuspended and lysed in RIPA buffer (cell-lyses buffer) and centrifuged again. The few µl of lysate was directly put on the nitrocellulose membrane which was then blocked with blocking buffer. Since the ADAP protein is 6x his tagged. The membrane was blotted against anti-his-HRP labelled antibody followed by washing with TBS-T and further developed using Westar Nova 2011 chemiluminescence substrate (Cyanagen) and signals were detected with an Advanced Fluorescence and ECL Imager.

2.2.3 Protein Expression in *E. coli* cells

Bacterial cell expression system was used for the protein expression of ADAP-full length and other fragments of ADAP. Before starting the expression, the plasmids were transformed in the expression strain for example BL21_DE3 and Rossetta were used in this work. All the plasmids were transformed in expression strain competent cells and plated on LB plates containing appropriate antibiotic. BL21 Rossetta strain contain chlorophenicol, so chlorophenicol was used along with vector antibiotic like Kanamycin since all the ADAP genes were cloned in pET28a vector. A single colony from the LB plate after incubating at 37°C overnight was grown in 10-15ml primary culture in LB medium at 37°C overnight at 120 rpm of constant shaking containing appropriate antibiotic (Kanamycin in case of pET28a and Cholophenicol for Rossetta). The following day, 10ml of pre-culture was added to 1L of fresh medium to initiate cell growth containing antibiotics, again incubated at 37°C with constant shaking. Labelled proteins were expressed in minimal medium containing 15N-labelled ammonium chloride as a sole nitrogen source. The components of Minimal medium are mentioned in **Table2.15**. If no isotope labelling was needed, then the expression was done in 2YT medium or LB medium. The cultures were induced with 1mM IPTG once the optical density at a wavelength of 600nm (OD600) reaches between 0.5 and

0.8. The cells were grown at different temperatures after IPTG induction depending on the construct (see **section 2.2.3 d and e**).

2.2.3.1 Protein expression for NMR experiments:

Table 2.15: The composition of the minimal medium (antibiotic resistance: kanamycin). The medium contains ^{15}N labelled ammonium chloride as a sole nitrogen source.

Component	Amount
100x Trace element solution	10 ml
1 M $MgCl_2$	1 ml
1 M $CaCl_2$	300 µl
10x M9 salt solution	100 ml
Thiamine [1 mg/ml]	1.5 ml
Biotin [1 mg/ml]	1.5 ml
40% Glucose	10 ml
$^{15}NH_4Cl$	750 mg
Kanamycin (35 mg/ml) / Ampicillin (100mg/ml)	1 ml
H_2O	Ad 1000 ml

2.2.3.2 Expression of Deuterated 15N protein

Full deuteration of protein was used to reduce the relaxation of protein and to get a better spectrum of IDPs. Bacterial growth in D2O cultures is limited so an intermediate 50% D2O pre-culture step is added. This was done by growing a 10ml pre-culture overnight in normal LB medium containing appropriate antibiotic on day 1. Then on day 2, the cells from the pre-culture were centrifuged at 2000xg at 4°C. The cells in the pellet were resuspended in a new pre-culture prepared in 20ml D20 instead of LB medium containing all the ingredients mentioned below prepared in D20 stocks except labelled ammonium chloride. For pre-culture, unlabeled ammonium chloride was used.

Table2.16: Components used for preparing culture for the expression of deuterated 15N recombinant protein.

Component (prepared in D2O culture)	Amount
100x Trace element solution	10 ml
1 M $MgCl_2$	1 ml
1 M $CaCl_2$	300 µl
10x M9 salt solution	100 ml
Thiamine [1 mg/ml]	1.5 ml
Biotin [1 mg/ml]/powder	1.5 ml/pinch
Deuterated glucose	1g
(D-glucose_1,2,3,4,5,6,6-D7)	
$^{15}NH_4Cl$	750 mg
Kanamycin (35 mg/ml) / Ampicillin (100mg/ml)	1 ml
D_2O	Ad 1000 ml
NOTE: For the pre-culture use unlabelled NH_4Cl.	

2.2.3.3 Expression of amino acid-specific labelled protein

To perform the amino acid specific labelling of protein, for example only phenylalanine, valine and alanine were specifically 15N labelled in ADAP1-100 construct. On day 1 the pre-culture was prepared using the appropriate antibiotic. The next day, 2L of 2YT medium supplemented with appropriate antibiotic (Kanamycin in this case) was inoculated with the preculture and grown it until the OD_{600} reaches 0.5. Then the cells were centrifuged at 3000xg at 4°C for 10 minutes. The cell pellet was resuspended in 500ml of M9 medium (components are listed below) deficient in ammonium chloride, supplemented with 500mg of each amino acid and 400mg of ^{15}N labeled amino acids of interest. The cells were recovered for 15-20 minutes by shaking at 37°C, 180rpm, induced with IPTG after 20 minutes and finally harvest after 3-4 hours of induction by centrifuging at 4000xg at 4°C for 15 minutes.

Table 2.17: Components used for preparing culture for the expression of 15N labelled specific amino acids in a recombinant protein for NMR.

Component (for amino acid-specific labelling)	Amount
100x Trace element solution	5 ml
1 M $MgCl_2$	0.5 ml
1 M $CaCl_2$	150 µl
10x M9 salt solution	50 ml
Thiamine [1 mg/ml]	0.75 ml
Biotin [1 mg/ml]	0.75 ml
40% Glucose	5 ml
All amino acids	500 mg
^{15}N specific amino acids	200-400mg
Kanamycin (35 mg/ml) / Ampicillin (100mg/ml)	0.5 ml
H_2O	Ad 500 ml

2.2.3.4 Expression of His-tagged ADAP constructs

All the ADAP constructs were in pET28a vector transformed in expression strain BL21 (Rossetta) competent cells for protein expression except ADAP-hSH3 domains and ADAP486-783 (dbl), these were transformed in BL21(DE3) strain. ADAP full-length and ADAP1-381 were expressed at 18°C overnight after IPTG induction while all other constructs are expressed at 37°C for 3-4 hours or 30°C overnight after the induction. The samples were collected before and after 1mM IPTG induction and run on SDS PAGE to check the expression before proceeding for purification.

2.2.3.5 Expression of GST tagged 14-3-3 construct

GST-tagged 14-3-3 construct was cloned in pGEX-4T-2 and kindly provided by Annika Manns from FMP. This construct was transformed in BL21(DE3) cells for expression. The protein was expressed at 37°C for 3 hours after 1mM IPTG induction. The samples were collected before and after IPTG induction and run on SDS PAGE to confirm the expression.

2.2.4 Protein purification

2.2.4.1 Sonication

After overexpression of the proteins, the cells were harvested by centrifugation at 3000xg and 4°C for 10 mins. The supernatant was discarded, and the cell pellet was resuspended in 20ml of the lysis buffer used for IMAC, GST or Strep-tactin affinity chromatography. The lysis buffer also contained 1 tablet of EDTA-free Protease inhibitor cocktail, 50U Benzonase, 1 pinch of lyophilized RNAse and 10mM $MgCL_2$. The cells were sonicated until the color of solution changed to grey. To remove the cell debris, cells were spun down at 15,000xg (fixed angle rotor) for 20 mins at 4°C. The supernatant was filtered through a 0.45µm membrane filter before proceeding for the first step affinity purification.

2.2.4.2 Affinity purification

2.2.4.2.1 His-tag

The filtered lysate was first loaded on a manual column containing Ni-beads equilibrated with lysis buffer. After the lysate was passed through the beads, to get rid of the unbound non-specific proteins, beads were washed with buffer containing 10mM of Imidazole. The His-tagged proteins were eluted using buffer containing 250mM Imidazole. However, a buffer with lower pH of 2-4 could also be used for eluting his-tagged proteins.

2.2.4.2.2 GST-tag

Glutathione Sepharose beads were used to purify GST tagged proteins. GST is a 26kDa protein and expressed in pGEX-41 vector as a tag. After loading the lysate on to the beads, the non-specific proteins were carefully washed off. The wash buffer contained 50mM Tris-HCl pH 8 and the recombinant protein was then eluted by using 40mM of glutathione in wash buffer to compete with the beads.

2.2.4.2.3 Strep-tag

Strep-tag consists of a short peptide of 8 amino acids (WSHPQFEK) which binds tightly to strep-tactin beads.. The buffer to wash off the non-specific proteins contains 50mM Tris, 100mM NaCl, 1mM beta-mercaptoethanol and 1mM EDTA (pH 8). The elution of recombinant protein of interest was done using either 50mM biotin or 2.5mM desthiobiotin in the wash buffer. Desthiobiotin is an analog of biotin which could be removed from the beads using regeneration buffer containing HABA (4-hydroxyazobenzene-2-carboxylic acid).

The eluted fractions from these purifications were further analyzed on SDS PAGE. The elution protein was then concentrated using Viva-spin column of suitable molecular weight cut-off at 4000xg (swing rotor) or 8000xg (fixed angle rotor) at 4°C until the volume reaches to 1ml.

2.2.4.3 Affinity tag cleavage

ADAP was cloned with Thrombin cleavage site (LVPRGS) inserted between His-tag and the first amino acid of the protein and could be cleaved off before or after concentrating the protein. To remove the affinity tag the eluted protein was incubated with 1U of thrombin per mg protein at 4°C overnight or 37°C for 1-2 hours depending on the stability of the protein.

2.2.4.4 Size exclusion chromatography

Size exclusion chromatography was the final step of the protein purification process. Analytical Superdex 200 gel filtration column was used to purify ADAP full length or different fragments of ADAP. The column was first equilibrated with the final buffer suitable for the protein prior to loading the protein sample. All the ADAP fragments were purified in a final buffer containing 10mM HEPES, 50mM NaCl, 1mM DTT, pH7.4, while ADAP/SKAP55 complex is eluted in a buffer of 50mM Tris, 100mM NaCl buffer, 1mM BME, 1mM EDTA, pH8 and their purity was confirmed by SDS-PAGE

2.2.4.5 SDS PAGE

The size and purity of proteins in solution was analyzed by sodium dodecyl sulfate polyacrylamide gel electrophoresis (SDS-PAGE). At least 1µg of the protein was mixed with 5xSDS loading buffer and the samples were then run on a 12% polyacrylamide gel prepared according to Laemmle or a 4-20% Mini-PROTEAN TGX gradient gel (Bio-Rad, for western blotting or Mass Spec.) at 200-280V. The gels were subsequently stained with Coomassie (R250) and de-stained using de-staining solution (composition described below). The size of the proteins was estimated by comparing the resulting bands to a Mark12 Unstained Standard or See-Blue Pre-stained Protein Standard (Thermo Fischer) run on the same gel [160] [161].

SDS sample loading buffer (5X): 10% (v/v) glycerol, 500mM DTT, 3% (w/v) SDS, 0.5% bromophenol blue, 312.5mM Tris-HCl, pH 6.5

SDS Running buffer (10X): 250mM Tris-HCl, 1.92M Glycine, 1% SDS in H_2O, pH 8.3

Coomassie staining solution: 0.25% Coomassie brilliant blue R250, 50% Methanol, 10% acetic acid

De-staining solution: 50% Methanol and 10% acetic acid

2.2.4.6 Western blotting

To specifically detect proteins purified from different systems, western blotting was applied apart from another analytical technique i.e. Mass Spectrometry. In this case, the proteins were run on a commercial 4-20% gradient acrylamide gel. The gel is placed on a nitrocellulose membrane with a pore size of 0.45µm (Bio-Rad) soaked in transfer buffer and both are placed between layers of soaked Whatman-paper. The blotting was carried out in a tank-device (Invitrogen) for 55 min at 100V. The transfer of protein bands on the membrane is assumed by seeing the bands of pre-stained marker. The transfer of bands on membrane could also be confirmed by ponceau staining. Subsequently, the membrane was blocked with 5% milk powder in TBS supplemented with 0.05% Tween 20 (TBS-T) for 1 h at room temperature or overnight at 4°C followed by a washing step with TBS-T, 3 times. The membrane was then incubated with the primary antibody for 1 h at room temperature or 4°C overnight, washed 3 times with TBS-T and incubated for 1 h with the secondary antibody. After washing with TBS-T, the membrane was developed using Westar Nova 2011 chemiluminescence substrate (Cyanagen) and signals were detected with an Advanced Fluorescence and ECL Imager (Intas).

TBS (10X): 200mM Tris, 1.5M NaCl pH 7.4

TBS-T: 1X TBS, 0.05% Tween 20

Blocking buffer: 5% milk powder in TBS-T

2.2.4.7 Measurement of protein concentration

The concentration of proteins containing aromatic residues was measured at an absorbance of 280nm on nano-drop. The measured absorbance was divided by the specific absorbance which was computed using the online protparam software on the expasy site.

$$concentration\ (Protein) = \frac{A280}{Specific\ absorbance}\left(\frac{mg}{ml}\right)$$

2.2.5 *In vitro* actin polymerization assay

Basic principle

As described in the introduction when actin polymerizes it makes a long double helical filament. To start the process of polymerization, it requires the formation of a stable actin nucleus where two or more actin monomers come together and form dimer or oligomer. Once the nucleus is formed, the actin monomers start to add on to the nucleus from both ends making a long filament, a step called elongation. This assay is based on the principle that pyrene-fluorophore on monomeric actin excites at 385nm and emits at 395 nm. However, when pyrene-actin starts to polymerize into a double helical filament **(Fig. 1.7b)**, the two or more pyrene molecules come in close proximity, make an excimer (excited dimer) and the emission shifts to 420nm. The change in fluorescence intensity of pyrene-actin resulting from addition of ADAP or ADAP/SKAP55 proteins was measured over time at 420±10nm on a fluorescence reader. In vitro actin polymerization assay is performed to investigate the polymerization effect of ADAP and its fragments or SKAP55 proteins on actin. In this assay, 10% pyrene labelled monomeric actin is used.

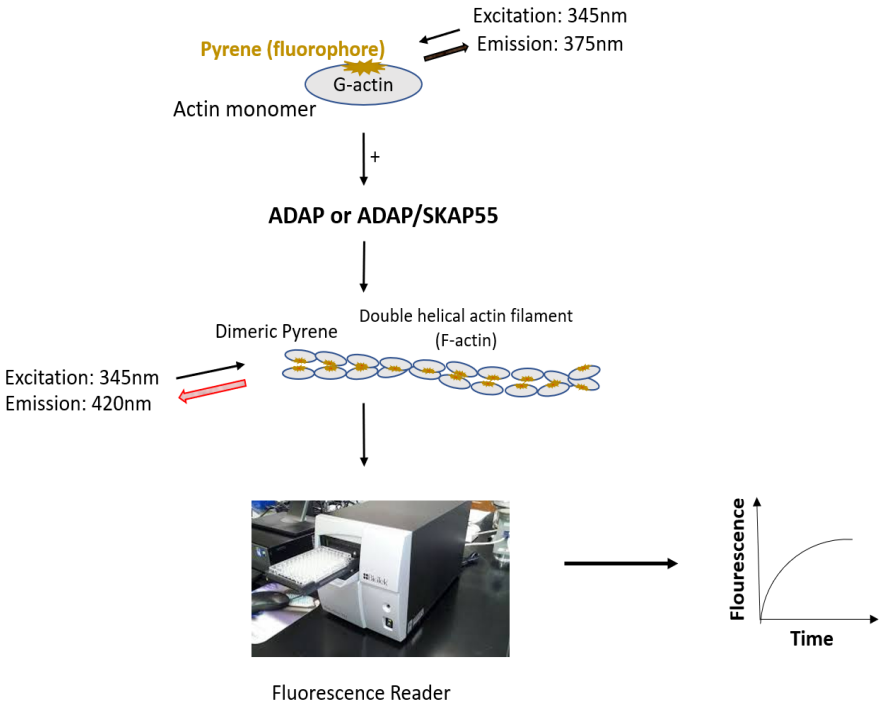

Fig 2.1: Schematic representation of experimental setup of *in vitro* actin polymerization assay. The monomeric actin used in this assay is pyrene labelled. The monomeric form of fluorophore pyrene has excitation wavelength of 385nm and emission at 395nm. When actin polymerizes in the presence of a polymerizing protein, it forms a double helical filament and pyrene molecule bound to actin come in close proximity and the emission wavelength shifts to a higher wavelength, so the emission is measured at 420 ± 10nm. The change in fluorescence intensity with time is measured on TECAN plate reader (new machine available in the lab). However, few of the measurements are done on the old plate reader Victor.

1mg of lyophilized pyrene-actin (from Hypermol) is dissolved in 3ml of cold de-ionized autoclaved water making a stock concentration of 7.9µM. For all the tests, actin concentration is used 5µM in 40µl final volume. First a baseline is measured for actin without any test protein for 5 times with 10sec interval, then test protein or buffer is added, volume make-up with the reference buffer and the fluorescence change is measured for 1-3 hours at an interval of every 10 seconds. The data is analyzed and plotted as fluorescence intensity versus time. The half time to maximal polymerization is calculated according to Doolittle et. al. [162].

2.2.6 *In vitro* co-sedimentation assay/ bundling assay

To investigate if a protein is interacting with filamentous actin or involved in bundling of F-actin, an in vitro co-sedimentation assay is performed. This assay is based on the principle that if a protein shows bundling activity, the protein and F-actin (filamentous actin) co-sediment in the pellet to a certain extent when centrifuged at low speed 12000g and the read out is the SDS PAGE.

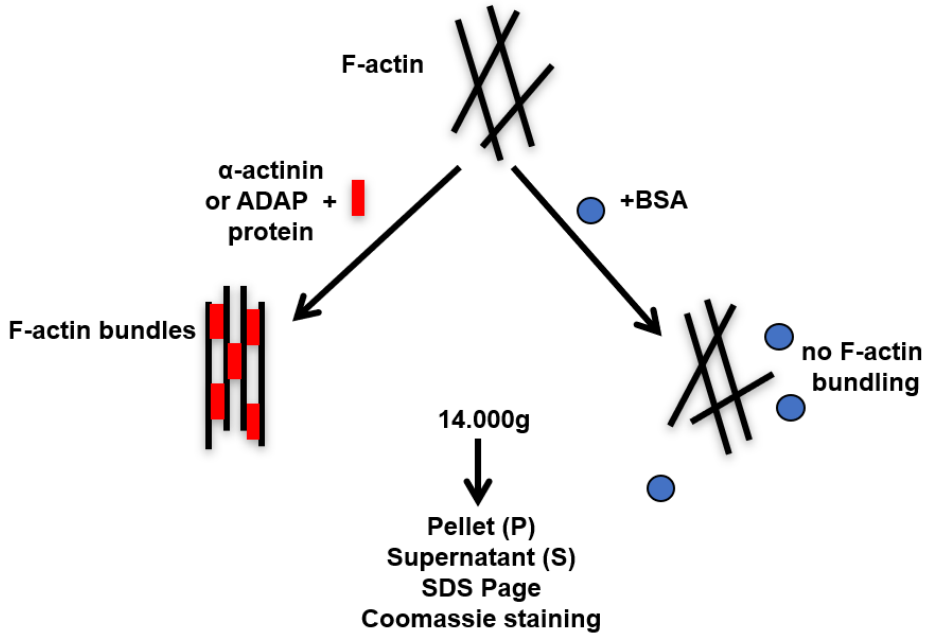

Fig 2.2: Schematic of *in vitro* F-actin bundling assay. The pre-polymerized actin is incubated with a positive control (we used alpha-actinin), a negative control (BSA) and test proteins for 30 minutes. The tubes are centrifuged at 14,000g for 15-20 minutes at RT and the supernatant is removed in a new tube and pellet is resuspended in water and checked on an SDS PAGE.

The commercial monomeric actin is polymerized with actin polymerization buffer (F-buffer) to a concentration of 10µM and incubated at room temperature for 15-30 minutes to ensure the complete polymerization. Then the 10µl of 10µM or 50µM test protein is added to the polymerized actin and again the mixture is incubated for 30 minutes followed by centrifugation for 15 minutes at RT. Several controls are needed to validate the results. For

each test protein, a control without F-actin (i.e., test protein with F-buffer) to rule out the possibility of self-precipitation. Furthermore, F-actin without any test protein (F-actin with protein buffer) to make sure that F-actin itself does not form bundles or precipitate more than the protein samples. BSA is used as a negative control and actinin is the positive control. After the centrifugation step, the supernatants are carefully put into a new-tubes and the pellets are re-suspended in 15µl water. The supernatants and pellets are ultimately run on SDS PAGE. The analysis of F-actin band on SDS PAGE was performed using ImageJ software and plotted with GraphPad version 8.

2.2.7 *In vitro* phosphorylation Assay

Tyrosine Phosphorylation with Fyn Kinase: ADAP-full length, ADAP/SKAP55 proteins or C-terminus of ADAP were phosphorylated with Fyn Kinase, the similar way as described previously ([32]).

2.2.8 Crosslinking Mass Spectrometry

2.2.8.1 *In vitro* Crosslinking and Digestion

Crosslinking MS was performed to confirm the direct interaction between ADAP and actin using a crosslinker [163] [164]. DSSO was the crosslinker used in this experiment to crosslink pre-polymerized filamentous actin with different fragments of ADAP. The commercial monomeric actin was polymerized to a final concentration of 1mg/ml with actin polymerization buffer containing cations and high concentration of AMPpnp (a non-hydrolysable analog of ATP). The very clean ADAP full length or different fragments of ADAP were mixed with filamentous actin of ~0.35mg/ml concentration of each protein in a final volume of 70µl. These two proteins were crosslinked by adding 0.05mM of DSSO (in other words 1:100v/v) to the mixture, which was then incubated at room temperature for 20 mins and repeated. The reaction was quenched by adding 1M Tris (pH 8.0) to a final concentration of 20mM and the mixture was incubated for 30 mins at RT followed by addition of equal amount of ABC buffer as volume of mixture. To this mixture, 8M crystalline urea and 5mM DTT was added to denature protein and reduce the di-sulfide bonds. The reaction was incubated at 56°C for 30 mins. At this point the pH of the reaction mixture should be basic for the activity of enzymes, so the pH was checked by pH paper. The endo-proteinase enzyme Lys-C was added at an enzyme to substrate ratio of 1:75 and incubated at 37°C for 2-4 hours. The urea concentration was diluted to 2M using ABC buffer for the addition of Trypsin enzyme with 1:100 of enzyme to substrate ratio and incubated overnight at 37°C. The following day, digestion was stopped by adding 1% of Formic acid. The cleaved peptides were further purified using Stage Tip [165].

DSSO stock concentration: 50mM (1mg DSSO dissolved in 50µl DMSO)

Quenching solution: 1M Tris, pH 8.0

Ammonium Bicarbonate (ABC): 50mM ABC in water, pH 7.8

2.2.8.2 Peptide purification by Stage Tip

Desalting of samples was performed with Stage Tips packed with C18 solid phase extraction disks using 16-guage punches. The peptides in an acidic solution of pH ~2-3 binds to the C18 material which was eluted with elution buffer containing 50% acetonitrile in 0.1% formic acid. The stage-tips were activated by adding 100µl of Methanol and centrifuged at 2000xg for 2-3 mins until the tip (C18 material) was dried. The stage tips were washed with 200µl Buffer A and centrifuged again but this time the C18 material was not let dried completely. The samples were loaded onto the tip followed by a washing step with buffer A and centrifuged at 2000xg until the tips were dry [166]. The peptides were then eluted in 100µl Buffer B in an Eppendorf which was further transferred to a glass vial. Eluates were dried via vacuum centrifugation, and stored at -20°C [166].

Buffer A (Wash Buffer): 0.1% Formic acid in water

Buffer B (Elution Buffer): 50% ACN in 0.1% Formic acid

2.2.8.3 Measurement and analysis of DSSO-crosslinked samples by mass spectrometry

The dried peptides were solved in 100 µl 1% ACN / 0,05 % TFA and injection volume of 1 µl was used. LC-MS analysis was performed using an UltiMate 3000 RSLC nano LC system coupled on-line to an Orbitrap Fusion mass spectrometer (Thermo Fisher Scientific). Reversed-phase separation was performed using a 50 cm analytical column (in-house packed with Poroshell 120 EC-C18, 2.7µm, Agilent Technologies) with a 120 min gradient. Cross-link acquisition was performed using an LC-MS2 method. The following parameters were applied: MS resolution 120,000; MS2 resolution 60,000; charge state 4-8 enabled for MS2; stepped HCD energy 21, 27, 33.

Cross-linking Data analysis was performed using XlinkX standalone with the following parameters: minimum peptide length=6; maximal peptide length=35; missed cleavages=3; fix modification: Cys carbamidomethyl=57.021 Da; variable modification: Met oxidation=15.995 Da; DSSO cross-linker=158.0038 Da (short arm = 54.0106 Da, long arm = 85.9824 Da); precursor mass tolerance = 10 ppm; fragment mass tolerance = 20 ppm.

MS2 spectra were searched against a special database (created from the submitted sequences for Actin and ADAP). Results were reported at score cutoffs (n_score = $10^{(-8)}$; n_score_MS2 = $10^{(-3)}$).

2.2.8.4 Mass spec sample preparation

To prepare the protein samples for MS analysis, the proteins were run on SDS gel. The gel was stained and de-stained in a clean box. The protein bands from de-stained gel of interest are cut in very small pieces (~1mm size) using a sterilized cutter and transferred into a low binding 0.5ml Eppendorf tube. Then 200µl of de-staining buffer was added to tubes containing small pieces of gel and incubated at 45°C for 15 mins at constant shaking. The buffer from the tube was carefully discarded and the tube was re-filled with 200µl of Trypsin buffer, again incubated at 45°C for 15 mins and then supernatant was removed carefully. If the gel pieces still look blue, then the upper two steps were repeated. After this, 100µl of ACN was added to the gel pieces for 10mins at 45°C and removed carefully after 10 mins. The gel pieces shrink after ACN incubation. To the dried gel pieces, 1µg of trypsin enzyme was added in 30µl of ABC buffer to fully cover the pieces, followed by an incubation at 37°C overnight. Next day, the digestion was stopped by adding 30µl of stop solution. The supernatant was collected in a sterilized glass vial or Eppendorf tube. To the gel pieces 10µl of ACN was added and incubated for 10 mins at RT. The tube is shortly spinned down and the remaining supernatant was collected and combined with the first supernatant in glass vial. The supernatant was dried in vacuum centrifuge (speed vac.) for 1-2 hours depending on the volume. The dried peptides were either stored at -20°C if not using immediately or re-dissolved in 10µl of 5%ACN and 0.1% TFA and measured.

Trypsin Buffer (ABC): 50mM Ammonium Bicarbonate, pH 7.8

Distaining buffer: 50mM ABC/ACN (1:1v/v)

Enzyme Solution: 5µl of Trypsin enzyme of stock concentration 1µg is mixed in 95µl ABC

Stop Solution: 0.5% TFA (Trifluoroacetic acid) in ACN (Trifluoroacetic acid)

2.2.9 Negative stain Electron Microscopy

The basic principle of this technique is that the background of the sample is stained with heavy metal, uranyl acetate is used most commonly, and the specimen is left untreated, thus visible due to the contrast and measured on a transmission electron microscope (TEM). In this method, a low voltage electron beam is transmitted through an ultra-thin

section of microscope which passes through the specimen to image and the magnification of the image is achieved by electromagnetic field, unlike the light microscope where the magnification of the image is obtained by optical lenses. This method can be used to image structures of macromolecules with atomic resolution from nm to µm [167]. The limiting factor is the thickness of the specimen, as it limits the transmission of electrons. Additionally, for biological specimens, sample preparation is critical for electron micrographs.

The samples from *in vitro* polymerization assay were diluted to a final concentration of 50-100 ng/µl and an aliquot of 4 µl was applied to glow-discharged carbon/formvar-coated 400 mesh copper grids (S162-4, Plano GmbH) for 1 minute. Grids were blotted manually with Whatman No. 1 filter paper and stained by addition of 4 µl 1% uranyl acetate for 1 minute. After blotting, grids were dried for at least one hour and stored at room temperature until use. Imaging was conducted on a FEI Talos L120C transmission electron microscope (TEM) equipped with a CETA 16M CMOS detector. Data was acquired manually under “Low dose” conditions with FEI TIA Software applying a defocus between -1 and -2 µm.

2.2.9.1 Gradient Fixation for EM

To improve the ADAP/SKAP55 complex sample for electron microscopy, another sample preparing technique called gradient fixation using a crosslinker ‘glutaraldehyde’ was tried. For this, all the buffers were prepared fresh and filtered before adding glutaraldehyde. On the gradient mixing column, buffer A was added to the Left column and buffer B on the right. The gradient of sucrose was created by slowly opening the valve and let the solution fill the tube used in ultra-centrifugation. 200µl of 1mg/ml or more concentrated protein was added on the top of the gradient solution gently through the wall of the tube and centrifuged for 16 hours at 21,000g at 4°C. After 16 hours, the total solution was divided in smaller volumes like 200-400µl /fraction and 30µl of each fraction was checked on SDS-PAGE. The fractions containing protein were collected and prepared for EM. To remove the high sugar from the sample, it was diluted with normal protein buffer and concentrated through the vivaspin columns and repeated for at least 3-4 times. The protein was concentrated to a final volume of 100µl and the cryoEM grids were prepared with this material.

Buffer A: 10% sucrose in 20mM Hepes, 100mM NaCl, pH 7.5 (5g sucrose in 50ml solution)

Buffer B: 30% sucrose in 20mM Hepes, 100mM NaCl, pH 7.5 + 0.1% glutaraldehyde (5g sucrose in 50ml solution and 200µl glutaraldehyde from 25% stock)

2.2.10 Nuclear Magnetic Resonance

Basic principle

Nuclear magnetic resonance (NMR) spectroscopy is an effective technique to study molecular interactions at atomic level. This is based on the behavior of the angular momentum (spin) of atomic nuclei in a magnetic field. Only isotopes with a spin quantum number different from 0 are NMR-active and thus ^{1}H, ^{13}C and ^{15}N atoms are eligible for NMR spectroscopy. However, proteins and other biomolecules mainly contain ^{12}C and ^{14}N isotopes as they are of high natural abundance. Thus, in order to visualize carbon and nitrogen atoms, proteins need to be labeled with NMR-active nuclei by bacterial expression in minimal medium containing ^{13}C glucose and ^{15}N ammonium chloride as sole carbon and nitrogen sources **(section 2.2.3).**

In a homogeneous magnetic field, nuclear spins align and perform gyroscopic motion about the magnetic field axis at the nuclear Larmor frequency. Nuclei with a spin quantum number of half (½) can occupy either of two states with a slight preference for the lower energy level. Transitions between energy levels are induced by irradiation of electromagnetic waves when the resonance case exists. During relaxation, the nuclear spins return to the equilibrium state inducing a decaying cosine function called FID (Free Induction Decay), detected by a coil.

The chemical environment of the nucleus influences the exact magnetic field that acts on the nucleus. This results in the different Larmor frequencies. The NMR spectrum shows the chemical shifts, which are the measured Larmor frequencies of every nucleus normalized to the Larmor frequency of a reference compound in ppm (parts per million) [168].

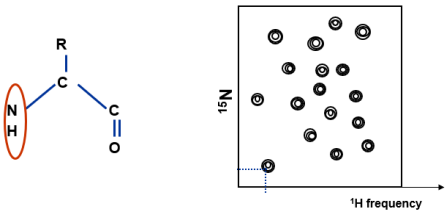

Fig. 2.3. Schematic representation of a 2D ^{1}H-^{15}N-HSQC spectrum. In a ^{1}H-^{15}N-HSQC spectrum, proton and nitrogen atoms are correlated so that each NH group of the protein backbone gives rise to a resonance signal in the spectrum. (adapted from Dr. Jana Sticht).

Based on the sequence of defined pulses and incrementable waiting times between them, magnetizations can be transferred and thus correlations between atomic nuclei can be displayed in multidimensional spectra. In the two-dimensional ^{1}H-^{15}N-HSQC (Heteronuclear single quantum correlation) spectrum, the frequency of the amide proton is linked to the frequency of the nitrogen atom. That is, each signal results from a bond of a proton to a nitrogen atom. For each NH group of the protein backbone, a signal is generated

in the spectrum **(Fig. 2.3)**. This allows the investigation of a peptide or protein with information about individual amino acids. An exception is proline, which is not detected due to the lack of a proton in the backbone. The amino acids asparagine, glutamine, tryptophan, lysine and histidine generate additional resonances resulting from the NH2 or NH group of their side chains.

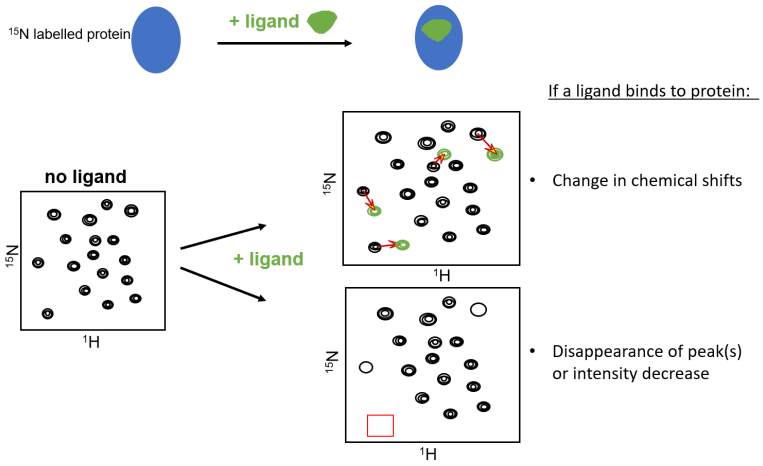

Fig. 2.4: Schematic representation of 2D ^{1}H-^{15}N-HSQC spectrum indicating interaction between two molecules. Chemical shift changes result from the change in chemical environment of the residue upon ligand binding. Disappearance of peaks or overall intensity change would imply the formation of a bigger complex, which tumbles slowly in the magnetic field. (adapted from Dr. Jana Sticht).

To see an interaction between two proteins or a protein and a ligand, first a reference spectrum is measured which is usually the ^{15}N-labelled protein alone. Then the unlabeled ligand is added to the protein, if there is interaction between the two molecules then the resulting spectrum shows differences in the resonances when compared to the reference **(Fig. 2.4)**. HSQC titrations, adding increasing concentrations of ligand to the protein sample, can additionally reveal the strength of the interaction, either showing fast or slow exchange as compared to the NMR timescale represented by peaks shifting linearly with ligand concentration or peaks of the free protein loosing intensity while peaks of the bound state increase in intensity with ligand concentration, respectively.

In our HSQC interaction experiments, ADAP proteins were recombinantly expressed under deuterated conditions containing ^{15}N-NH_4Cl and deuterated glucose **(section 2.2.3 for more details)**. ADAP_1-100 was expressed in non-deuterated conditions. The overexpressed proteins were purified as described above in section 2.2.4. HSQC spectra were acquired on a Bruker Avance III 700 MHz spectrometer equipped with a 5 mm triple resonance cryoprobe at 300K with 32 scans (deuterated) or 64 scans (non-deuterated) and 160 data points in the indirect dimension. 25µM ^{2}H-^{15}N- or ^{15}N-labeled protein was mixed with 25µM G-actin (recombinantly expressed) or non-polymerizing actin (purchased from

Hypermol company) in a final volume of 550µl containing 10% D_2O, pH 6.5. Experiments with G-actin and non-polymerizable actin were performed in 10mM HEPES, 50mM NaCl, 0.4mM ATP pH 6.5 or 7.5 buffer. Experiments with F-actin were performed in buffer containing 500mM KCl, 10mM ATP, 10mM HEPES pH 6.5. NMR spectra were processed with TopSpin3.2 (Bruker, Billerica, USA) and analyzed using CcpNMR Analysis (version 2.4.2.) [169].

For backbone assignments, ^{13}C-^{15}N-labeled ADAP_1-100 and ADAP_100-200 were recombinantly expressed in M9 minimal medium containing ^{15}N-NH_4Cl and ^{13}C glucose. The overexpressed proteins were purified as described above and measurements were performed in 10mM HEPES, 50mM NaCl, pH 6.5 with 10% D_2O). HNCA, HN(CO)CA, HNCO, HN(CA)CO, HNCACB spectra were recorded at 300K for 500µM ^{13}C-^{15}N-labeled ADAP_1-100. HNCA, HN(CO)CA, HNCO, HN(CA)CO, HNCACB, (H)N(CA)NH spectra were recorded at 300K and HNCA, HN(CO)CA, (H)N(CA)NH were recorded at 280K for 400µM ^{13}C-^{15}N-labeled ADAP_100-200. 3D experiments were acquired with 8-32 scans and 25-50% NUS. Backbone assignments for 85% of the non-proline residues of ADAP_1-100 and 75% of the non-proline residues of ADAP100-200 could be assigned using CcpNMR Analysis (version 2.4.2.). Assignments were transferred to the spectra of ADAP1-381 whenever unambiguously possible. Overlapping peaks were excluded from the peak intensity analysis. Chemical shift differences were calculated using the following formula [169].

$$\boldsymbol{\Delta\delta(1H,15N) = (\delta(1H)2 + (0.15 * \delta(15N))2)1/2}$$

2.2.11 Peptide Docking Models

The CABS-dock server (http://biocomp.chem.uw.edu.pl/CABSdock) [170, 171] [172] was used to dock various fragments of ADAP_1-381 to a single actin (chain C extracted from PDB 6fhl [173]) or an actin dimer (chains C and E extracted from PDB 6fhl). In case ADAP fragments contain lysines that were shown to crosslink to lysines in actin, these were included as soft distance restraints of 10Å between the Lysine residues in the coarse-grained model.

3. Results

3.1 ADAP polymerizes actin filaments

Co-localization of ADAP with actin in lamellipodia [86] and defective F-actin content observed in ADAP deficient T cells suggest a possible role of ADAP in actin reorganization. In order to verify this hypothesis, the direct or indirect interaction of ADAP with actin and its potential role in actin polymerization was investigated *in vitro*. To begin with the aim of uncovering the mechanism of actin binding, ADAP full-length and different fragments of ADAP were recombinantly expressed as described in methods (**section 2.2.6**). In the following subsections the results of recombinant expression and *in vitro* actin polymerization are presented.

3.1.1 Generation of recombinant ADAP and ADAP/SKAP55 proteins

ADAP full-length and different fragments of ADAP (please see section 3.1.4) were cloned into prokaryotic expression vector (pET28a) and expressed in *E. coli* either in complex medium (2YT) or in minimal (M9) medium for isotopic labeling as it is required for NMR experiments. For the purpose of protein purification, the N-termini of the proteins were

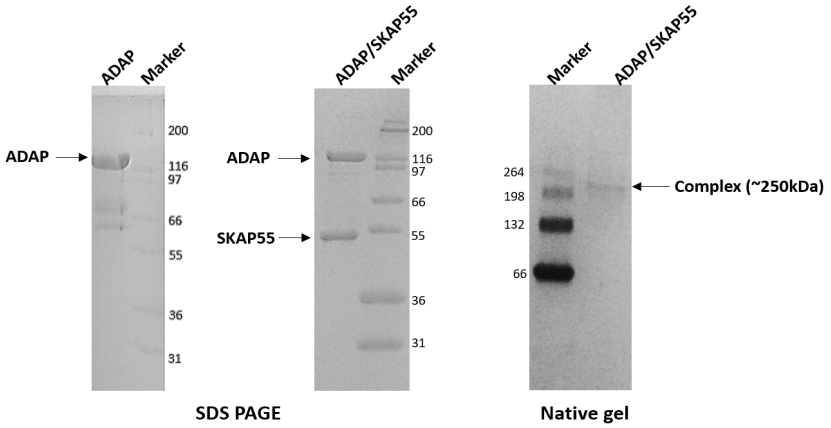

Fig. 3.1: Purified ADAP protein and ADAP/SKAP55 complex on SDS PAGE. (left) ADAP full-length is expressed in bacterial expression system using pET28a vector and **(middle)** ADAP/SKAP55 complex is co-expressed in Sf9 insect cell system using pFasBacDual vector. **(right)** ADAP/SKAP55 complex on native gel. (SDS-PAGE: 15%, 250 Volts, 35 minutes, Marker: Mark 12 Unstained Standard. Non-reducing (right) gel 4-20%, 100 Volts, 90 minutes, Marker: BSA Standard.)

fused to a 6x histidine-tag, purified by Ni-NTA affinity chromatography using imidazole in the elution buffer.

Since SKAP55 is unstable in the absence of ADAP [61], insect cell (Sf9) expression system was used to co-express ADAP and SKAP55 proteins using pFastBacDual vector. ADAP/SKAP55 proteins form a complex while co-expressing. Subsequently, the complex was purified through the Strep-tag affinity purification using 5mM desthiobiotin or 50mM biotin in the elution buffer. All the proteins after affinity purification were re-purified by size exclusion chromatography on a superdex_200 column in a final buffer containing 20mM Hepes and 50mM NaCl of pH 7.5 and their purity was confirmed by SDS-PAGE **(Fig. 3.1)**. ADAP has molecular weight of 86.1 kDa but it runs on SDS PAGE at ~120kDa, while molecular weight of SKAP55 is 41 kDa and it runs on SDS PAGE at ~55kDa. ADAP and SKAP55 proteins as part of the complex are speculated to make a dimer of heterodimer as the complex runs at 250kDa on a non-reducing/native gel **(Fig. 3.1)**. The proteins obtained were then used in the *in vitro* polymerization assay.

3.1.2 ADAP polymerizes actin *in vitro*

The ability of ADAP to nucleate and polymerize actin was probed by using the recombinantly expressed ADAP full-length as well as stable ADAP/SKAP55 complex, which is a predominant form of ADAP in T cells **(Fig. 3.1)**. Different concentration of these proteins was mixed with pyrene-labeled actin and change in fluorescence intensity was measured over time in an *in vitro* actin polymerization assay **(see methods section 2.2.5 for details)**.

At first, the protein buffer (the buffer in which the proteins were purified and stored at the end of size exclusion purification) was added to the pyrene-actin to rule out the possibility that actin polymerizes in buffer alone. As expected, the protein buffer did not lead to any change in fluorescence intensity **(black curve in Fig. 3.2 a, b)**. On the other hand, ADAP/SKAP55 complex as well as ADAP in the absence of SKAP55 were observed to induce rapid polymerization in a dose dependent manner without the addition of any other protein **(Fig. 3.2a, b)**. These results indicate that ADAP acts as a facilitator of actin polymerization. Stoichiometric amounts of ADAP or ADAP/SKAP55 complex were sufficient to achieve full polymerization of G-actin.

The polymerization rate of ADAP/SKAP55 complex appeared to be faster than that of ADAP alone, which is also inferred from the calculation of T-half values for these proteins

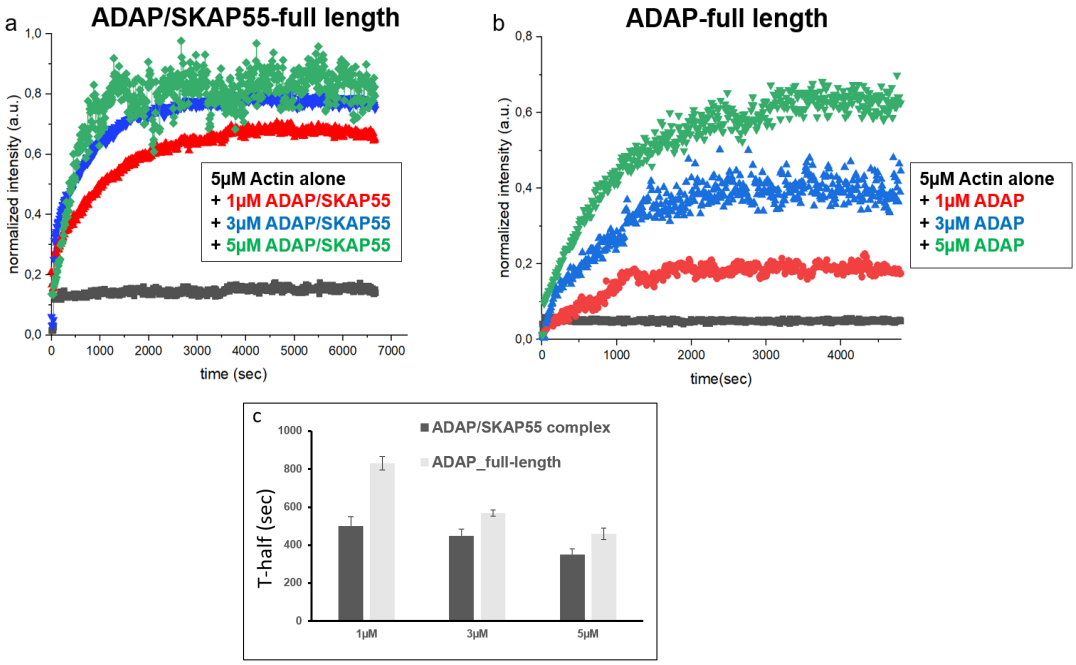

Fig. 3.2: *In vitro* actin polymerization by ADAP and ADAP/SKAP55 complex. Polymerization curves representing the change in fluorescence intensity of pyrene actin with respect to time (measured at an interval of 10 seconds), at different concentrations (1μM, 3μM and 5μM) of (a) ADAP/SKAP55 complex (b) ADAP-full length. (c) Time to half maximal polymerization (T-half) is calculated and plotted for ADAP/SKAP55 (dark grey) and ADAP-full length (light grey) for three different concentrations.

at three different concentrations **(Fig. 3.2c)**. This suggested that a further investigation is required into the role of SKAP55 and its contribution to actin polymerization activity. As SKAP55 is instable in the absence of ADAP, SKAP55 alone cannot be used in the assay. But it is known that SKAP55 is stabilized by the interaction of its SH3 domain with the proline-rich region of ADAP [79], therefore an artificial construct was created containing

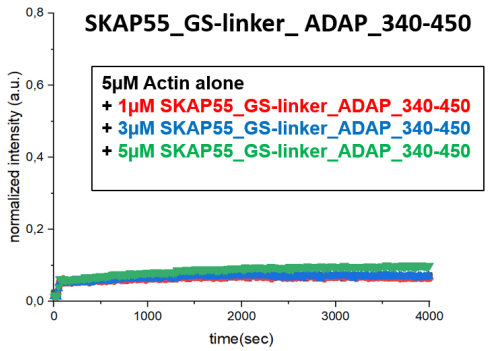

Fig. 3.3: SKAP55-ADAP_340-450 is inactive on polymerization in vitro. Polymerization curves representing the change in fluorescence intensity of pyrene actin with respect to time (measured at an interval of 10 seconds), at different concentrations (1μM, 3μM and 5μM) of SKAP55_GS-linker_ADAP_340-450.

SKAP55 linked to ADAP_340-450 (proline rich region) through a glycine-serine linker of 11 amino acids. This construct was expressed in bacterial expression system under T7 promoter, purified in a similar way as ADAP-full length and the proper composition of the complex was confirmed by LC-MS. The different concentrations of protein were tested in the *in vitro* polymerization assay **(Fig. 3.3)**. Interestingly, SKAP55/ADAP_340-450 seemed to be inactive on polymerization even when a 1:1 ratio of pyrene-actin and SKAP55 was used.

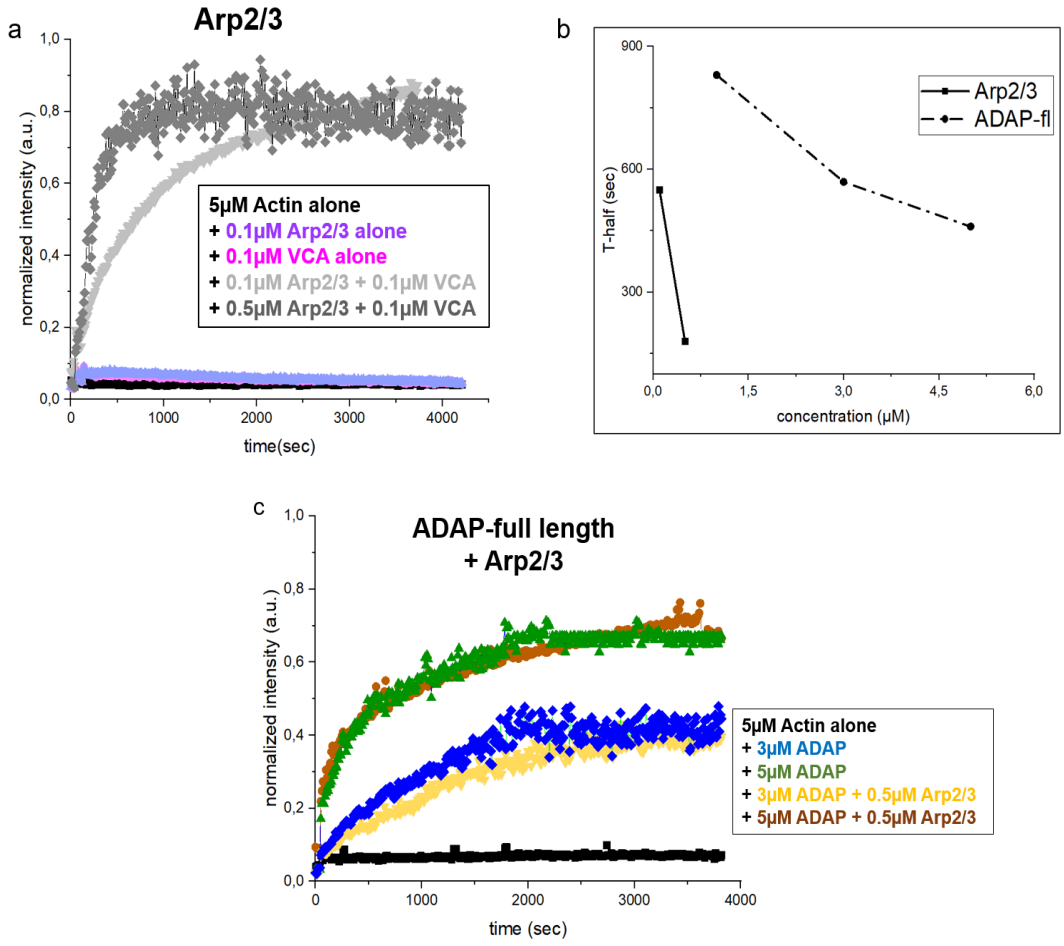

Fig. 3.4: ADAP and Arp2/3 proteins do not interact and polymerize actin at different rates. (a) 0.1µM and 0.5µM Arp2/3 complex in combination with 0.1µM of VCA were added to pyrene-actin. 0.1 µM VCA and 0.1µM Arp2/3 were used as controls to check their ability to polymerize actin in the absence of each other. (b) The time to half maximal polymerization was calculated for ADAP and Arp2/3 proteins based on the polymerization curves of the two proteins (Fig. 3.4a and 3.2b). (c) 3µM and 5µM of ADAP with and without 0.5µM Arp2/3 proteins were added to 5µM pyrene actin and change in fluorescence was measured with time.

Interestingly, ADAP has no sequence homology to any of the already known regulators of actin polymerization. Considering that Arp2/3 has already been shown as a *de novo* actin nucleator factor [126, 136, 139], so Arp2/3 was used in the *in vitro* polymerization assay to compare the activity levels of the two proteins **(Fig. 3.4a)**. The time to half maximal

polymerization ($T_{1/2}$) was calculated (as described in *Doolittle et.al. 2013 [162]*), which suggests that these two proteins polymerize actin at significantly different rates and that filament formation is 20-50 times faster in the presence of Arp2/3 complex when compared to ADAP-full length **(Fig. 3.4b)**. It was further checked if Arp2/3 is a regulator of ADAP-induced polymerization. No change in polymerization activity of ADAP was observed upon addition of Arp2/3 proteins in the *in vitro* polymerization assay **(Fig. 3.4c)**. The presence of Arp2/3 proteins neither suppresses nor stimulates the activity of ADAP. This indicates that there is no functional impact of Arp2/3 on polymerization activity of ADAP.

The results presented in this section establish that both ADAP and ADAP/SKAP55 are able to polymerize actin *in vitro*, while SKAP55 is inactive on its own but helps in enhancing ADAP's polymerizing activity. It was also found that ADAP and Arp2/3 proteins do not interact with each other and polymerize actin at different rates.

3.1.3 Effect of tyrosine phosphorylation on actin polymerization activity of ADAP

ADAP contains multiple tyrosine residues which become phosphorylated upon TCR or chemokine receptor stimulation in cells [90, 91]. Therefore, the impact of tyrosine phosphorylation on polymerization activity of ADAP was investigated next. The protein was phosphorylated *in vitro* by recombinantly expressed Fyn kinase **(as described in methods section 2.2.7)** at room temperature for 2 days and the phosphorylation efficiency was confirmed by mass spectrometry by analyzing the tyrosine residue at position 571 (Y571), since it has been identified as a major phosphorylation site on ADAP in activated T cells [90, 91]. A phosphorylation efficiency greater than 70% at Y571 indicates that all other tyrosine sites (Y595, Y625, Y651, Y771 and Y780) are phosphorylated, as also reported by *Kuropka et.al.* in 2015 [91]. Different concentrations of phosphorylated and unphosphorylated ADAP (incubated in the same way but without Fyn kinase) were added to pyrene-actin. However, no influence of tyrosine phosphorylation was seen on polymerization activity of ADAP. **(Appendix figure 2)**

3.1.4 Molecular dissection of N-terminus of ADAP

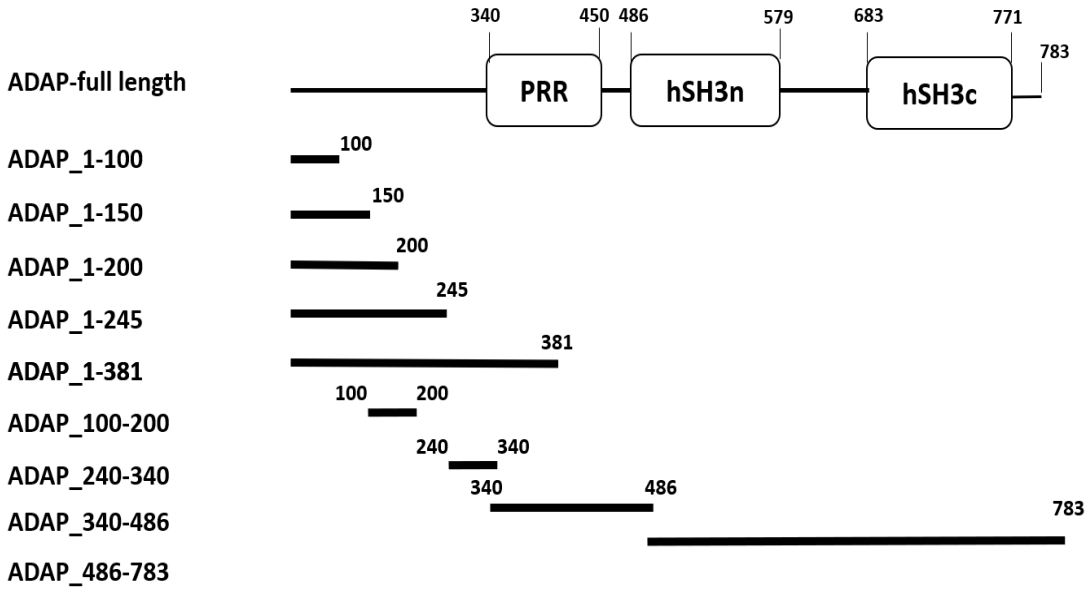

Fig. 3.5: Various fragments of ADAP generated to narrow down the region responsible for the polymerization activity. All the fragments were cloned in pET28a vector with an N-terminal His-tag and expressed in bacterial cell expression system. The over-expressed proteins were then purified by affinity tag purification and re-purified by size exclusion chromatography.

Subsequently, to narrow down the region in ADAP crucial for polymerization activity, ADAP was dissected into smaller fragments **(Fig. 3.5)** and their ability to polymerize actin was checked individually. All these fragments were cloned into pET28a vector containing an N-terminal 6xHis-tag and then expressed and purified as described in **section 3.1**. An N-terminal fragment of ADAP covering the first 381 amino acids of the protein (ADAP_1-381) showed a level of actin polymerization which is comparable to ADAP-full length while an ADAP_1-245 construct maintained only partial activity **(Fig. 3.6a)**. On the other hand, no polymerization was observed either for ADAP constructs consisting of the C-terminal fragment (ADAP_486-783) or for constructs comprising the SKAP binding region (ADAP_340-486 and ADAP_340-579) even when a 5:1 stoichiometry of ADAP to actin proteins was used in the assay **(Fig. 3.6a and appendix figure 3)**. Following a similar pattern, protein fragments containing only 100 residues like ADAP_1-100, ADAP_100-200, and ADAP_240-340 **(Fig. 3.6a and appendix figure3)** were unable to catalyze actin polymerization, indicating a length dependency.

These results suggest that the N-terminus of ADAP_1-381 is crucial for polymerization activity and that the first 150 residues represent the minimal fragment required for polymerization. Subsequent constructs were designed to check the activity of the C-

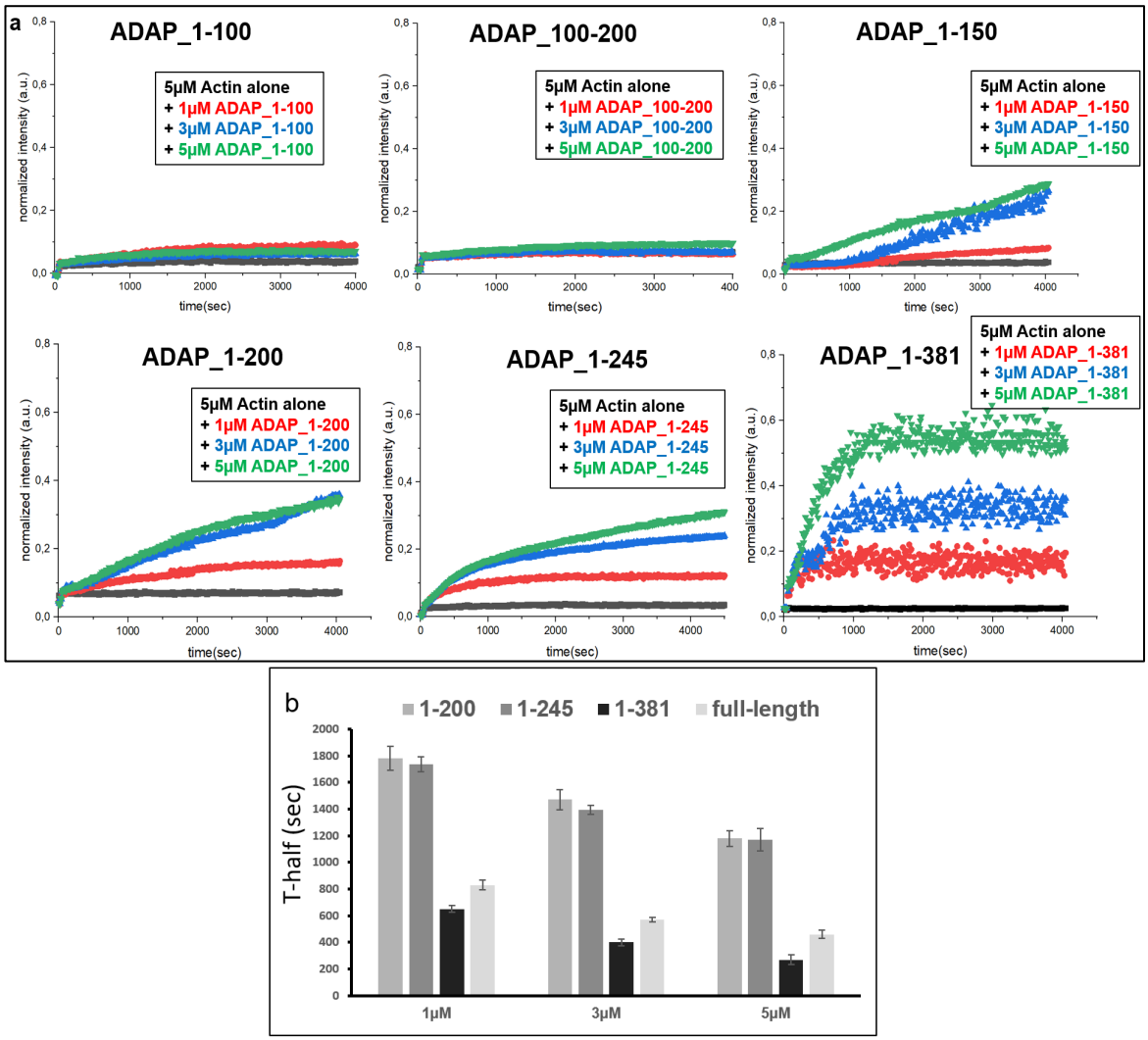

Fig. 3.6: The N-terminus ADAP_1-381 is responsible for polymerization activity in ADAP. (a) Different ADAP fragments (shown in Fig 3.5) were checked for polymerization activity. The N-terminal fragments 1-100, 100-200 of ADAP do not induce actin polymerization. At equimolar concentrations (5μM), the shorter fragments like 1-150, 1-200 and 1-245 show weak activity as compared to ADAP_1-381. (b) T-half is calculated and plotted for ADAP_1-200, 1-245, 1-381 and ADAP-full length. The T-half of ADAP-full length and ADAP_1-381 is observed to be very similar which implies that the polymerization activity comes from the N-terminus of ADAP. (Pyrene actin concentration 5μM was kept constant in all the samples, change in fluorescence intensity was measured on TECAN plate reader at an interval of 10sec, at excitation wavelength 385nm and emission 410nm).

terminus of ADAP_1-381 **(Fig. 3.7a)**. ADAP_150-381, 200-381 and 240-381 showed no to very little activity when added to pyrene-actin **(Fig. 3.7b)**. This directly implied that the

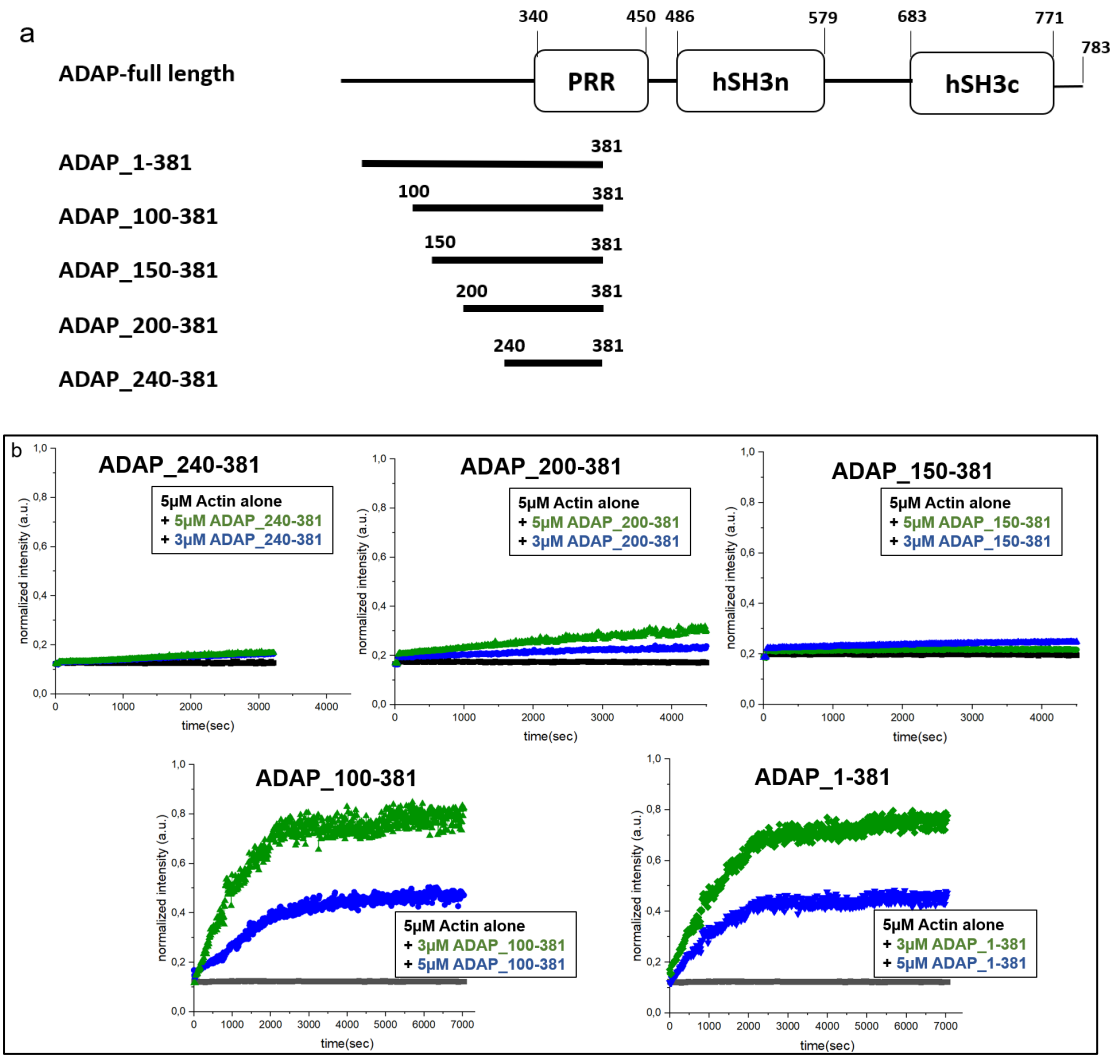

Fig. 3.7: The N-terminus of ADAP_1-381 is crucial for polymerization activity but not the first 100 residues. (a) Dissection of ADAP_1-381 into smaller fragments. (b) 3μM and 5μM of all the fragments were added to 5μM pyrene-actin and followed for intensity change. 240-381 and 150-381 showed no activity in polymerization. Activity of 200-381 on polymerization was very little when compared to 150-381. 100-381 fragment exhibited same polymerization activity as 1-381.

extreme N-terminus of ADAP is crucial for initializing the polymerization process. However, ADAP_100-381 was found to be as active as ADAP_1-381, suggesting that the first 100 amino acids are not sufficient on their own for polymerization activity **(Fig. 3.7b)**.

3.1.5 No individual motifs in ADAP_1-381 account for polymerization activity

The 381 N-terminal residues of ADAP are predicted to be intrinsically disordered **(appendix figure 4)** and include several abundant proline, lysine and leucine containing motifs such as LKP or PKP. A few of these motifs were removed at a time to identify a potent region or a patch of 20-30 residues responsible for the polymerization effect of ADAP. A series of mutants, each containing 20-30 amino acid deletions along the sequence of the first 381 amino acids of ADAP did not reveal any individual site to compromise the polymerizing activity of ADAP. The impact of each deletion was checked in multiple replicates with three independent repetitions and further compared to the activity of 1-381 wild-type protein. Surprisingly, all the individual mutants showed activity and fluorescence-intensity increase when used in *in vitro* polymerization assay as shown in **(Fig 3.9a)**.

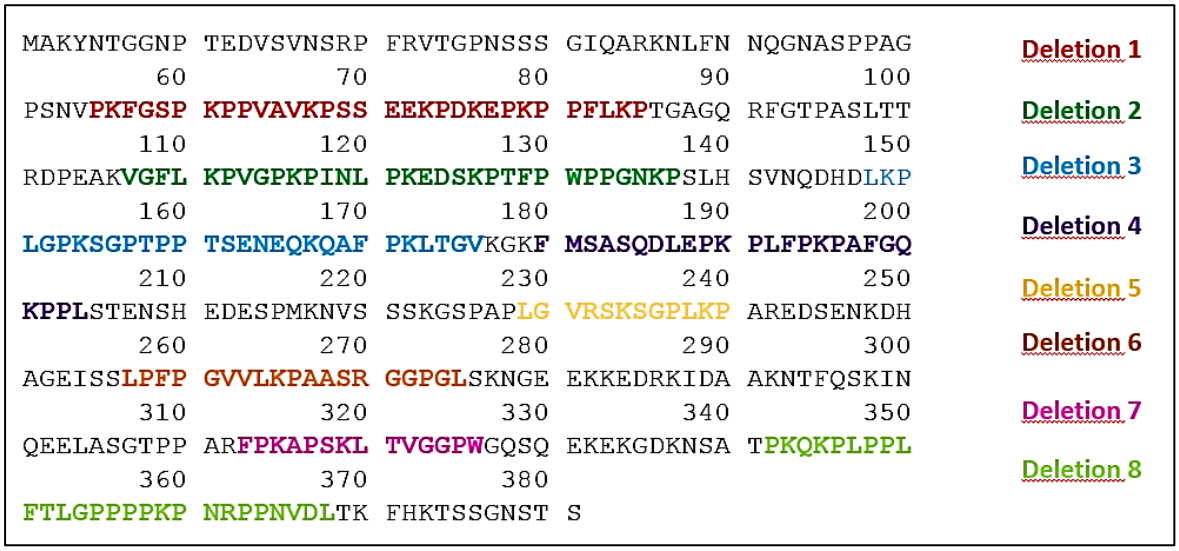

Fig. 3.8: Deletion mutants created in the sequence of ADAP_1-381. Series of deletion mutants named 1-8 with 20-30 residues deleted in ADAP_1-381 sequence.

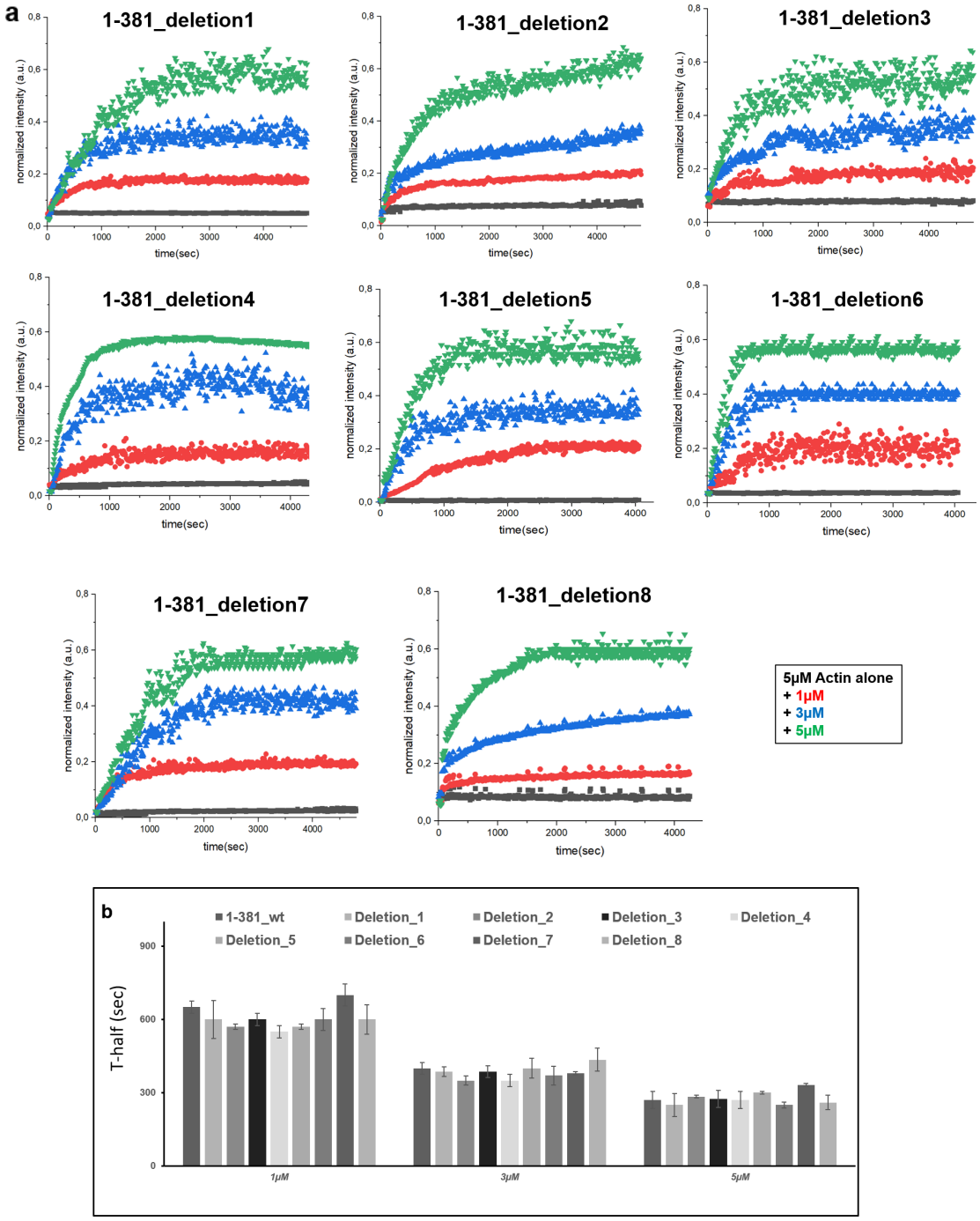

Fig. 3.9: All deletion mutants are as active as ADAP_1-381 wild-type on polymerization. (a) The impact of each deletion was checked in multiple replicates with three independent repetitions and further compared to the activity of 1-381 wild-type protein. All the deletion constructs showed activity and fluorescence increase when used in *in vitro* polymerization assay. (b) The analyzed T-half of polymerization effect of all eight deletions was similar to the wild-type protein, which indicated that none of the analyzed sets of amino acids in 1-381 alone is responsible for this activity.

The analyzed half-time of polymerization for all eight deletions was similar to the wild-type protein **(shown in Fig. 3.9b)**, which indicates that there is likely no single linear motif in the ADAP_1-381 sequence responsible for this activity.

These results show that there is indeed a composite effect of the N-terminal region that confers actin polymerization promoting properties and no individual motifs can be defined that are required for activity.

3.2 ADAP induces bundling of the actin filaments *in vitro*

Interestingly, a visible precipitation of actin was also observed in *in vitro* which was induced by the ADAP fragments that were able to polymerize G-actin. The proteins such as α-actinin and fascine [151] in the cell are specialized and known only for the purpose of organizing individual actin filaments into long and dense bundles, a process termed as actin bundling. However some proteins can polymerize actin as well as induce bundling (for example Formin I in plants [137]). This was the motivation to investigate the actin bundling properties of ADAP using low speed *in vitro* co-sedimentation assay. The latter consisted of mixing the pre-polymerized filamentous actin (F-actin) with ADAP-full length or different fragments of ADAP, then centrifuging them at 12,000g for 30 mins followed by SDS-PAGE. This assay is based on the concept that if a protein shows bundling activity, the protein and F-actin co-sediment in the pellet to a certain extent when centrifuged at low speed **(section 2.2.6)**.

Pre-polymerized filamentous actin (F-actin) alone does not sediment on its own into the pellet and addition of BSA should have no effect on this. Results for these two negative controls after the centrifugation are shown in **Fig. 3.10**, where SDS-PAGE was performed for supernatant and pelleted material. A faint band in the pellet indicates a small degree of self-association of actin **(Fig. 3.10)**. F-actin in the presence of α-actinin (a known actin-bundling protein [149]) was used as a positive control. Expectedly, F- actin could be observed as a thick and intense band on SDS PAGE which is in line with literature **(Fig. 3.10)**. To our observation actin was also found to be co-precipitated by ADAP full-length as well as N-terminal fragments ADAP_1-381 and 1-245, which indicated formation of actin bundles **(Fig. 3.10)**. The bundling activity of ADAP was comparable to α-actinin **(the bar diagram in Fig. 3.10)**. The fact that ADAP_1-100 was not able to bundle actin suggests again that the first 100 amino acids are not sufficient on their own or that residues 100-245 contain motifs essential for bundling actin. Similar to the polymerization assay, the C-terminus of ADAP (residues 486-783) was unable to bundle actin. The bundling ability also indicates the direct binding of ADAP to filamentous actin. In summary, ADAP full length and the N-terminal fragments of ADAP (1-381, 1-245) not only polymerize actin but also bundle filamentous actin.

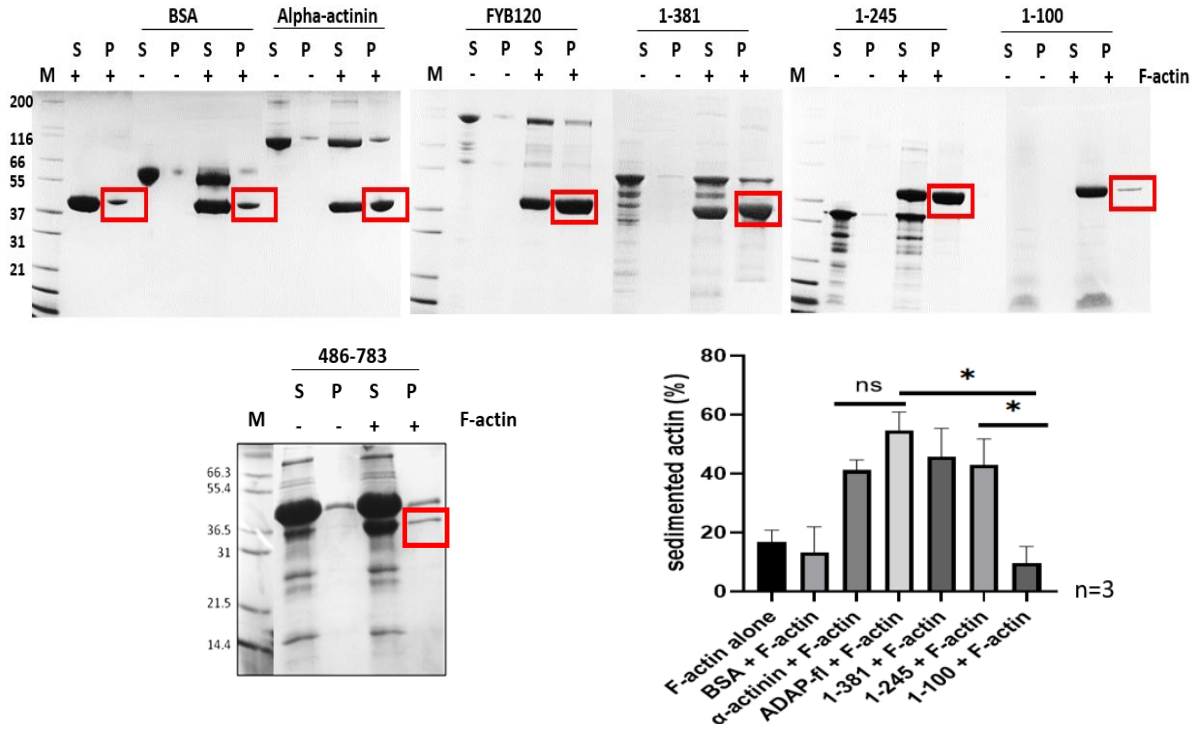

Fig. 3.10: Low speed actin co-sedimentation assay (also called actin bundling assay) confirms that ADAP-full length and ADAP_1-381 can bundle actin. F-actin was mixed with protein and centrifuged at low speed for 30mins at room temperature. The supernatant and the resuspended pellet were analyzed on SDS PAGE. Similar to the positive control (α-actinin), ADAP-full length and the N-terminal ADAP-fragments (1-245, 1-381) show increased bundling of filamentous actin (F-actin) as compared to the negative controls (BSA or F-actin alone). The C-terminus of ADAP (486-783) showed no bundling activity. Plot showing the percentage of sedimented filamentous actin as judged from SDS-PAGE band intensity from the co-sedimentation assay. (SDS-PAGE 4-20%, 200 Volts, 40 minutes, M: Marker (Mark 12) Unstained Standard, S: Supernatant, P: Pellet, F-actin: filamentous actin).

3.3 Distinct bundles formed by ADAP/SKAP55 and ADAP

The actin filament formation and bundling by ADAP/SKAP55, ADAP-full length and ADAP_1-381 were further confirmed by electron microscopy in collaboration with Dr. Tarek Hilal (from research center of electron microscopy at FU Berlin). The grids for negative stain were prepared with monomeric actin mixed with either ADAP/SKAP55, ADAP-full length, ADAP1-381 or actin polymerizing buffer and measured at a transmission electron microscope at 120 kV **(see section 2.2.11)**. The topology of actin in the presence of ADAP/SKAP55, ADAP-full length and ADAP1-381 revealed distinct types of bundles, while no bundles were observed in case that filaments were formed by actin polymerizing buffer **(appendix figure 5)**. For ADAP/SKAP55 complex in the presence of monomeric actin, long

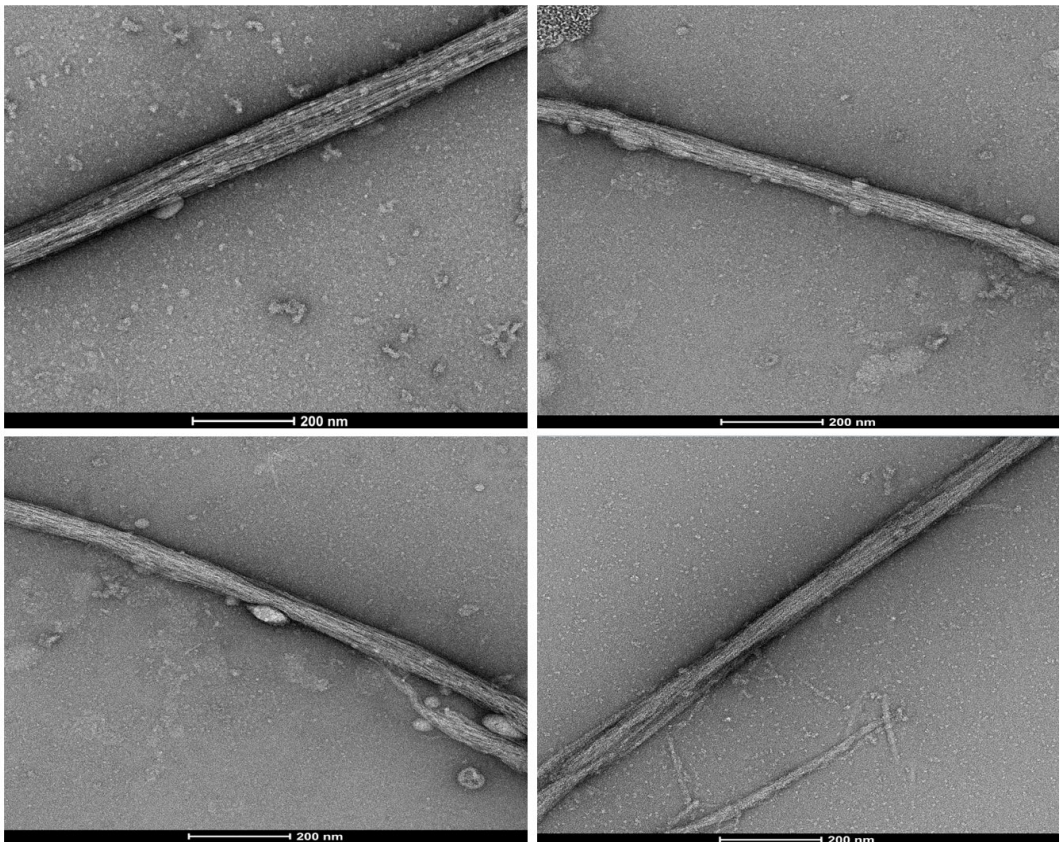

Fig. 3.11: Negative stain EM of actin filaments and bundles formed by ADAP/SKAP55 complex. ADAP/SKAP55 complex with actin showing long and linear filaments in uniformly shaped bundles along with some circular shaped structures in-between the filaments.

filaments were observed which formed thick and ordered bundles of a length of several hundred nanometers **(Fig. 3.11)**. However, the actin bundles formed by ADAP-full length and the N-terminal ADAP_1-381 looked very different from the bundles formed by ADAP/SKAP55 complex **(Fig.3.11, 3.12 a and b)**. Actin filaments and bundles formed by ADAP-full length in the absence of SKAP55 were loose, non-uniform and did not show a well-defined pattern **(Fig. 3.12a)**. This feature was exacerbated in the case of ADAP_1-381, with actin fibers forming dense and more irregular polymers **(Fig. 3.12b)**. This suggests that the intrinsic polymerizing activity as well as the ability to cross-linking actin filaments of the N-terminus of ADAP become more constrained in the presence of the cognate ADAP/SKAP55 complex, which is a large module consisting of several folded domains, such as hSH3, SH3 and PH domains.

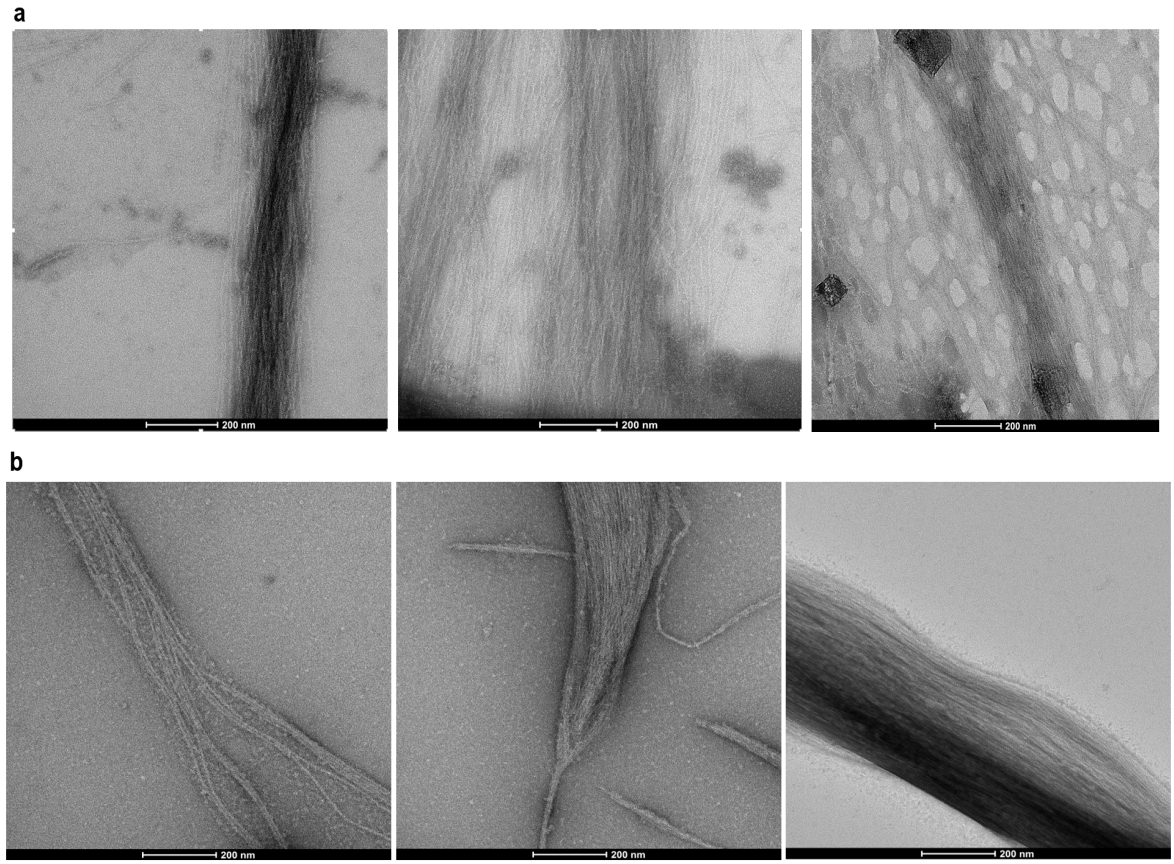

Fig. 3.12: Negative stain EM pictures of actin filaments and bundles formed by ADAP-full length and ADAP_1-381. (a) actin bundles formed by ADAP-full length containing loosely packed filaments. (b) non-uniform highly dense actin bundles formed by ADAP_1-381.

For ADAP_1-381 in presence of actin, some sort of protein islands or phase separated structures were observed surrounding the actin filaments **(as seen in Fig. 3.13)**. This phenomenon was not observed in case of ADAP/SKAP55 complex or ADAP-full length.

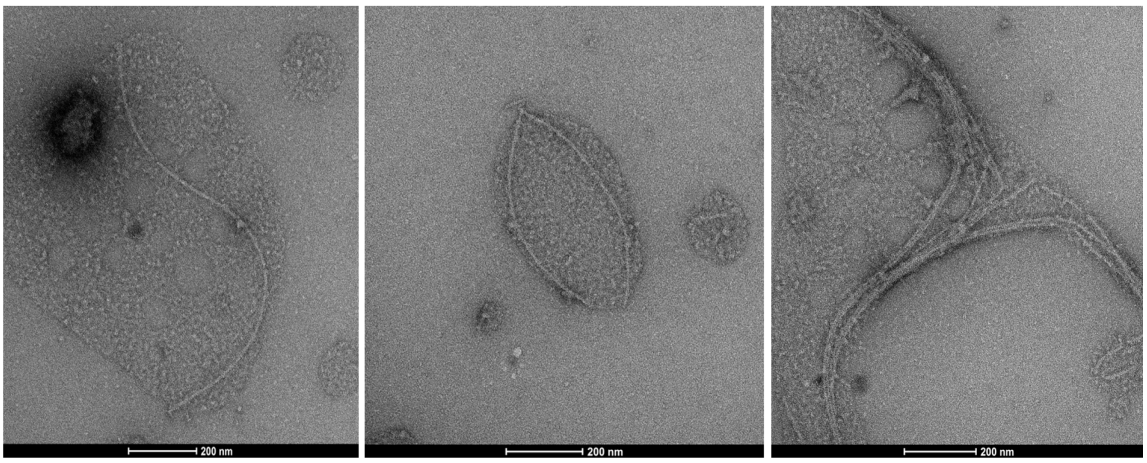

Fig. 3.13: Negative stain EM pictures of ADAP_1-381 forming co-separated structures with actin to form filaments.

Thus, the ADAP N-terminus might act to concentrate actin in a manner that facilitates polymerization as well as bundling.

3.4 Polymerization activity of ADAP in the presence of profilin

Profilin is an actin-monomer-binding protein and an actin-elongator which plays an important role in actin re-organization in cells. It binds to ADP-actin and catalyzes the nucleotide exchange (replaces ADP with ATP) as well as adds ATP-actin to the barbed end of the filament via its binding to proline rich sequences present on the elongating factors like Ena/VASP or formin proteins [126] [143] **(Fig. 3.14)**. The effect of profilin on the polymerizing activity of ADAP was probed by mixing 5µM profilin with different concentrations of ADAP. It was observed that addition of equimolar profilin to pyrene-actin in the absence of ADAP did not show any fluorescence change. This verified that profilin cannot nucleate actin and also confirmed that there are no actin seeds or nucleus already present in the stock solution, and the actin used in the assay is monomeric, otherwise an increase in fluorescence would be seen with time **(pink curve in Fig 3.15b)**.

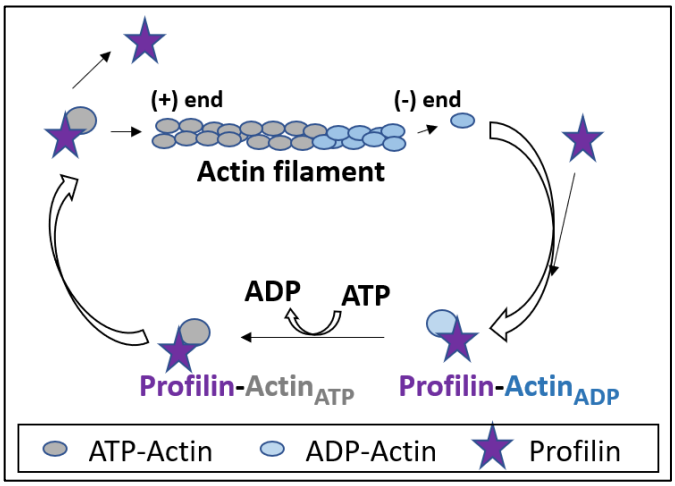

Fig. 3.14: Cartoon representation of profilin binding to actin, ADP replacement to ATP and addition of ATP-actin to the barbed end of the filament by profilin.

No significant change in the polymerizing activity of ADAP was observed when mixed with equimolar concentrations of profilin **(green curve in Fig. 3.15a and b)**, however the lower concentration of ADAP showed better activity in the presence of profilin by not attaining an early saturation and continued fluorescence increase to the end **(blue curve in Fig. 3.15a and b)**. The reason for this observation could be that ADAP nucleated filaments have free barbed ends and profilin elongates filaments by adding actin to that end, indicated by the constant increase in fluorescence until all monomeric actin is incorporated into filaments. To investigate this further, another protein was used, which acts on the barbed end, as described in the following section **(section 3.5)**.

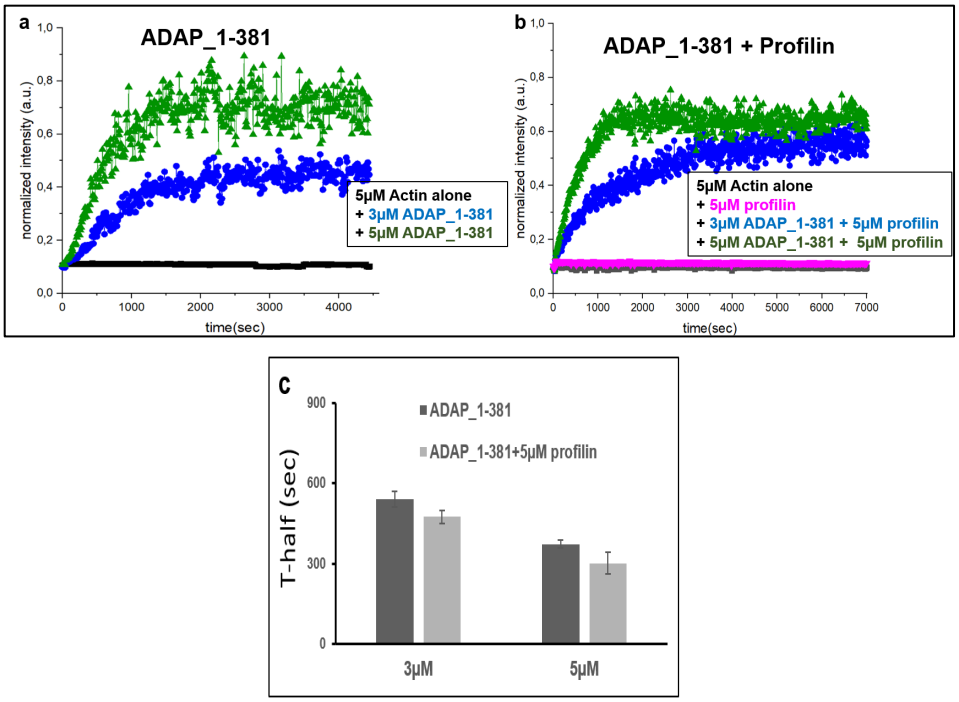

Fig. 3.15: Profilin improves the polymerization activity of ADAP. (a) Polymerization by two different concentrations (3µM and 5µM) of ADAP_1-381 in the absence of profilin. (b) The effect of profilin on actin polymerization activity of ADAP was checked by adding 5µM profilin either alone or in combination with 3µM and 5µM ADAP. (c) The half-time to maximum polymerization (T-half) was calculated for ADAP_1-381 with and without profilin and plotted for different concentrations. (5µM pyrene actin concentration was used and kept constant in all the samples, measured on TECAN plate reader using excitation at 385nm and emission at 410±10nm).

3.5 Effect of barbed end capping protein on the polymerizing activity of ADAP

As described in **section 1.8**, actin filaments consist of two ends, a fast-growing barbed end (or plus end) and a slow growing pointed end (or minus end) **(Fig. 3.14 and 1.7)**. There are proteins which polymerize actin through either end of the filament [126]. To figure out if ADAP polymerizes actin through barbed end or pointed end, a capping protein 'CapZ' was used in the *in vitro* polymerization assay. CapZ is a factor that binds to and caps the fast-growing plus end of the actin filament thereby preventing the addition or loss of actin at the barbed end of the filament [126, 174]. Thus, if ADAP polymerizes actin from the barbed end, then in the presence of CapZ the fluorescence intensity should not increase with time. On the other hand, if ADAP binds and polymerizes through the pointed end then there should be no inhibition of polymerization in the presence of CapZ.

At first, I checked if CapZ alone has the ability to polymerize actin. No change in fluorescence intensity upon adding CapZ to pyrene actin was seen **(pink curve in Fig. 3.16b)**. This confirmed that CapZ is inactive in polymerizing actin on its own.

In the next step, CapZ was added to ADAP along with pyrene-actin and an instant polymerization was observed which was clearly faster than ADAP in the absence of CapZ **(Fig 3.16a and b)**. This outcome established that ADAP polymerizes through the pointed

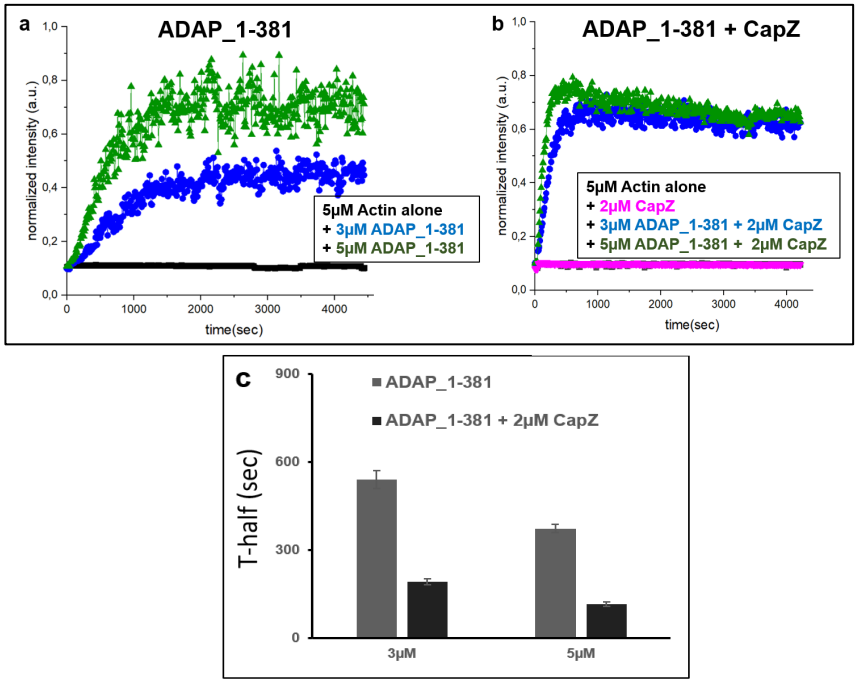

Fig. 3.16: ADAP polymerizes through the pointed end. (a) 3µM and 5µM of ADAP1-381 were added to pyrene actin and change in fluorescence was measured with time at an interval of 10 seconds. (b) 2µM of CapZ was added to different concentrations (3µM and 5µM) of ADAP. (c) The half-time to maximum polymerization was calculated for ADAP_1-381 with and without CapZ and plotted for different concentrations of ADAP. (5µM pyrene actin concentration was used in all the samples, measured on TECAN plate reader using excitation at 385nm and emission at 410nm).

end as the barbed end is blocked by CapZ in this case. The initial polymerization rate also seemed to be enhanced by approximately 10-20 times in the presence of CapZ, which might be due to the stabilization of actin seeds or intermediate filaments by capping protein **(Fig 3.16c)**.

These results show that actin binding proteins like profilin and CapZ, both have a positive impact on the polymerization activity of ADAP and since both the proteins are known to act on the barbed end of the actin filament, it is a reasonable indication that ADAP polymerizes actin through the pointed end of the filament.

3.6 Insights into ADAP-actin binding at molecular level by Nuclear Magnetic Resonance (NMR) spectroscopy

In order to probe the interaction between ADAP and actin at the molecular level, NMR spectroscopy was used which allowed to assign interacting epitopes for isotope labeled ADAP protein fragments. The isotope labelled ADAP proteins were expressed as described in methods **(section 2.2.3)**. The human β-actin used in the NMR experiments was recombinantly expressed using Sf9 insect cells (by following the approach mentioned in Ref. [175]). The construct was kindly provided by Noritaka Nishida (AIST Japan).

3.6.1 Insect cell expression and purification of recombinant actin

The expression of actin bound to thymosin β-4 protein with a linker containing a chymotrypsin cleavage site between the two proteins of approximately 50kDa size, was verified on SDS-PAGE before harvesting the insect cells. Subsequently, cells were sonicated and the protein was purified as described in the methods section **(2.2.4)**. The IMAC purification always showed a thick expression band with only very little impurities **(Fig. 3.17a)** and yielded protein in the range of 10-20 mg per liter of insect culture.

After performing ion exchange chromatography, the fractions showing the right size of approximately 42kDa were collected and checked on SDS-PAGE **(Fig. 3.17b)**. The chromatogram showed multiple peaks indicating the combination of different protein species even though they were not distinguishable by SDS-PAGE. The polymerizable actin was then isolated using ultracentrifugation **(Fig 3.17c)**. The pelleted actin was resuspended and dialyzed in monomeric actin buffer (G-buffer) overnight and was then used for NMR experiments.

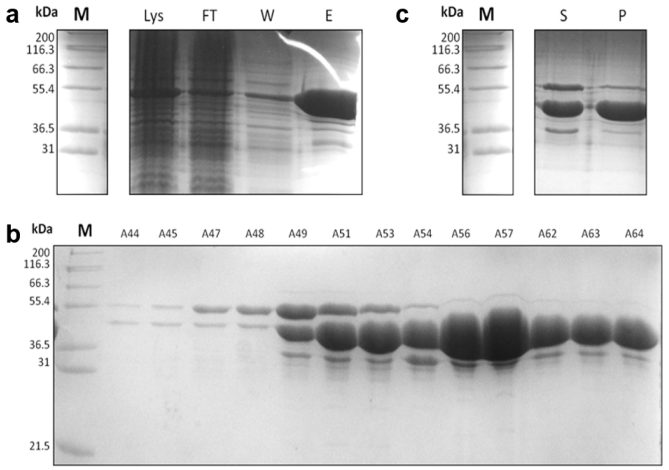

Fig. 3.17: The purification process of the human β-actin. (a) Immobilized metal ion affinity chromatography of the actin: Most of the protein visible in the lysate (Lys) could have been enriched in the elution (E). Small amounts of protein are found in the flow-through (FT) and Wash (W). (b) Ion exchange chromatography (Bio-Rad chromatography system, column: MonoQ GL 5/50, flowrate: 1 ml/min, linear NaCl gradient 0-0.5 M, fraction size: 0.33 ml) after digestion with chymotrypsin. The fractions A49-A64 were collected which contain intact actin with the expected size. Minor impurities due to unspecific digestion are visible in most of the fractions. (c) Ultracentrifugation (40 minutes, 80.000 g) of the actin sample after addition of actin polymerization buffer (F-buffer): With this purification step, all forms of actin that are not able to polymerize such as residual uncut or unspecifically cut actin are found in the supernatant (S), whereas polymerized actin is found in the Pellet (P). SDS-PAGE (15%, 250 Volts, 35 minutes, Marker: Mark 12 Unstained Standard):

3.6.2 hSH3 domains of ADAP do not interact with monomeric actin

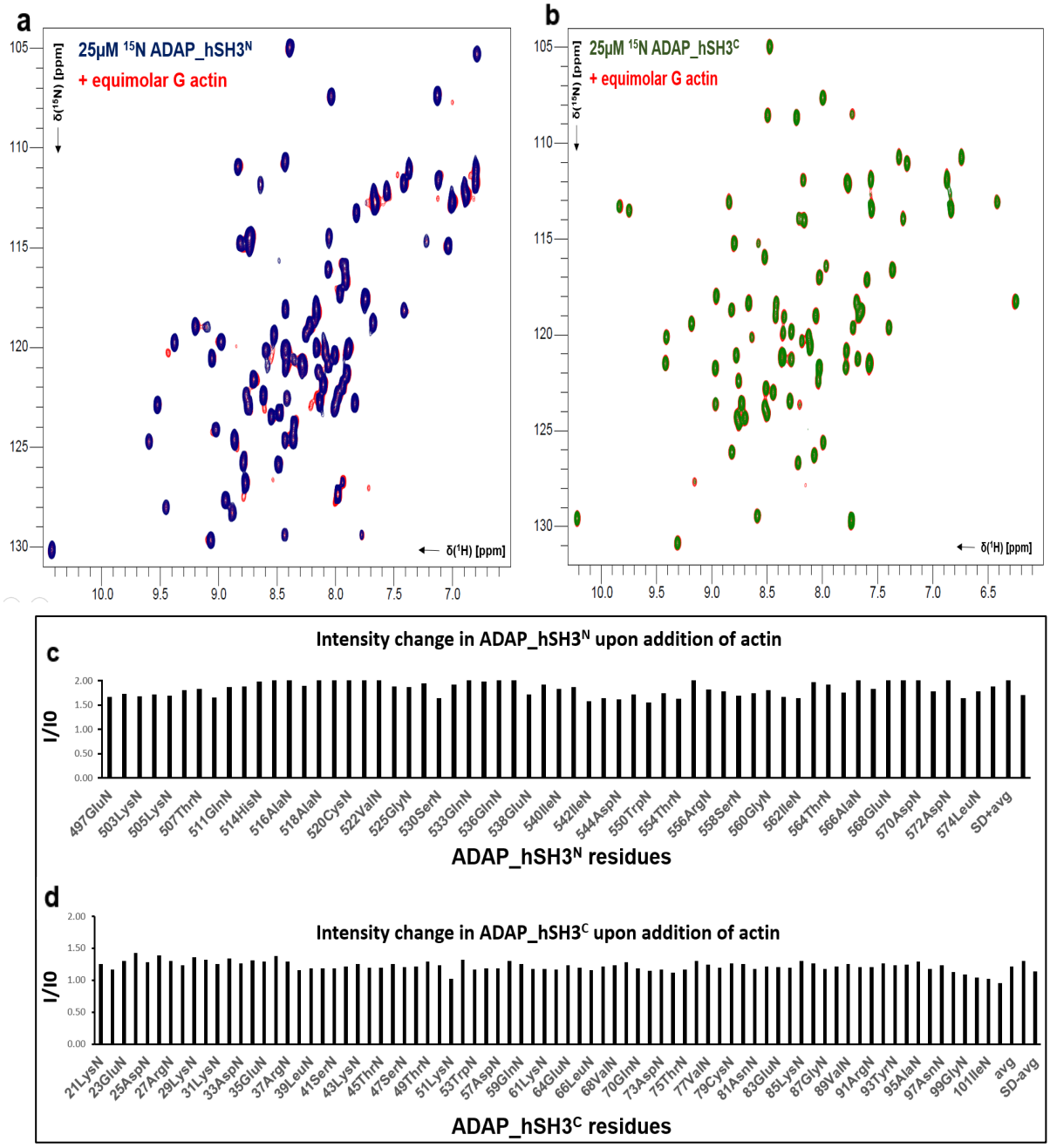

Fig. 3.18: The SH3 domains of ADAP do not interact with monomeric actin. Overlay of ^{15}N-HSQC spectrum of isolated (a) hSH3^{N} domain in the absence of actin (blue) and in presence of equimolar amounts of G-actin (red). (b) hSH3^{C} alone (green) and in presence of equimolar amounts of G-actin (red). (c-d) Peak intensity changes for (c) hSH3^{N} domain and (d) hSH3^{C} domain of ADAP upon addition of G-actin indicating no significant changes.

To begin with, ^{1}H-^{15}N-labeled ADAP_hSH3^{N} and ADAP_hSH3^{C} were measured as reference. In the next step, equimolar amounts of recombinantly expressed G-actin (monomeric form of actin) were mixed with ^{15}N-labeled ADAP_hSH3^{N} and hSH3^{C} and acquired ^{1}H-^{15}N-HSQC spectra were compared to the reference spectra **(Fig 3.18)**. The

spectra obtained upon addition of monomeric actin to domains did not show any clear changes in chemical shift or peak intensity **(Fig 3.18a-d)** which demonstrated that the folded domains of ADAP do not bind to G-actin. This result reconciles well with observations in **section 3.1.4 and 3.2,** showing that the C-terminus of ADAP is not involved in actin interaction, polymerization or bundling.

3.6.3 Interaction of intrinsically disordered region ADAP_1-381 with actin

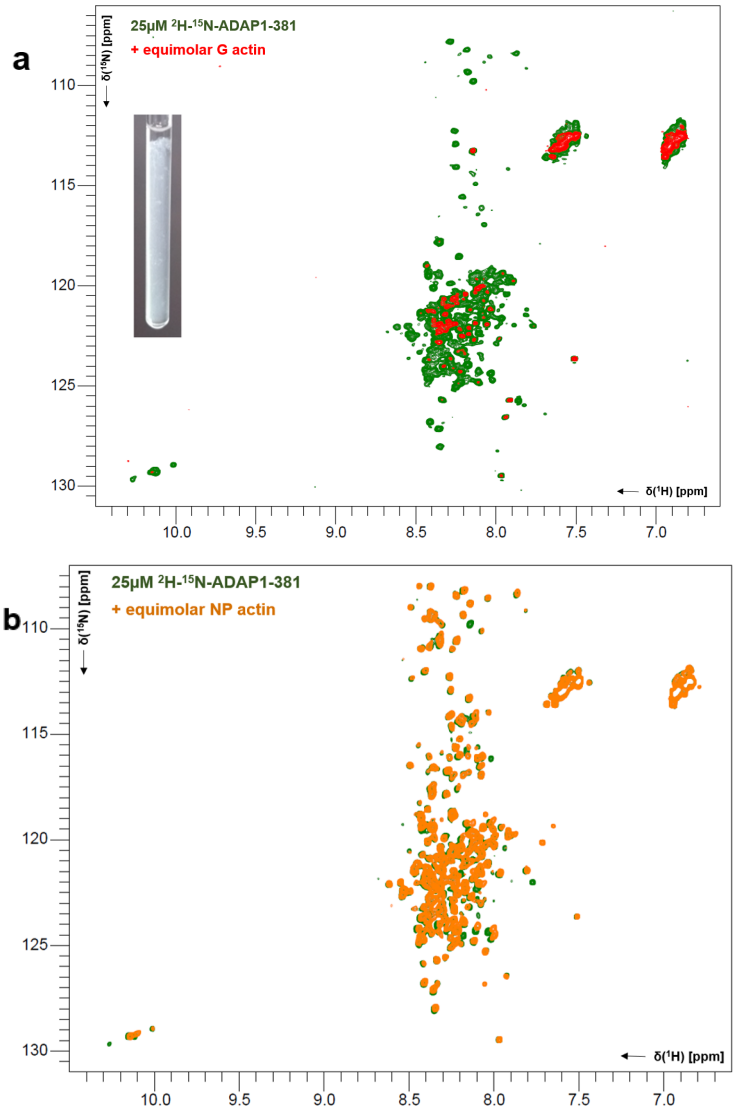

Fig. 3.19: The N-terminus of ADAP directly interacts with actin. (a) ^{1}H-^{15}N HSQC spectra of ADAP_1-381 (green) mixed with recombinantly expressed G-actin (red). The inset showing G-actin immediately turned turbid when mixed with ADAP_1-381 in the NMR tube. The line broadening and vanishing of peaks indicate strong binding with actin. b) ^{1}H-^{15}N HSQC ADAP_1-381 in the absence (green) and presence of non-polymerizing (NP) actin (orange).

To examine the role of the N-terminus of ADAP in actin binding, ADAP_1-381 was expressed in deuterated conditions to get a better spectrum, since it is predicted to be

unfolded using theoretical structure prediction sites such as PSIPRED [176, 177]. Similar to the previous measurement, in the first step a reference ^{1}H-^{15}N-HSQC spectrum of ^{2}H-^{15}N-labeled ADAP_1-381 was acquired. With its low chemical shift dispersion in the proton dimension, it displayed the hallmarks of an intrinsically disordered protein. Subsequently, equimolar amounts of recombinantly expressed G-actin were mixed with ^{2}H-^{15}N-labeled ADAP_1-381, inducing an immediate polymerization and bundling indicated by the visible turbidity observed in the NMR tube **(Fig. 3.19a, inset)**. The fingerprint HSQC-spectrum displayed severe line-broadening and loss of intensity for a subset of resonances when compared to the reference, which occurs in the case of larger protein assembly formation **(Fig. 3.19a)**. One possible explanation is that only certain regions of ADAP are dynamically immobilized by the interaction with bundled actin filaments. This result further supports the direct interaction between ADAP_1-381 and actin, however, it does not answer the question whether ADAP's N-terminus possesses the capacity to bind to G-actin in a bi- or multivalent manner which likely is a prerequisite to promote initial nucleation and filament formation. The unfolded N-terminus of ADAP might be responsible for providing the flexibility required for the formation of a dense but somewhat random network of filaments as seen in the EM images **(Fig. 3.12b)**.

The recombinantly expressed G-actin immediately polymerized and precipitated in the NMR tube in the presence of ADAP_1-381 resulting in the line-broadening beyond detection of most of the peaks. Considering this fact, a non-polymerizing monomeric actin (NP actin) which contains a cleavage in the loop critical for inter-monomer contacts in the filament, was used in the further experiments [132]. Mixing of equimolar amounts of NP actin to ADAP_1-381 did not result in any visible precipitation of actin or peak vanishing **(Fig. 3.19b)**. However, less severe but still significant line broadening and clear chemical shift changes were observed for several resonances for ADAP_1-381 in the bound state with monomeric actin. Since it is an unfolded region of ADAP and many peaks are concentrated to the centre and overlapped with each other, it was difficult to analyse the spectra and assign peaks.

To resolve this problem and further obtain sequence specific epitope information in the actin bound state, a divide-and-conquer approach was applied by using smaller ADAP fragments of 100 residues such as ADAP_1-100, ADAP_100-200 and ADAP_ 240-340 **(section 3.6.4)**. These 100 amino acid fragments were also tested in *in vitro* actin polymerization assays and were found to be inactive **(Fig. 3.5 and 3.6)**.

3.6.4 Motifs in ADAP_1-100 and 100-200 fragments interact with actin

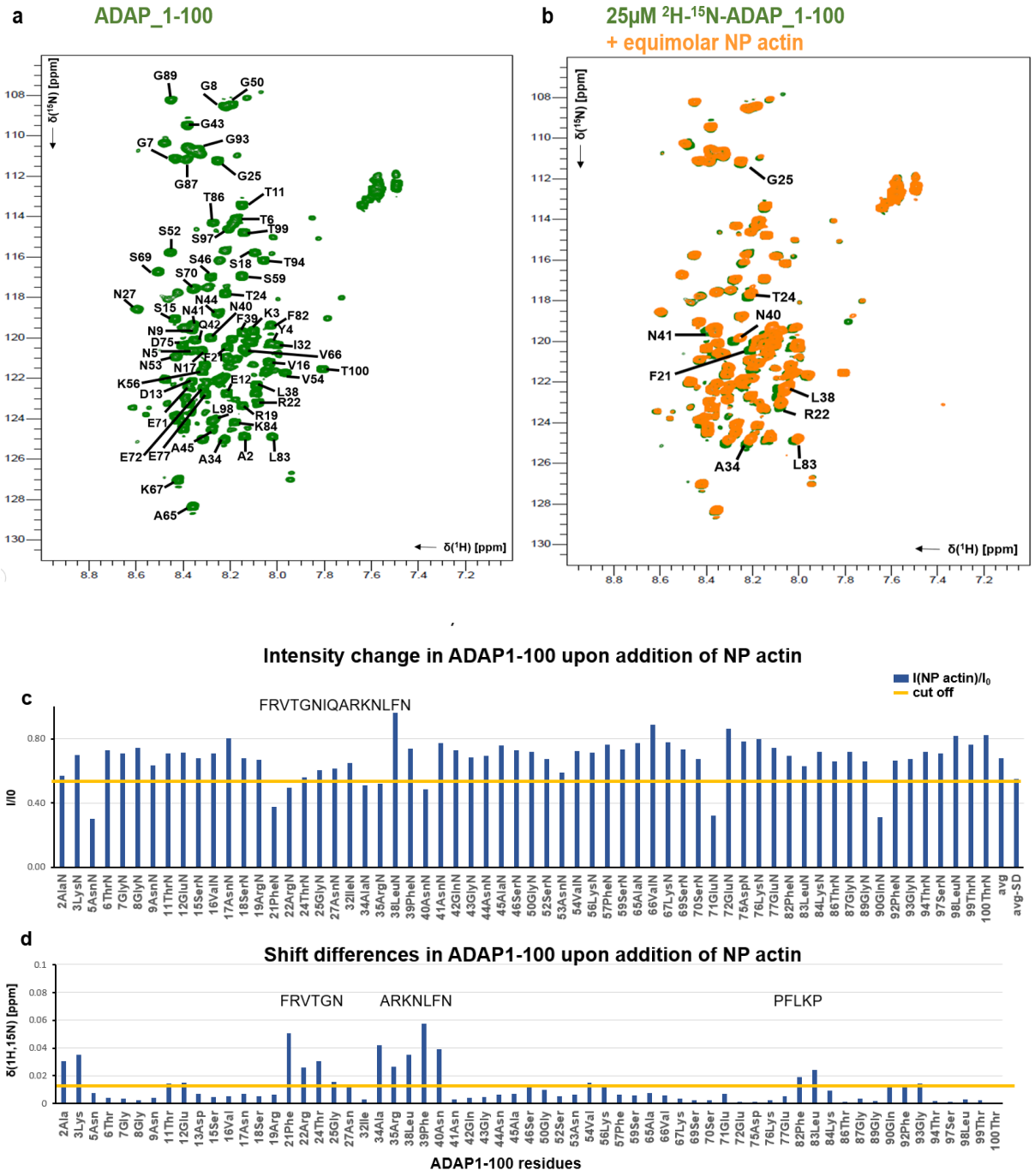

Fig. 3.20: ADAP_1-100 interacts with actin. (a) Backbone assignment of ^{13}C-^{15}N-ADAP_1-100 in 20mM Hepes, 50mM NaCl, 2mM DTT, pH 6.5, (b) Overlay of ^{1}H-^{15}N-ADAP_1-100 in the absence (in green) and in the presence of non-polymerizing actin (orange). Marked residues are clearly shifted in the presence of actin. (c) The graph shows the change in intensity in ADAP (I_0) upon addition of NP actin (I). (d) Chemical shift changes upon addition of NP actin plotted for ADAP_1-100 residues. Both the graphs indicate major changes in the regions of 21-40, 82-83 and 90-93. (The analyses of ADAP_1-100 spectra with and without actin was performed with ccpNMR_2.4).

Similar to ADAP_1-381, ^{1}H-^{15}N-labeled ADAP_1-100 and ^{2}H-^{15}N-labeled ADAP_100-200 in the absence and presence of non-polymerizable monomeric actin were recorded **(Fig. 3.20b and 3.21b)**. The spectra showed clear changes in the line width and chemical shifts, indicating direct interaction between the individual fragments and actin. To examine the interacting residues and define the motifs, HNCA, HN(CO)CA, HNCO, HN(CA)CO, HNCACB spectra were recorded at 300K for 500µM ^{13}C-^{15}N-labeled ADAP_1-100.

HNCA, HN(CO)CA, HNCO, HN(CA)CO, HNCACB, (H)N(CA)NH spectra were recorded at 300K and HNCA, HN(CO)CA, (H)N(CA)NH were recorded at 280K for 400µM ^{13}C-^{15}N-labeled ADAP_100-200. The backbone resonance assignments were carried out by Dr. Jana Sticht resulting in assignment of 85% of the non-proline residues of ADAP_1-100 and 75% of the non-proline residues of ADAP_100-200 using CcpNMR Analysis (version 2.4.2) **(Fig. 3.20a and Fig. 3.21a)**. These two fragments were chosen for the assignment as the major resonance changes were seen in these two fragments upon addition of non-polymerizable monomer actin, individually as well as in the context of ADAP_1-381 **(Fig. 3.19b, 3.20 and 3.23)**.

Further analysis of ADAP_1-100 revealed epitopes involved in actin interaction. A larger motif spanning the residues 21-40 and shorter motifs 82-83 and 90-93 appeared to be involved in the interaction with monomeric actin **(Fig. 3.20)**. When inspecting the binding of first 100 residues with actin in the context of ADAP_1-381 construct, it was found that similar interactions are maintained in the larger fragment **(Fig. 3.23)**. These results confirm a direct interaction of the N-terminus of ADAP with G-actin.

After assigning the backbone resonances for ADAP_100-200, the spectra in free state and in the presence of NP actin were analysed. Some defined regions clearly showed intensity changes and chemical shift differences. An epitope could be allocated in the region 110-118, since peak intensities were affected upon addition of non-polymerizable actin **(Fig. 3.21)**. It was also observed that several short motifs, both in ADAP_1-100 (such as 82-83) and ADAP_100-200 (131-139 and 148-149) displayed line broadening or chemical shift differences upon addition of NP actin, but these effects were restricted to few amino acids only. This might suggest additional transient interactions with actin by these sites.

NMR measurements were also carried out on another fragment, ADAP_240-340, which was also inactive in polymerizing actin. When ^{2}H-^{15}N-ADAP_240-340 was measured in the absence and presence of non-polymerizable actin, many significant intensity changes and chemical shift distances were observed **(Fig. 3.22)**. This suggests that there might be more

motifs in this region but maybe not essential because ADAP fragments such as 1-150, 1-

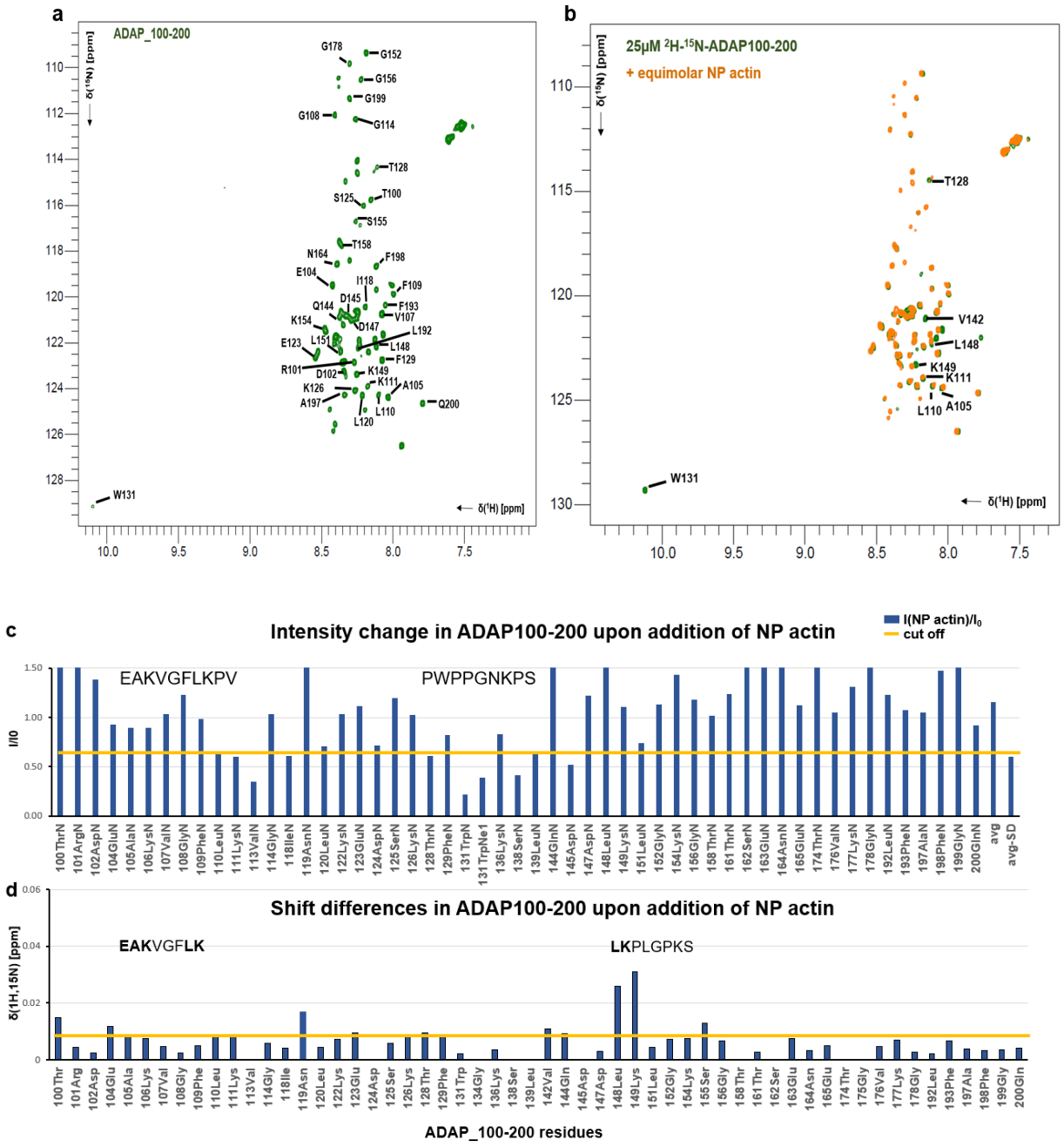

Fig. 3.21: ADAP_100-200 interacts with actin. (a) Backbone assignment of ^{13}C-^{15}N-ADAP_100-200. (b) Overlay of ^{2}H-^{15}N-ADAP_100-200 in the absence (in green) and in the presence of non-polymerizing actin (orange). Marked residues are clearly shifted in the presence of actin. (c) The graph shows the change in intensity in ADAP (I0) upon addition of NP actin (I). (d) Chemical shift changes upon addition of NP actin plotted for ADAP_100-200 residues. Both the graphs indicate major changes in two different regions. (The analyses of spectra with and without actin was performed on ccpNMR_2.4)

200 and 1-245 already polymerize actin at least partially.

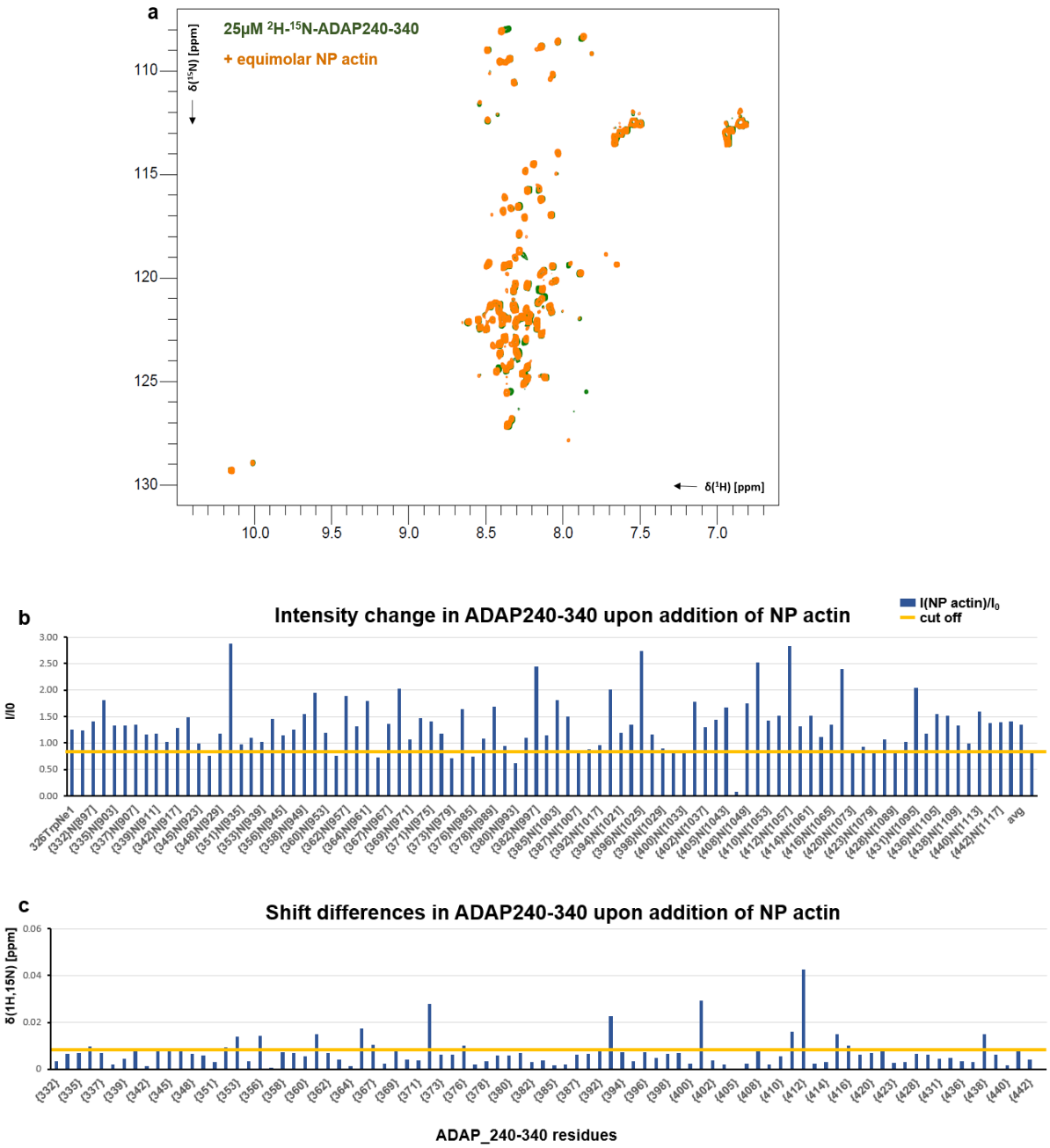

Fig. 3.22: Minor interactions between ADAP_240-340 and monomeric actin (a) Overlay of ^{2}H-^{15}N HSQC spectra of ADAP_240-340 in the absence and presence of non-polymerizable actin (NP actin). (b) Changes in intensity is plotted for residues in ADAP_240-340 upon addition of NP actin (blue). No major changes are seen in this fragment in the presence of NP actin. The peaks are not assigned and given an arbitrary number, so not a clear binding region could be observed. (c) Chemical shift differences plotted for ADAP_240-340 residues upon addition of NP actin. (The analyses of spectra with and without actin was performed on ccpNMR_2.4)

3.6.5 Analysis of ADAP_1-381 spectra in the presence of NP actin

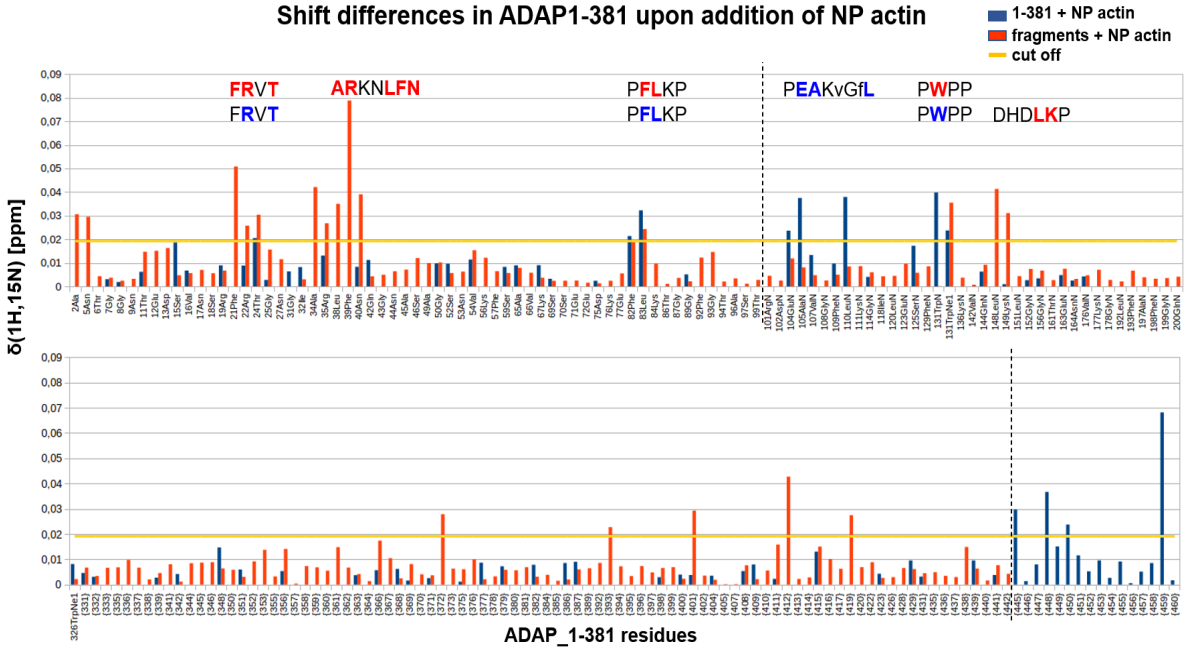

Fig. 3.23: Chemical shift differences plotted for the individual fragments (shown as red bar) and common peaks in larger fragment ADAP_1-381 (shown as blue bar).

Assignment of the fragments were helpful in analyzing ADAP_1-381 spectra with and without non-polymerizing actin **(shown in Fig. 3.19b)**. The assignments from shorter fragments (ADAP_1-100 and 100-200) for the clearly visible and non-overlapping peaks in ADAP_1-381 spectra were transferred, and the remaining unassigned peaks were numbered arbitrarily. The chemical shift differences were plotted and observed to have mostly the same residues affected in case of individual fragments as well as in the context of ADAP_1-381. When inspecting the binding of first 200 residues with actin in the context of ADAP_1-381 construct, it was found that similar interactions are maintained in the larger fragment **(Fig. 3.23)**.

However, due to the massive peak overlap in the intrinsically disordered large fragment (ADAP_1-381) many peaks cannot be assigned or analyzed. This clearly limits the number of analyzable peaks for ADAP_1-381 **(blue bars in Fig. 3.23)** in comparison to the analyzable peaks in the spectra of the shorter fragments **(red bars)**. For example, in ADAP_1-381 only some peaks of the larger motif in ADAP_1-100 covering residues 21-40 are analyzable and only one of these shows a significant shift. In contrast, the motif 104-110 shows significant chemical shift differences in ADAP_1-381 but not in ADAP_100-200 but it rather showed significant line-broadening, implying that the artificial N-terminus in the fragment ADAP_100-200 might influence the interaction.

Also, the interaction of this IDP might be highly dynamic and transient, as no disorder-to-order transition seems to occur in ADAP fragments upon interaction with actin. These properties might make observable chemical shift and peak intensity differences less pronounced and precise.

In summary, these results confirm a direct interaction of the N-terminus of ADAP with actin. A single binding site cannot be identified but rather short motifs from all over the sequence seem to interact with actin.

3.7 Epitopes obtained from NMR are further confirmed by crosslinking Mass Spectrometry

To investigate the interaction between ADAP and actin at lower concentrations, cross-linking mass spectrometry was performed using a lysine crosslinker (DSSO_disuccinimidyl sulfoxide) and observed inter-crosslinks of lysines in its relative vicinity (up to 7-25 Å in space between Cα-Cα atoms of different amino acids) [163] [165] [178] **(section 2.2.8)**.

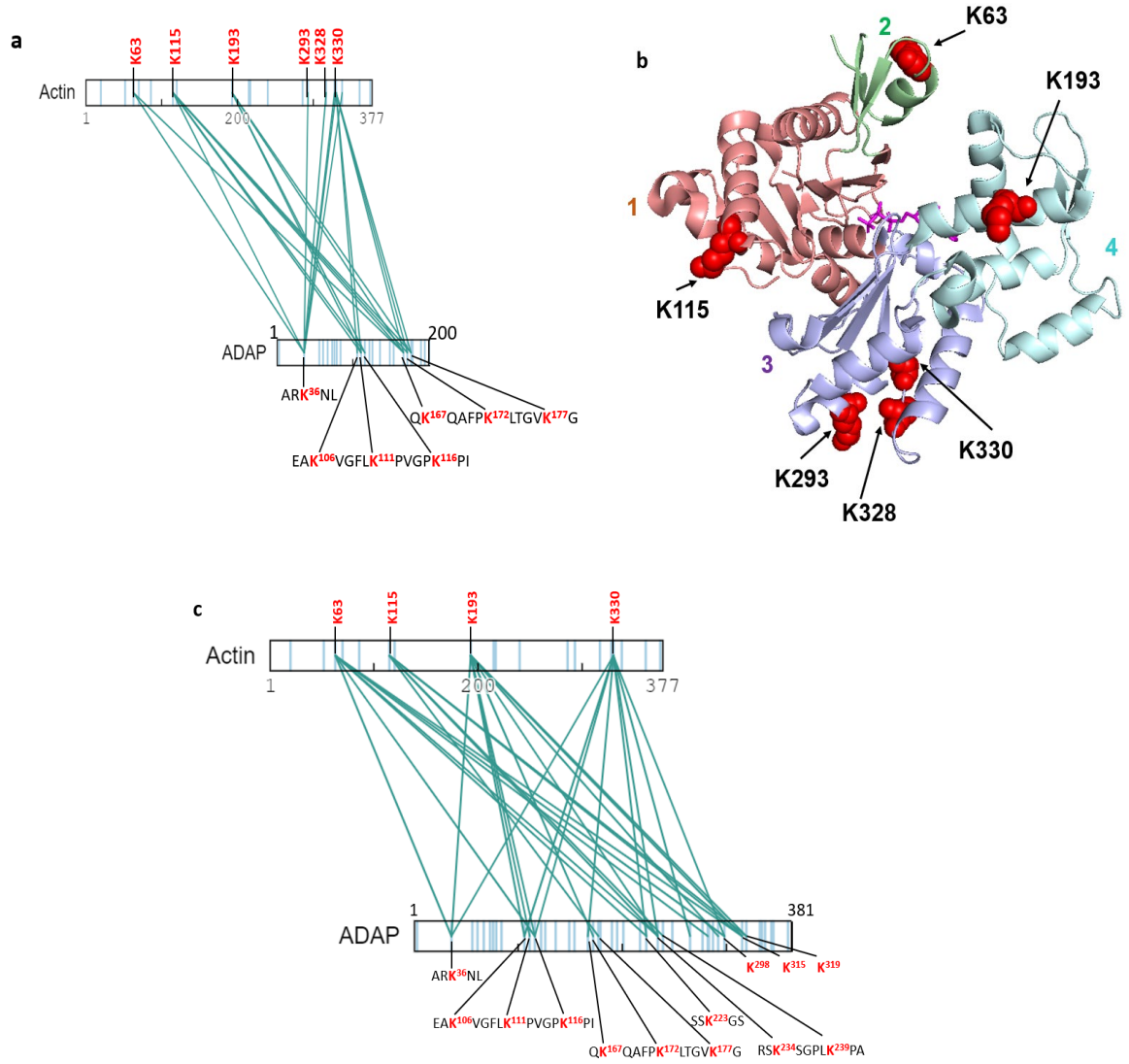

Fig. 3.24: Crosslinking MS confirms the interacting epitopes on ADAP. (a) Cross-links between ADAP_1-200 and NP-actin are shown as green lines while the cross-linked lysine residues are shown in red. (b) Crosslinked lysine residues are indicated as red spheres on subdomains of actin monomer (pdb:3HBT) (color code, domain 1: salmon, domain 2: green, domain 3: light-blue, domain 4: pale-cyan, ATP: magenta). (c) Inter-crosslinks between ADAP_1-381 and NP-actin show the same lysine residues interacting in shorter fragment.

The fragment ADAP_1-200, which covers both the fragments used in NMR (ADAP_1-100 and 100-200), mainly showed crosslinks to K63, K115, K193, K293, K328 and K330 on NP actin which are spread on all four domains of actin (PDB 3hbt [133]) **(Fig. 3.24b)**. ADAP_1-

200 showed crosslinking via K36, K106, K111, K116, K167, K172 and K177 to non-polymerizable monomeric actin confirming the corresponding NMR-derived epitopes **(Fig. 3.20 and 3.21)**. The same crosslinks were reproduced when longer fragments such as ADAP_1-381 and ADAP_100-381 were used **(Fig. 3.24c and appendix figure 6)**. The exact crosslinked lysines or the nearby residues on ADAP were also found in NMR to be involved in direct binding with monomeric NP actin.

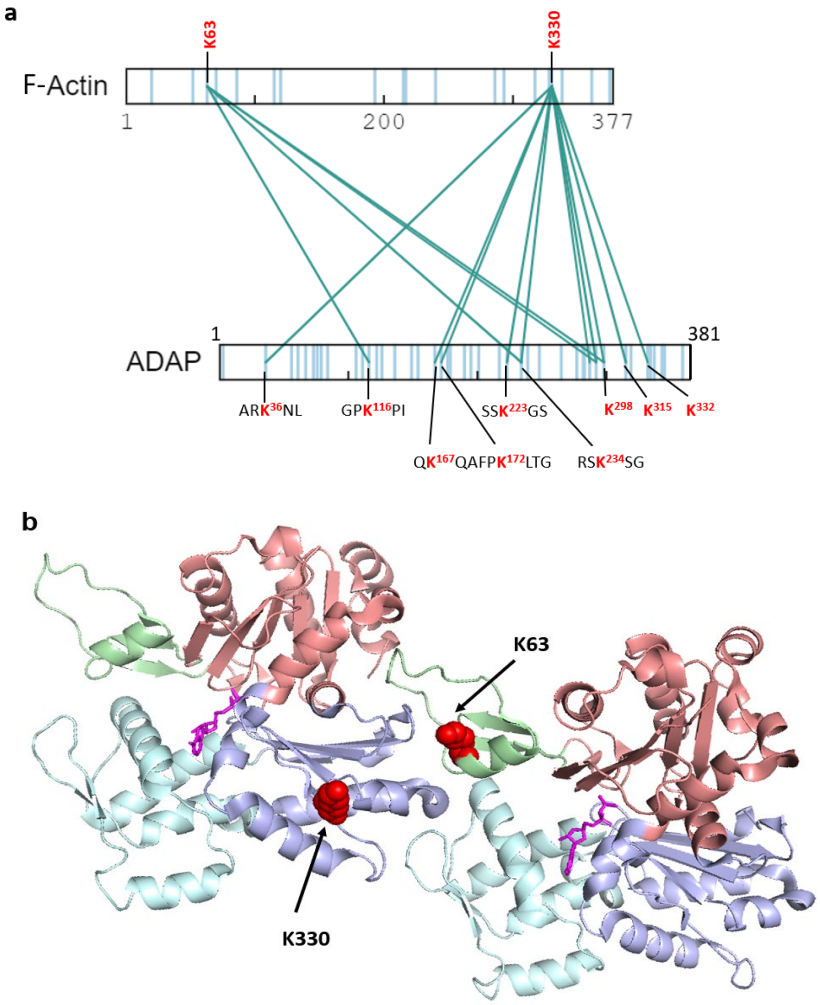

Fig. 3.25: Crosslinking mass spectrometry confirms interaction between ADAP and F-actin. (a) Cross-links between ADAP_1-381 and pre-polymerized actin (F-actin) are shown as green lines while the cross-linked lysines are presented in red. (b) Crosslinked lysine residues are indicated as red spheres on actin dimer chosen from F-actin (dimer from pdb:6FHL) (color code, domain 1: salmon, domain 2: green, domain 3: light-blue, domain 4: pale-cyan, ATP: magenta).

On the monomeric actin four different sites from all the actin sub-domains were observed to crosslink with ADAP. However, one of these sites is eventually excluded after the filament is formed. XL-MS data of ADAP_1-381 in the presence of F-actin indeed indicate that the epitope between monomers of two separate actin strands is no longer available for ADAP binding **(Fig. 3.25)**. Interestingly, of the four sites in G-actin identified to cross-link with ADAP-fragments only two remained to be observed in these experiments, namely K63

and K330 shown on actin dimer of PDB:6fhl [173] **(Fig. 3.25b)**. These lysines are on opposite ends of the actin monomer but become spatial neighbors in the filament **(Fig. 3.25b)**.

Interestingly, ADAP-full length showed crosslinks to F-actin only through the N-terminus and no intermolecular crosslinks were observed from the C-terminus of ADAP **(appendix figure 7)**. This finding was reproduced when a construct containing only the C-terminus (ADAP_486-783) was crosslinked to F-actin showing no crosslinks between the two proteins. Impact of tyrosine phosphorylation was also interrogated to see if the phosphorylated C-terminus of ADAP shows any crosslinks to F-actin. Phosphorylation of ADAP was achieved *in vitro* with Fyn kinase and confirmed by mass spectrometry. The phosphorylated C-terminus showed similar results as the unphosphorylated ADAP **(appendix figure 8)**. These results confirmed the binding, polymerization and bundling of actin by the N-terminus of ADAP.

In summary, various motifs from all over the sequence of ADAP_1-381 were observed to bind with monomeric actin in NMR. The interaction through those motifs was further confirmed by cross-linking MS through the lysines. The C-terminus of ADAP neither showed direct interaction with monomeric actin (confirmed by NMR) nor to F-actin (confirmed by cross-linking MS).

3.8 Competition between ADAP and cofilin for the binding site on actin filament

Cofilin is an actin severing and depolymerizing factor. It is known to bind to both monomeric and filamentous actin and has a higher preference for ADP-actin compared to ATP-actin [130, 142, 148, 154]. It also binds on the side of the actin filament and induces a structural rearrangement that leads to disassembly of filaments and depolymerization of actin [126, 130]. It was reported in the literature [130] to decorate actin filaments at a position identical to the position which is proposed to accommodate the ADAP interaction motifs based on the constraints obtained from NMR and crosslinking mass spectrometry results **(Fig. 4.7b)**.

To confirm our model of ADAP-actin complex formation, ADAP-induced actin polymerization was monitored in the presence of cofilin **(Fig. 3.26)**. Addition of Cofilin to pyrene-actin in the absence of ADAP did not show any increase in fluorescence with time indicating that cofilin is not able to polymerize actin on its own which is in line with the literature **(pink curve in Fig. 3.26b)**.

In the next step, two different concentrations of ADAP_1-381 were used and the concentration of cofilin was kept constant. Following this, a rapid polymerization of actin was observed by ADAP in the presence of cofilin that peaked at a time between 10-15 minutes. Afterwards, depolymerization by cofilin was dominant leading to filament disassembly, which generated a sharp fluorescence decay **(Fig. 3.26 a and b)**. It is already known from the literature that cofilin stabilizes the filaments [121], so a possible explanation of observed rapid increase in fluorescence in the first few minutes is that cofilin helps in enhancing the polymerization activity of ADAP by keeping the filaments stable. However, once the filament is formed cofilin probably outcompetes ADAP and initiates depolymerization detected as a decrease in fluorescence after 10-15 minutes for two different concentrations of ADAP **(Fig. 3.26b)**.

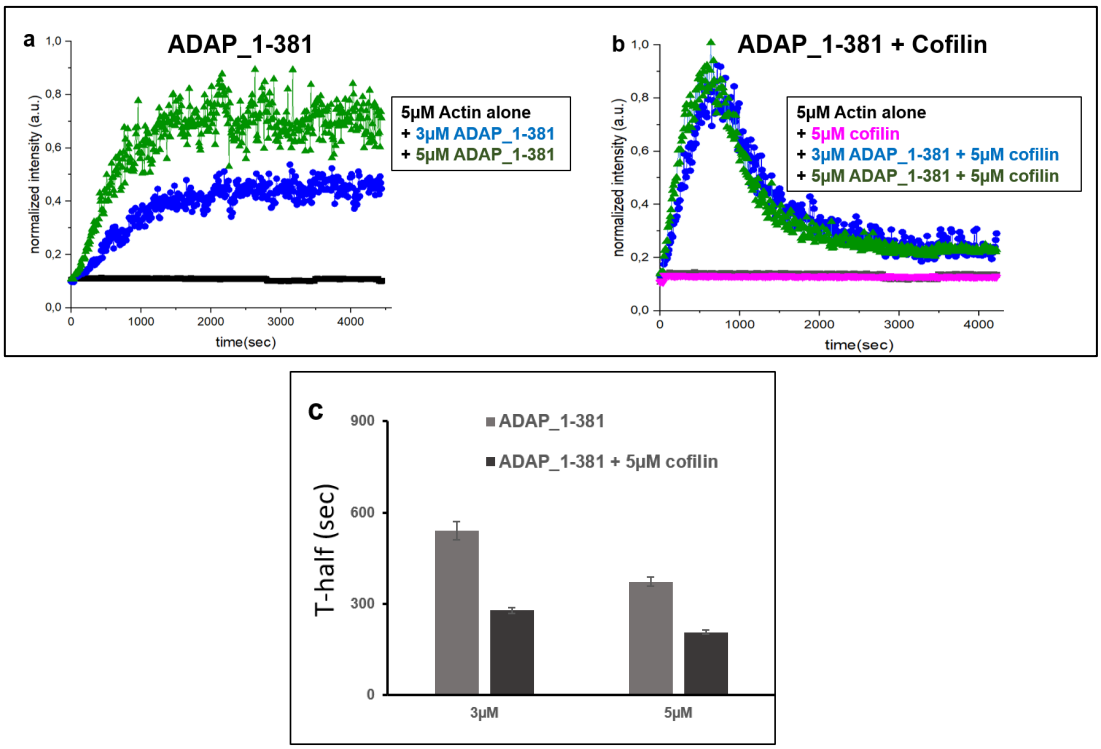

Fig. 3.26: Polymerization activity of ADAP is affected in the presence of cofilin. (a) 3µM and 5µM of ADAP1-381 was mixed with 5µM of pyrene actin and change in fluorescence was measured with time (b) Polymerization activity of different concentrations of ADAP_1-381 (3µM and 5µM) in the presence of 5µM cofilin added to 5µM of pyrene-actin. (c) The half-time to maximum polymerization was calculated for ADAP_1-381 with and without cofilin and plotted for different concentrations of ADAP. (5µM pyrene actin concentration was used in all the samples, measured on TECAN plate reader using excitation at 385nm and emission at 410nm).

To further probe this hypothesis, the concentrations of ADAP and actin were kept constant (i.e. 5µM) and used different concentrations of cofilin (reducing the amount of cofilin in a step-by-step manner) in the *in vitro* polymerization assay. This resulted in a different initial polymerization activity of ADAP as well as in a slower depolymerization by cofilin **(Fig. 3.27)**. These experiments suggest that the initial ADAP-mediated filament formation is

assisted by cofilin, while the depolymerization activity of cofilin leads to a delayed depolymerization of F-actin by out-competing ADAP's ability to bind and polymerize actin.

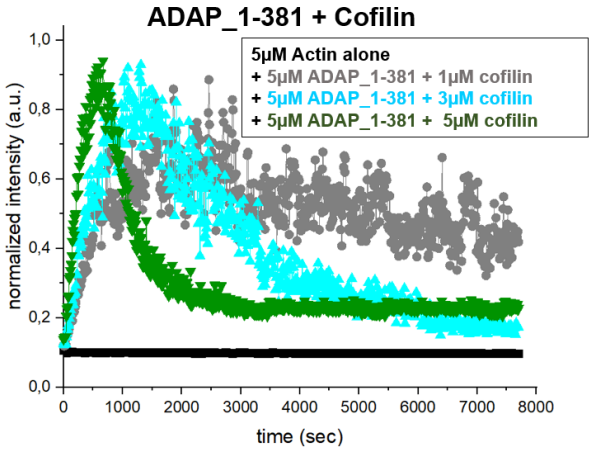

Fig. 3.27: Effect of cofilin on polymerization activity of ADAP. Different concentrations of cofilin (1, 3 and 5μM) were added to 5μM of ADAP_1-381 and pyrene-actin. Change in fluorescence intensity was monitored over time.

However, when cofilin was added to pyrene-actin in the presence of ADAP/SKAP55 complex, no decay in fluoresence intensity was observed even at equimolar concentrations at later time points **(Fig. 3.28)** which was a different observation from previous result when ADAP_1-381 was used in presence of cofilin **(Fig. 3.26b and 3.27)**.

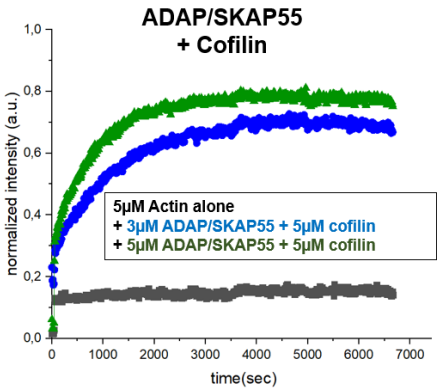

Fig. 3.27: Effect of cofilin on polymerization activity of ADAP/SKAP55 complex. Polymerization activity of different concentrations of ADAP/SKAP55 complex (3μM and 5μM) in the presence of 5μM cofilin added to 5μM of pyrene-actin.

4. Discussion and Outlook

Adhesion and degranulation promoting adaptor protein (ADAP) is known to play a central role in inside-out and outside-in signaling in T cells [30, 49, 70, 75, 90] [179] [37], processes that also involve in remodeling of the actin cytoskeleton. Here, the direct interaction of ADAP with monomeric and filamentous actin was confirmed by various *in vitro* methods. The ability of ADAP-full length to polymerize actin was shown by polymerization assay using pyrene-actin. The region responsible for the polymerization activity was narrowed down to ADAP_1-381 by dissecting ADAP into small, overlapping fragments and probing their activity in the polymerization assay. This divide-and-conquer approach helped in establishing that the extreme N-terminus ADAP_1-150 is crucial for initiating the polymerization activity. However, it was not possible to nail down a single motif or region responsible for activity. Interestingly, when the first 150 residues were deleted resulting in the construct ADAP_150-381, it showed no polymerizing activity at all, however ADAP_200-381 was slightly active **(Fig 3.7)**. That might be explained by a somewhat auto-inhibited conformation of ADAP_150-381 in the truncated construct, covering the slight remnant activity seen in ADAP_200-381. On the other hand, deleting the first 100 residues had no impact on the polymerizing activity, and showed similar activity to ADAP_1-381 **(Fig 3.7)**. This indicates that the first 100 amino acids on their own are not essential for polymerization, but they contribute to binding as indicated by NMR and crosslinking mass spectrometry results. However, residues 100-150 are only active in the presence of other patches of the protein. Our investigation into the N-terminal fragments of ADAP_1-381 **(Fig. 3.6)**, suggests that 100-150 show partial activity if 1-100 is present, but display higher activity if 1-100 is present along with 150-200 or 150-245 fragments. This example highlights that there are no single defined patches of amino acids or certain motifs are responsible for the polymerization activity of ADAP_1-381 as probed by creating various deletion mutations. The results rather indicate that these motifs interact together to be active. Most likely, the actin binding epitopes are present all over the sequence and when one such redundant motif is deleted, another one takes over. Some motifs seem to repeat similarly within the sequence such as the sequence in deletion 1 (75-**D**K**EPKP**P**F**L**KP**-85) matches with the one in deletion 4 (186-**D**L**EPKP**L**F**P**KP**-196). Also, the sequence present in deletion 2 (110-**LKP**V**GPK**-116) is similar to the one found in deletion 3 (148-**LKP**L**GPK**-154). Interestingly, the sequence of ADAP_1-381 contains 64 prolines, 46 lysines, 23 leucines, five times the motif LKP, six times PKP and twice the dipeptide PW.

In order to search for potentially important motifs, the sequence conservation of ADAP N-terminus was compared for several species **(Fig. 4.1 and appendix figure)**. ADAP contains many positively charged residues followed by one or more negatively charged amino acids (like D and E). Many motifs in the deleted regions of ADAP named as deletion 1-8 were found to be conserved in various species as exemplified here for sequence covering deletion 1 and 8 **(Fig. 4.1)** and shown for the rest of the ADAP in **appendix figure 9**. The conserved motifs covered in two of our deletions are presented in this section as an example to show that most of the amino acids covered in deletion 1 and 8 are conserved. In conclusion, there is no single stretch that is highly conserved, but many conserved patches, and often these conserved patches contain amino acids like P, K, L, F.

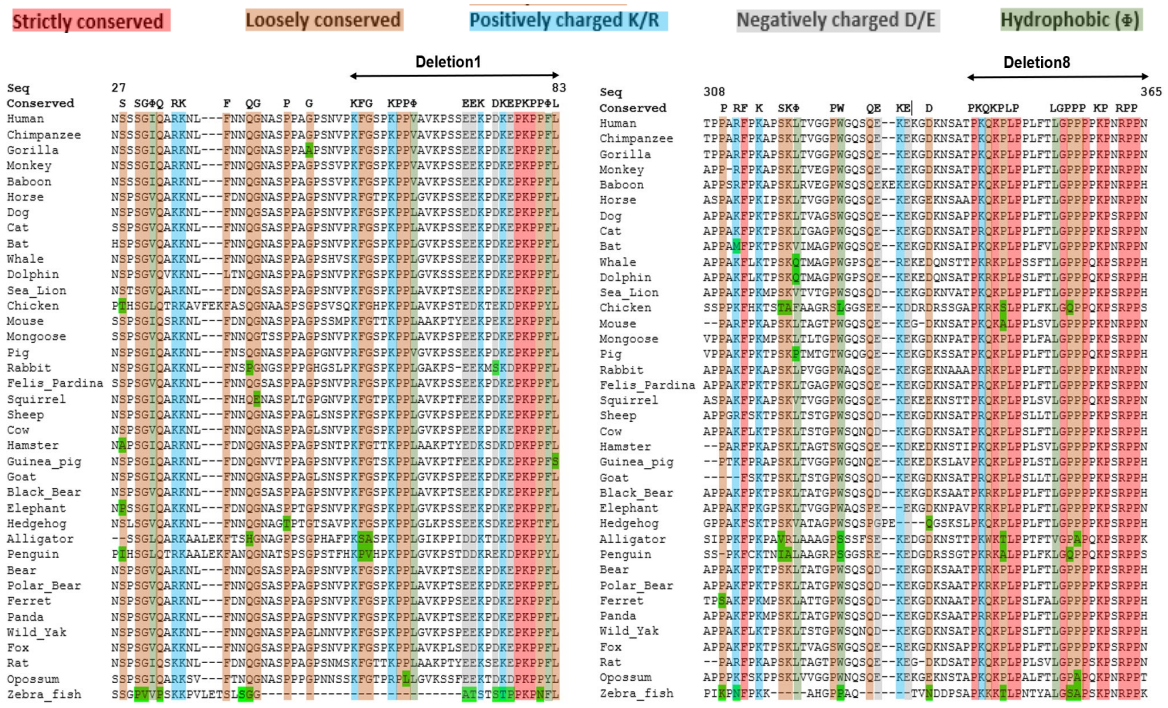

Fig. 4.1: Conserved motifs in N-terminus of ADAP among different species. The N-terminal 1-381 residues of ADAP were matched with the sequence in different species and scanned for conserved motifs. Sequence-stretches covering deletion_1 (left) and deletion_8 (right) is shown here. The conserved residues were marked according to their properties: amino acids strictly conserved in all the presented species are colored in red, the loosely conserved residues are colored in orange, conserved positively charged amino acids such as lysine and arginine are shown in blue, the conserved negatively charged amino acids (aspartate and glutamate) are shown in grey and the consistent hydrophobic amino acids are colored in light green.

Interestingly, enhanced polymerization activity was observed by ADAP in the presence of SKAP55 (ADAP/SKAP55 module) as compared to ADAP alone *in vitro* **(Fig. 3.2)**. However, SKAP55 showed no activity on polymerization when used in complex with ADAP_340-450 (proline rich region). This suggested that SKAP55 contributes indirectly to the polymerization activity of ADAP as part of the complex. One possible reason for this observation could be that ADAP in the presence of SKAP55 attains a conformation which

impacts the polymerization activity of ADAP. Alternatively, a shared epitope might be created upon complex formation of the two proteins which enhances polymerization activity.

On the other hand, a construct missing the first 340 amino acids in ADAP in complex with SKAP55 (i.e., ADAP_Δ340/SKAP55 also named as shorter ADAP/SKAP55 complex) was found to be equally active in polymerizing actin as ADAP/SKAP55-full length complex. This result seems to contradict our findings that the N-terminus of ADAP is crucial for polymerizing activity, obtained from ADAP dissections and confirmed by various *in vitro* assays. One possible explanation for the *in vitro* observation could be that the ADAP_Δ340/SKAP55 complex is expressed in insect cells, which also express other actin polymerizing factors. It might be that either any of these factors are co-purified along with the protein of interest or the purified protein contains post-translational modifications that modulate its polymerizing activity *in vitro*. To confirm this, it is planned to perform an in-solution trypsin digestion followed by mass spectrometry analysis of the protein to confirm the contamination with any other protein or occurrence of post-translational modifications.

The ADAP constructs which showed activity on polymerization were also found to be involved in bundling of actin filaments in the co-sedimentation assay. Actin bundles play an important role in the normal functioning of cells, such as the force generated via dense actin bundles which has been shown to be crucial for cell motility, establishment of cell/cell and cell-matrix adhesions [121]. Bundles are formed when actin filaments are maintained in close contact via crosslinking proteins [180, 181]. The well-studied bundling proteins such as α-actinin or fascin are not able to polymerize actin [151]. However, some proteins such as formins can polymerize actin and eventually move from the end to the side of the actin filaments. This ability of formin allows it to polymerize G-actin and also crosslink actin filaments into parallel or anti-parallel bundled structures [121]. ADAP is found to have a similar dual functional property, where on the one hand it polymerizes actin and on the other hand can also bundle filaments. However, the mechanism of action is certainly different, since formins use folded domains to interact with actin. The intrinsically disordered nature of ADAP utilizes several short motifs to interact with actin, thereby creating irregular and dense filaments, similar as observed for tau protein which is also unfolded however contains short motifs that bind to filamentous actin and bundle it [180].

The actin-polymerization by ADAP observed as an increase in pyrene-fluorescence in the *in vitro* polymerization assay was further confirmed by negative stain electron microscopy. Interestingly, the formation of filaments or bundles varied a lot depending on the proteins used such as ADAP/SKAP55 module polymerized actin faster and formed long-uniform

bundles **(Fig. 3.11)**. ADAP-full length and ADAP_1-381 showed same polymerization activity but according to the negative stain EM images, the bundles formed by ADAP_1-381 were highly dense and irregular **(Fig. 3.12)**. One possible reason for the formation of dense filament structures is that ADAP_1-381 is unfolded and smaller compared to ADAP full length or ADAP/SKAP55 complex which contain multiple fully folded domains. The resolution of bundles formed by ADAP proteins is not high enough for measuring the distance between filaments and counting the number of filaments in each bundle, which would be one of challenges for future investigations.

The direct binding of ADAP and actin was further confirmed by NMR spectroscopy where the addition of G-actin to ADAP_1-381 leads to an instant actin precipitation in the NMR tube resulting in loss of signal of resonances in the measured spectrum. This was one indication that the actin filaments generated are bound to the IDR (intrinsically disordered region) of ADAP, leading to the formation of a slow tumbling polymer containing both the proteins. The investigations using a non-polymerizable actin and smaller ADAP fragments resulted in the definition of epitopes directly affected by actin which were found to be similarly affected in the context of the longer ADAP_1-381 fragment. NMR results indicate that there are multiple short motifs which bind to actin and these motifs are not localized in close proximity but spread all over the sequence of ADAP_1-381 present at a distance from each other. Among those motifs, we found the dipeptide leucine-lysine to display chemical shift changes in ADAP_1-100 (L82, K83) and ADAP_100-200 (L148, K149), and this motif can be found five times as LKP tripeptide in ADAP_1-381. Taken together, the ability of ADAP to directly interact with, polymerize and bundle actin by its intrinsically disordered N-terminal region ADAP_1-381 reveals a new principle of how a multivalent scaffolding protein can modulate the actin skeleton.

4.1 Relevance of N-terminal domain (ADAP_1-381) in T cells

ADAP deficient cells exhibit defective TCR or chemokine receptor triggered stimulation, impaired LFA-1 activation/clustering and T cell-APC interaction [30, 61, 69, 70, 75, 76, 85].As described above, the intrinsically disordered N-terminal domain of ADAP (1-381) was confirmed to be the part essential for polymerization and bundling of actin in our *in vitro* assays. Therefore, to probe the functional consequences of depletion of ADAP_1-381, we collaborated with the group of Stefanie Kliche (Otto-von-Guericke University, Magdeburg), carrying out all the cellular experiments described below. Jurkat T cells were transfected with a suppression/re-expression vector, which suppresses the expression of endogenous ADAP by small hairpin RNA (shRNA) [182] and simultaneously re-expresses shRNA resistant Flag-tagged ADAP wild-type or ADAP mutants with a deletion of either the N-terminal 340 or 381 amino acids (named as ADAP_Δ340 and ADAP_Δ381 constructs) **(shown in Fig. 4.2)**. The transfected cells were then checked for the expression of re-expressed proteins by western blot and the cells were further analyzed for adhesion, migration, and total F-actin content under stimulated or un-stimulated conditions.

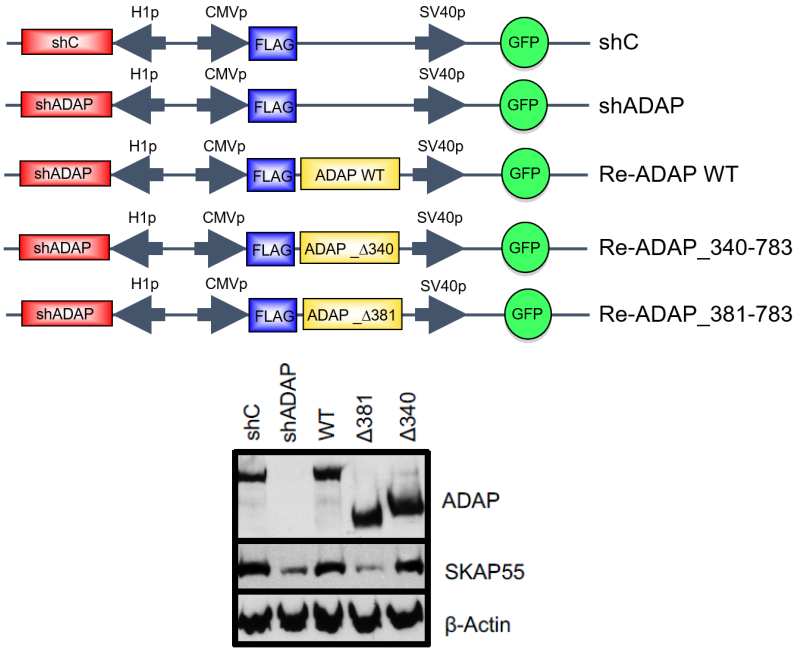

Fig. 4.2: Schematic representation of suppression/re-expression vectors of ADAP used in functional study. The Jurkat cells were transfected with the following vectors; **shC**: control vector expressing GFP (green fluorescent protein); **shADAP**: vector encoding shRNA against endogenous ADAP and cells will express GFP; **Re-ADAP WT**: vector encoding shRNA against endogenous ADAP, shRNA-resistant FLAG-tagged wild-type ADAP and GFP; **Re-ADAP_340-783**: vector encoding shRNA against endogenous ADAP and re-express shRNA-resistant FLAG-tagged ADAP_340-783 and GFP; **Re-ADAP_381-783**: vector encoding shRNA against endogenous ADAP and re-express shRNA-resistant FLAG-tagged ADAP_381-783 and GFP. The western blot analysis confirms the expression of ADAP wildtype and the mutants in the cells.

It has been shown that ADAP promotes chemokine-mediated adhesion and migration, using both an *in vitro* and *in vivo* approach [26, 30, 60, 90, 95]. Triggering of the chemokine receptor CXCR4 by its ligand CXCL12 induces both adhesion and migration [26]. To investigate whether the N-terminus of ADAP regulates migration, Jurkat T cells were transfected with the vectors described in **Fig. 4.2**. These transfected cells were seeded in an upper well of a transwell chamber coated with ICAM-1 and incubated for 2 hours in the absence or presence of CXCL12. The percentage of cells that migrated to the lower chamber was counted. ADAP knocked-down cells showed significantly reduced migration upon stimulation as compared to the cells containing the control vector shC **(black and white bars in Fig. 4.3a)**. This confirms the previously reported results in the literature. The migration ability of cells was restored upon re-expression of ADAP wild type (Re-ADAP WT). However, the re-expression of ADAP mutants missing the N-terminus (Re-ADAP_Δ340 and Re-ADAP_Δ381) failed to revive the ability as good as ADAP-full length but clearly shows better migration than cells with no ADAP expression **(Fig. 4.3a)**. Additionally, when stimulating Jurkat T cells with anti-CD3/CD28 antibodies, we observed a reduced ability of cells expressing ADAP_Δ340 and ADAP_Δ381 to adhere to ICAM-

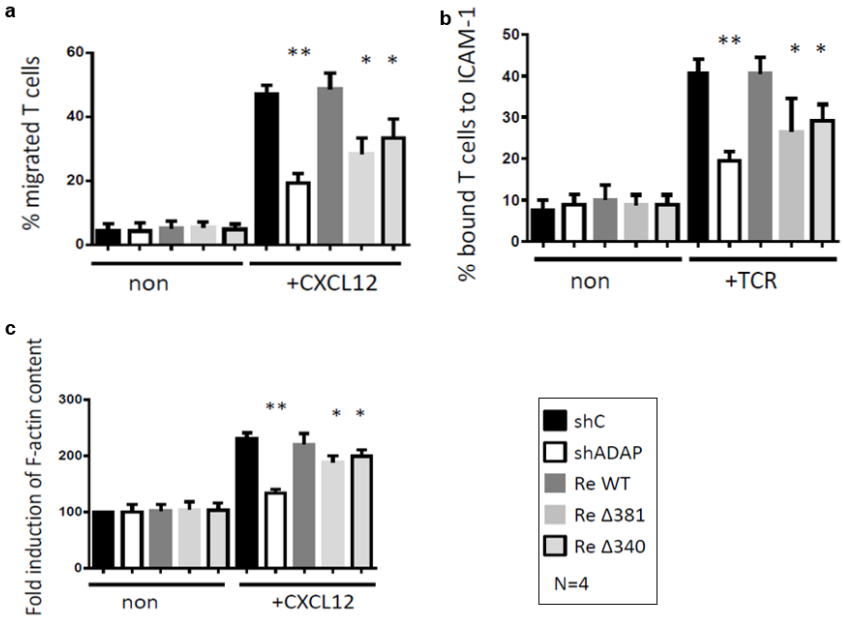

Fig. 4.3: The N-terminus of ADAP is crucial for adhesion, migration, and F-actin content. (a-c) Jurkat T cells were transfected with the constructs shown in **4.1** and incubated for 48 hours. (a) Cells were seeded into the ICAM-1-coated transwell inserts. Subsequently, cells were incubated in the absence or presence of CXCL12 in the lower chamber for 2h. Migrated T cells (located in the lower chamber) were counted and calculated as percentage of input. (b) Non-stimulated (non) or OKT3-stimulated (+TCR) cells were analysed for their ability to adhere to ICAM-1-coated plates. Adherent cells were counted and calculated as a percentage of input ($2x10^5$ cells). (c) Cells were stimulated with CXCL12, fixed, permeabilized, stained with Phalloidin-Alexa Fluor633 (F-actin) and analysed by flow cytometry. Data are presented as normalized MFI after gating on the transfected GFP-positive cells. Error bars represent mean ± SD of three independent experiments.

coated plates **(Fig. 4.3b)**. Thus, an important role for the unstructured N-terminus can be observed in Jurkat T cells.

Since cell motility is regulated by continuous actin polymerization and depolymerization [50, 123], the total F-actin content was analyzed in transfected cells by FACS using intra-cellular phalloidin staining after chemokine receptor stimulation. A significant reduction in the F-actin content was observed in ADAP-suppressed cells compared to the cells with endogenous or re-expressed ADAP **(Fig. 4.3c)**. It is interesting to note that re-expression of mutants that either retain (ADAP_Δ381) or do not retain (ADAP_Δ340) the SKAP55 binding region, both showed similar levels of significantly reduced F-actin content upon chemokine receptor stimulation, which is still higher compared to ADAP deficient cells **(Fig. 4.3c)**. This observation reconciles with our polymerization assay results where it was seen that SKAP55 does not have any direct effect on actin polymerization **(Fig. 3.3)**. Hence, it is reasonable to assume that ADAP/SKAP55 complex formation is not strictly required for the attenuation of actin-dependent functional properties, given that SKAP55 binds through interaction of its SH3 domain with residues 340-362 of ADAP [27].

Notably, F-actin reduction as well as motility and adhesion effects were more pronounced for cells depleted of ADAP full-length compared to both N-terminal deletion constructs **(Fig 4.3)**. This clearly suggests an additional influence of the C-terminal part of the protein although no polymerization or bundling activity was observed in our *in vitro* assays. However, it is well established that ADAP contains binding sites for Ena/VASP family members and also binds to Nck, an N-WASP/WASP effector, in a stimulation and tyrosine-phosphorylation-dependent manner [85, 90, 91, 93, 94]. This could account for executing the more ubiquitous actin-regulating machinery in a cell which might be a reason for the observed differences of constructs seen in **Fig. 4.3**.

Overall, the cellular results correlate with the *in vitro* results where we show that the N-terminus of ADAP (ADAP_1-381) is directly interacting with actin as well as influencing the actin polymerization (total F-actin content) and thereby affecting the adhesion and migration upon chemokine receptor or TCR stimulation.

4.1.1 Impaired T cell adhesion/migration and link to diseases

In order to participate in the adaptive immune responses, T cell trafficking from blood to lymphoid and non-lymphoid tissues is crucial for the continuous surveillance of APCs as well as for their motion to the sites of infection [123] [35]. These processes strictly depend

on activation of integrin LFA-1 [44] [38, 48] and on the actin cytoskeleton [121] [117]. Defects in actin dynamics directly influences cell motility and are generally linked to impaired migration [50, 121, 123]. In the case where migration is impaired, the chances of severe and recurrent infections in the body would likely increase because the T cells cannot perform their vigilance function. Even if such T cells encounter an antigen presenting cell, still these cells cannot form a stable interaction with the APCs due to defective integrins and such T cells will not be activated [44] [51, 52, 117]. Also, ADAP deficient cells showed reduced levels of actin content, and defects in actin pathways are also known to be involved in autoinflammatory diseases and primary immunodeficiencies [183] [184].

Levin et. al. studied patients containing a non-sense mutation 393G>A in fyb gene (encoding ADAP) where tryptophan (coded by TGG) at position 131 gets replaced with a stop codon (TGA), presumably leading to the formation of truncated ADAP and resulting in a condition called small-platelet thrombocytopenia [99]. The lymphocytes from these patients were shown to have reduced pseudopodium formation (a projection formed by actin cytoskeleton in the direction of cell movement) upon activation. Interestingly these observations are in good agreement with our results where we show that ADAP plays a role in regulating actin remodeling. Since the truncated ADAP not only misses most of the disordered N-terminus that polymerizes and bundles actin, but also the C-terminus which has the binding site for Ena/VASP and Nck proteins (known actin regulators). This also clearly explains the morphological impairment in the patient's lymphocytes. Additionally, another study has demonstrated the crucial role of ADAP in platelets where it was shown that ADAP deficient platelets were impaired in adhesion and defective in cell spreading under shear stress [185, 186]. These results again correlate with our observations from experiments with Jurkat T cells deficient of ADAP or re-expressing ADAP mutants with the missing N-terminus.

4.2 ADAP and other actin binding proteins

In order to put ADAP's function in actin polymerization in context with other well-known actin regulating proteins, its function was investigated in the presence or in comparison with other actin binding proteins such as cofilin, capZ or profilin.

Profilin is an actin-monomer-binding protein and is a key player for rapid elongation of filaments in the presence of nucleating proteins containing proline-rich regions such as formin and active Arp2/3 [121] [187]. When profilin was used in combination with ADAP in

the *in vitro* polymerization assay, it showed a positive impact on the polymerizing activity of ADAP **(Fig. 3.15)**. The observation that profilin improves actin polymerization by ADAP could be explained based on its mechanism in the presence of formin. It has been shown that the rate of elongation at free barbed ends by formin alone is slow ($10\mu M^{-1}s^{-1}$), whereas the rate in the presence of profilin increases ($90\mu M^{-1}s^{-1}$) [121] [143]. Thus, it might be that profilin binds to the proline-rich sequences on ADAP and improves polymerization as it does in combination with formin protein, where formin binds and polymerizes through the barbed end of the filament and actin monomers complexed with profilin (which binds to formin through the proline-rich region on latter) are also loaded on to the free barbed end. In this way these two proteins, an actin-elongator and a nucleator work simultaneously and enhance the overall polymerization rate.

Cofilin originally termed as 'cofilamentous protein' [148] is a ~21kDa protein and is known

Fig 4.4: Cofilin decorated actin filament. Cofilin in pink and F-actin is coloured in green. (PDB: 5YU8)

to bind to F-actin with a K_d<0.05μM and disassembles the filaments [142] [130] [180] [152] [154]. When cofilin was added to pyrene-actin in the presence of ADAP during the *in vitro* polymerization assay, it initially showed a positive impact on the polymerizing activity of ADAP followed by strong depolymerization **(Fig. 3.26b and 3.27)**. Based on this observation, it was hypothesized that cofilin binds and stabilizes the actin filaments formed by ADAP, hence the instant increase in fluorescence initially. At later time points, ADAP is outcompeted by cofilin which starts to depolymerize or disassemble the filaments seen as a sharp decay in fluorescence over time. However, it is known that cofilin has a preference for ADP bound actin compared to ATP-actin [126], which suggests that the ATP on the filaments gradually hydrolyze to ADP in the *in vitro* assay as well.

According to literature, on the structure of actin, the loop 241-245 **(colored in black in Fig 4.5)** has been shown to be critical for the formation of a filament and F-actin integrity which differs on the structure of monomeric actin [132] [133, 134, 150], while cofilin residues 154-158 are known to interact with residues 242-243 on actin [150]. Interestingly, ADAP 17-46, the epitope obtained from NMR analysis, docks at the exact position where cofilin 154-158

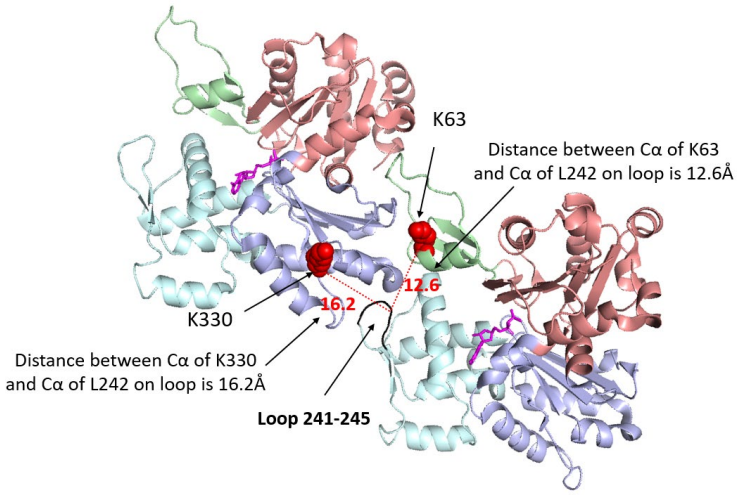

Fig. 4.5: ADAP and cofilin share the same binding site on actin. Crosslinked lysine resides on F-actin K63 and K330 are marked as red spheres on actin dimer (chain C and E of PDB 6fhl). (Color code, domain1: salmon; domain 2: light green; domain 3: light blue; domain 4: light cyan). Distance between Cα of K63 on domain2 or K330 on domain 3 and Cα of L242 on actin loop (residue where cofilin is known to interact) was measured to be within the binding limits.

sits on F-actin **(explained in section 4.3 and Fig. 4.6)**. ADAP shows crosslinking to K63 and K330 on F-actin which indicate that the nearby residues up to a distance of 25Å (between Cα-Cα atoms) are involved in binding. Therefore, we measured the distance from K63 or K330 to the crucial residues on the loop L242 or K243 and found it to be in the proximity of interaction showing a distance of 12-18 Å. This could indicate that ADAP is also interacting with these residues in the loop of actin and the observed crosslinking occurs through the nearby lysines such as 63 or 330 on actin. This suggests that ADAP and cofilin share the binding site on actin. This would fit with our polymerization results in the presence of cofilin protein where ADAP and cofilin were assumed to have the same interacting site on actin and ADAP is replaced by cofilin at later time points. However, no depolymerization by cofilin was observed when ADAP was used in complex with SKAP55 **(Fig. 3.28)**, it might be that cofilin cannot approach actin filaments due to the formation of bigger complex of ADAP/SKAP55 which hinders the binding site of cofilin on actin. ADAP polymerizes from the pointed end as seen in our results when a barbed end capping protein was used.

Capping protein CapZ is a heterodimer which binds to and caps the barbed end of the actin filaments with an affinity of K_d ~1nM and prevent addition or removal of actin subunits [155]

[174] [188]. When CapZ was used in the *in vitro* polymerization assay in the presence of ADAP_1-381, an enhanced polymerization activity by the latter protein was observed **(Fig. 3.16)**. This could be because CapZ binds and stabilizes the intermediate filaments [126, 155]. This observation also clearly suggested that ADAP polymerizes through the pointed end on the filaments.

4.3 Hypothetical model of ADAP/actin binding

In order to better understand the way ADAP polymerizes actin, also in comparison with other actin polymerizing proteins, a model of the ADAP/actin interaction was built by Dr. Jana Sticht based on NMR and MS results.

Based on the NMR investigations several regions all over the sequence were observed to be affected in ADAP_1-381 **(Fig. 3.23)**. However, in smaller fragments ADAP_1-100 and 100-200, specific epitopes were obtained such as residues 21-40 and 110-118 which showed clear chemical shifts and line broadening in the presence of non-polymerizing actin (NP actin) **(Fig. 3.20-3.23)**. The interaction of these regions with actin were further supported by cross-linking mass spectrometry showing for example K36, K111 or K116 located in the above-mentioned motifs on ADAP crosslinking to NP actin **(Fig. 3.24)**.

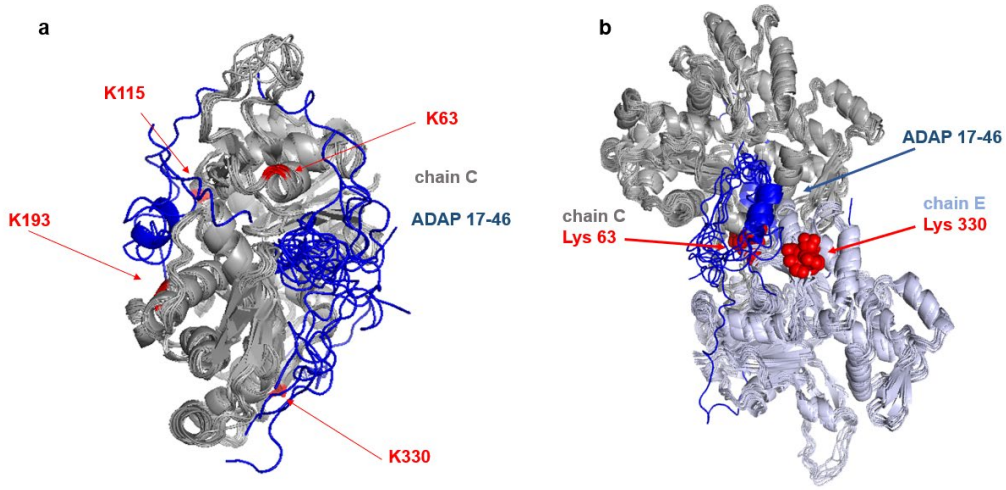

Fig. 4.6: Docking of ADAP peptide on monomeric actin and F-actin. (a) The 10 best docking models of ADAP residues 17-46 are shown in blue with the structure of actin in grey (chain C of PDB 6fhl). The CABS-dock server was used for docking using a 10Å distance between K36 of ADAP and K52, K115, K193, K330 and K338 of actin as soft restraints based on crosslinking MS results. (b) The 10 best docking models of ADAP residues 17-46 are shown in blue with the structure of actin dimer in grey and light blue (chain C and E of PDB 6fhl). The CABS-dock server was used for docking using a 20Å distance between K36 of ADAP and K63 of actin chain C and K330 of actin (marked in red spheres) chain E as soft restraints.

Thus, to get an idea about potential binding sites on monomeric actin the CABS-dock server (http://biocomp.chem.uw.edu.pl/CABSdock) [170, 171] was used, to dock ADAP residues 17-46 to monomeric actin (chains C of PDB 6fhl [173]), using crosslinking results as soft distance restraints. The docking results revealed two possible binding modes which are on opposite sides of the actin monomer **(Fig 4.6 a)**. This might imply a very transient and not a well-defined interaction.

However, in the case where pre-polymerized filamentous actin was used in crosslinking, all ADAP motifs were seen to converge onto just two binding sites on F-actin **(Fig. 3.25)**. The lysine residues K63 and K330 of actin which showed crosslinking are on the opposite ends of actin monomers but become spatial neighbors in the filament, implying that ADAP motifs might bind close to an actin-actin interface **(Fig. 3.25)**. Considering these constraints obtained for F-actin, the molecular docking was performed again which placed a short α-helical turn of the binding epitopes between two actin monomers along the filament **(shown in blue Fig. 4.6b)**. The observed cross-linked individual motifs consistently docked into the groove formed at the interface of the two actin monomers **(Fig. 4.6b)**. Interestingly, the WH2 motifs present in the known actin nucleating proteins are also known to form a helix

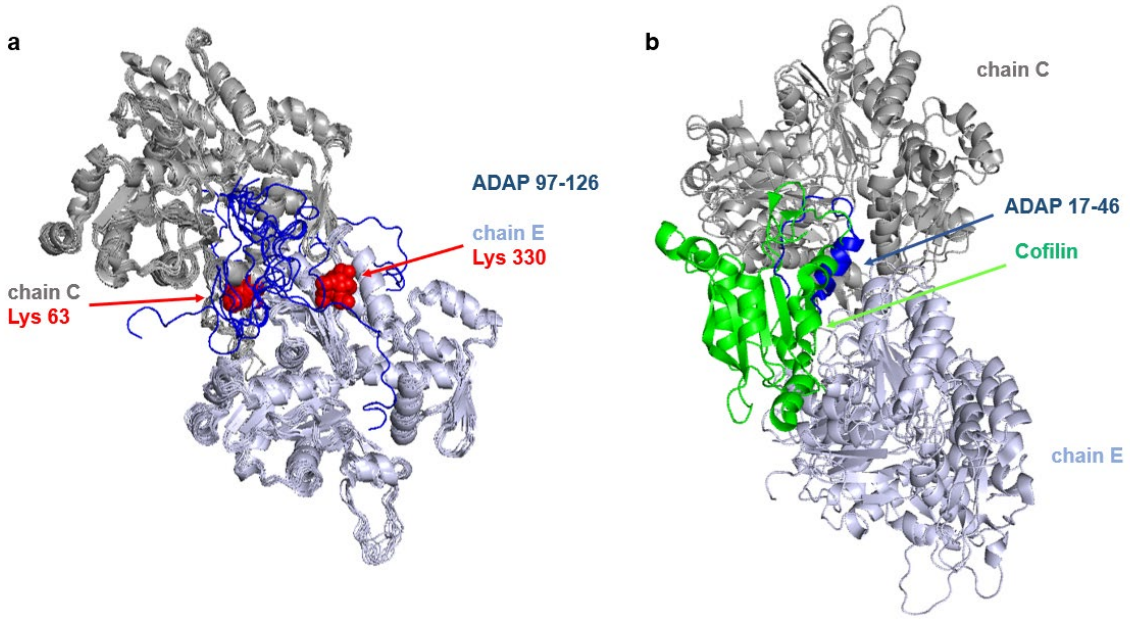

Fig. 4.7: Docking of ADAP peptides and cofilin on actin dimer. (a) The 10 best docking models of ADAP peptide 97-126 shown in blue with the structure of actin dimer (chain C and E of PDB 6fhl) to the constraint on actin Lys63 and Lys330 (marked as spheres in red on chain C and E) which docks to a very similar position as ADAP 17-46 in blue and to a region where ADAP 17-46 also binds. (b) Structure of cofilin (shown in green) bound to actin dimer showing that the binding site overlaps with the ADAP 17-46 (shown in blue) interaction site.

when interacting with actin but their sequence is distantly related to ADAP [126, 138, 139, 144, 189]. Additionally, ADAP residues 97-126 covering the other NMR-derived epitope also showed the propensity to dock to the same general site on actin, even though they were less well defined and binding in many different orientations **(Fig. 4.7a)**. Similar docking modes were also observed with other ADAP motifs that had shown crosslinks to F-actin.

Thus, it is a reasonable proposition that ADAP motifs iteratively connect the longitudinal interface of actin subunits along the filament. This insertion can happen along individual filaments but can also reach out to neighboring filaments. The disordered nature of the N-terminal fragment likely allows for the type of flexibility that is required for forming a dense and random network of filaments as it is seen in the EM structure **(Fig. 3.12b and 3.13).** Interestingly, the potential ADAP-actin interface identified by docking based on MS crosslinking overlaps with the binding site of cofilin **(Fig. 4.7b)**. This overlapping interaction of ADAP with cofilin on a filament certainly explains the *in vitro* polymerization results **(section 3.8)** where cofilin initially enhances the polymerization activity of ADAP and then out-competes the latter followed by a strong depolymerization of filaments.

4.4 Summary of the mechanism of actin-polymerization by ADAP

Taken together, NMR and crosslinking mass spectrometry establish that ADAP contains multiple redundant motifs which bind to actin monomers. However, the interaction between ADAP motifs and actin is not strong but transient based on NMR results as no disorder-to-order transition seemed to occur in ADAP upon interaction with actin. Also, a fuzzy complex with proteins remaining unstructured can result in high affinities [190]. In our hypothetical model we assume that more than one actin monomers transiently bind to the different motifs present in ADAP_1-381 sequence. Even though the interaction is transient, and actin is not continuously bound to ADAP, the presence of many ADAP molecules causes the continuous binding and unbinding of actin and increases the local concentration of actin. At certain point when the concentration of actin is high enough, the actin starts to polymerize on its own, similar to the phenomenon of phase separation where liquid droplets are formed due to transiently enhanced local concentration of participating molecules and binding motifs [181, 191, 192] [28]. Once the filament is formed, ADAP might remain on the sides of actin to bundle or crosslink the filaments or in-between the filaments. In our results, it is clearly seen that ADAP is not only a polymerizer but also an actin bundling protein. In

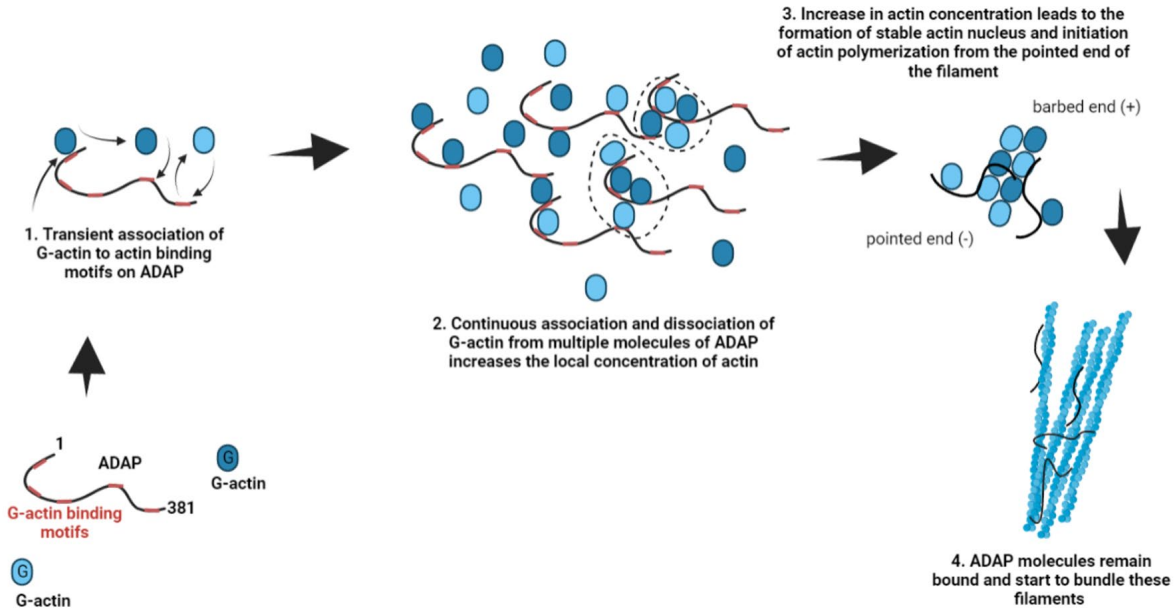

Fig 4.8: Hypothetical model of mechanism of action. ADAP_1-381 is unstructured and consists of multiple actin binding motifs. (1) The interaction between the G-actin and the motifs on ADAP is transient, which means that actin molecules continuously associate and dissociate from the motifs. (2) When multiple molecules of ADAP come together, the continuous binding and un-binding of actin to these motifs on ADAP increases the local concentration of actin. This could lead to the formation a stable actin nucleus (indicated under the dotted circle) and further the polymerization initiates. (3) On the filament ADAP remains bound and polymerizes actin from the pointed end, confirmed in our in vitro experiments using a barbed end capping protein. (4) Once the filaments are formed, ADAP crosslinks and bundles filaments by either binding in-between the filaments or on the side of the filaments.

conclusion, the actin-regulatory role of ADAP therefore might fine tune the actin machinery in the context of T cell activation.

4.5 Outlook of this research

In this work, many important questions regarding the mechanism and functioning of ADAP were answered. However, there are still some interesting observations which need further experiments to explain them. Some of them are listed below in this section.

4.5.1 PRE experiments to confirm actin binding

Crosslinking of ADAP and actin by DSSO gave us some rough idea about which domains of actin are involved in direct binding with ADAP and also the ^{15}N-labelled fragments used in NMR helped us to define interaction epitopes. However, to confirm these observations further, paramagnetic-relaxation enhancement (PRE)-NMR experiments could be used where one out of four available recombinantly expressed actin mutants (provided by Shimada group) will be utilized. Each mutant contains only one cysteine residue D56C, T201C, K215C and D292C **(Fig. 4.9)** while the other cysteine residues present on the

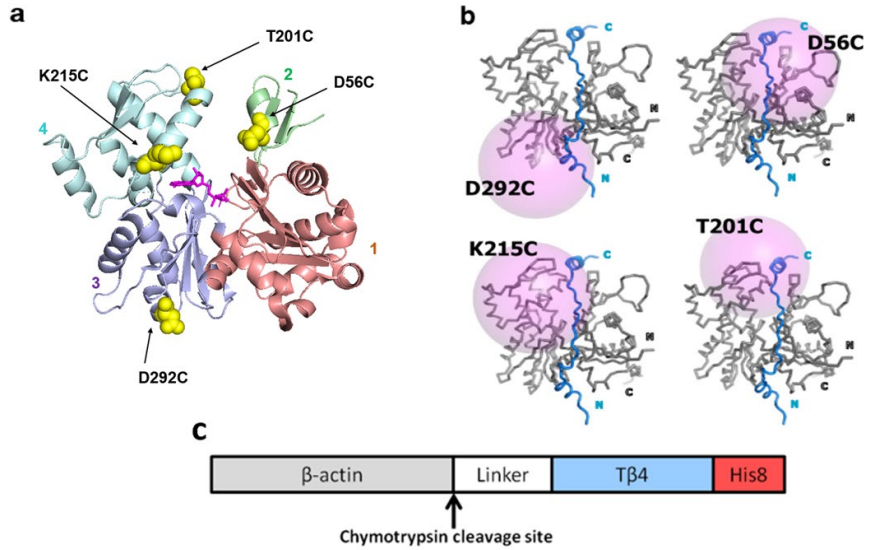

Fig. 4.9: Design of actin mutants containing one reactive cysteine for PRE-NMR experiments. (a) The position of four residues mutated to cysteine (D56, T201, K215 and D292) for MTSL tagging shown in yellow spheres on G-actin structure (PDB: 3HBT). (Color code; domain 1: salmon, domain 2: green, domain 3: light-blue, domain 4: pale-cyan, ATP: magenta). (b) The model structure of Tβ4 (blue) and actin (grey) drawn as a ribbon diagram. Pink spheres represent the estimated range (within 20Å from the mutated amino acid) that could be affected by PRE (picture taken from Huang et. al., 2016). (c) The schematic representation of the construct of actin mutant. The human β-actin is connected via a linker (ASRGGSGGSGGSA) to thymosin β4 (Tβ4), which keeps the actin in monomeric form (G-actin) until it's not cleaved off with the chymotrypsin enzyme. The construct contains a C-terminal 8x-histidine tag (His8) as a purification tag.

surface of actin are mutated to alanine (C272A, C374A) [175]. The cysteine is then labelled with MTSSL-tag (1-oxy-2,2,5,5-tetramethyl-d-pyrroline-3-methyl)-methanethiosulfonate). The attachment of MTSSL to a cysteine in the protein causes enhanced relaxation of the nearby NMR active nuclei (<25Å from the paramagnetic center) [175, 180, 193]. The MTSSL tag contains an unpaired electron of a nitroxyl radical and causes line broadening of the NMR signals.

Thereby, paramagnetic-relaxation enhancement method is an alternative NMR approach for the investigation of larger molecular weight complexes. A PRE-NMR experiment of a protein complex containing a spin label at a specific site gives a long range distance information [175].

4.5.2 ADAP and cofilin binding site on actin

According to the docking model of ADAP and actin based on NMR and crosslinking mass spectrometry results and in line with the polymerization results of ADAP in the presence of cofilin, it can be hypothesized that the two proteins share a similar binding site on actin.

To further test if the binding site of ADAP on F-actin overlaps with cofilin, an NMR experiment can conceivably be performed containing ^{15}N-labeled ADAP_1-381 or individual fragments with either non-polymerizing actin or pre-polymerized filamentous actin in the presence or absence of an excess of cofilin. According to our previous NMR results, upon mixing of ADAP and actin many significant chemical shifts as well as intensity changes were observed for some of the motifs in ADAP. If these changes were not observed in the presence of cofilin, this would imply that cofilin could compete with ADAP for actin binding and would further confirm that the binding sites overlap.

4.5.3 Structure of ADAP/SKAP55

The ADAP/SKAP55 module seems to make a larger complex of around ~250kDa based on the size exclusion chromatography and native gel profile **(Fig 3.1)**. Electron microscopy was used in order to try to solve the structure of this complex. The negative stain electron microscopy images of ADAP/SKAP55 complex were observed to make circular doughnut-shaped structures **(Fig 4.10)**. The shining dots in the structure seen in **Fig. 4.10b** could be the folded domains as this complex consists of two structured hSH3 domains in ADAP, and a dimerization domain, a lipid-binding PH and the ADAP binding SH3 domain in SKAP55. However, the resolution of the images was not sufficient to solve the structure due to the presence of aggregates and other contaminating particles seen on the grid. In addition, crosslinking the complex with 0.1% glutaraldehyde was tried using the GraFix (gradient fixation) approach described in section 2.2.9. But no improvement in the images was observed. As a next step, further optimization of the sample preparation of ADAP/SKAP55 complex could be done to obtain a higher resolution structure. In case the structure can be solved it will provide more information about the binding partners of the two proteins as well as the folding of the intrinsically disordered N-terminal region of ADAP in the presence of actin and its mechanism of action.

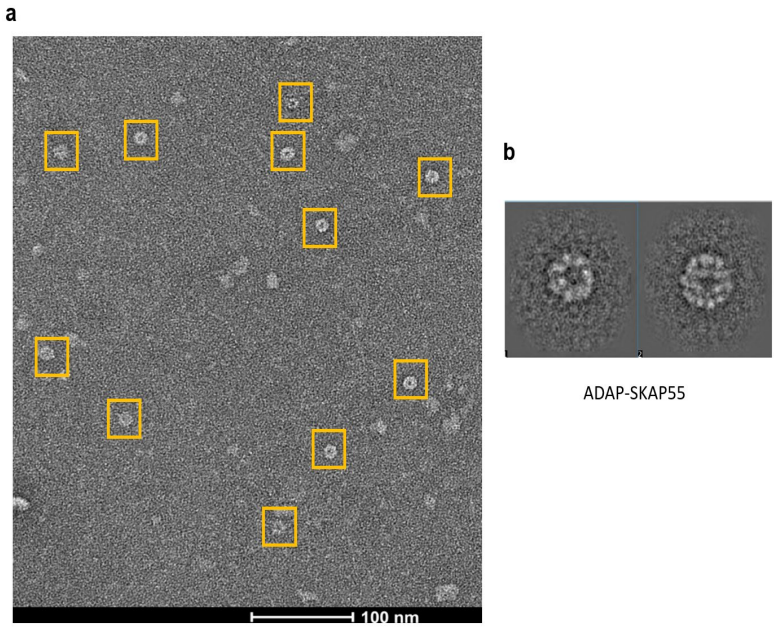

Fig. 4.10: Negative stain EM images of ADAP/SKAP55. (a) Negative stain images of ADAP/&SKAP55 complex. Many circular shaped identical structures are visible marked with yellow box. (b) Zoom-in of the two particles.

4.5.4 Regulator of the polymerization activity of ADAP

According to our *in vitro* results, tyrosine phosphorylation had no impact on the polymerization activity of ADAP. It is still unclear what regulates the polymerization activity of ADAP. Although there are no tyrosines on the disordered N-terminus of ADAP but contains few serine residues. Some of these serines (specifically S235) are shown to get phosphorylated and interact with 14-3-3 proteins (unpublished data and [194] [195]. When recombinantly expressed 14-3-3 proteins were used in 1:1 ratio of 14-3-3 to actin in the *in vitro* polymerization assay in the presence of various concentrations of ADAP_1-381 (1, 3 and 5µM), it was observed that ADAP could not polymerize actin at all which was different in the absence of 14-3-3. However, it has already been shown in literature that 14-3-3 protein can sequester soluble actin and inhibit actin polymerization *in vitro [196]*. The same thing was observed in cells using antibody for actin where more G-actin was found when 14-3-3 protein was overexpressed, not only this but also knockdown of 14-3-3 led to excessive polymerization. It was also hypothesized that the C-terminus of 14-3-3 binds directly to actin [196]. Moreover, this interaction is sufficient to inhibit polymerization in the absence of some of the co-factors [196] [197] [198]. However, it would still be interesting to probe the effect of 14-3-3 protein on the serine phosphorylated ADAP_1-381 (phosphorylation using HPK-1 kinase) and to further elucidate the regulator of ADAP's polymerization activity.

Summary

Adhesion and degranulation-promoting adaptor protein (ADAP) is known to play an important role in indirectly regulating integrins upon T-cell receptor or chemokine receptor stimulation and as a result is crucial for T cell migration and adhesion. ADAP has also been reported to bind to the known actin regulators Ena/VASP and Nck. Here, in this work we show that ADAP interacts with actin directly and induces actin polymerization *in vitro*. The region responsible for the polymerization activity was narrowed down to the disordered N-terminal 381 residues of ADAP. ADAP also induces bundling of actin filaments in an *in vitro* co-sedimentation assay. The fragments of ADAP that showed activity in polymerization assays were also active on bundling actin filaments. The formation of filaments and actin fibers by ADAP and various ADAP fragments were confirmed by negative stain electron microscopy showing bundles of distinct sizes and patterns when comparing ADAP_1-381, ADAP-full length and the ADAP/SKAP55 complex. The involvement of the N-terminus of ADAP in actin remodeling was further confirmed in Jurkat T cells where adhesion and migration was seen to be impaired and total F-actin content was significantly reduced upon stimulation in cells expressing ADAP missing its N-terminal region. NMR investigations also confirmed the binding of ADAP to monomeric as well as filamentous actin and provided information about multiple epitopes in the N-terminal 200 residues of ADAP involved in direct interaction with monomeric actin. Further confirmation of these epitopes was obtained from crosslinking mass spectrometry where short ADAP motifs, often enriched in lysine-proline dipeptides were found to bind to all four sub-domains on monomeric actin suggesting a multivalent interaction mode. In contrast, the same ADAP motifs were seen to converge to the actin dimer interface along the axis of the F-actin filament. The enhanced actin polymerization activity of ADAP in the presence of actin binding proteins like profilin (a barbed end actin elongator) and CapZ (a barbed end capping protein) indicate that ADAP polymerizes through the pointed end of the actin filament. However, the addition of cofilin initially leads to enhanced polymerization activity by ADAP followed by strong depolymerization. This suggests that cofilin has an overlapping binding site with ADAP on the filament as also suggested by our docking models. Overall, these results direct towards a novel mechanism of actin polymerization by the intrinsically disordered region of ADAP, which enhances the local concentration of actin by a sponge-like, multivalent mode of interaction that leads to instant polymerization, formation of filaments and actin bundles.

Zusammenfassung

Das Adhäsions- und degranulationsfördernde Adaptorprotein (ADAP) spielt bekanntermaßen eine wichtige Rolle bei der indirekten Regulierung von Integrinen nach Stimulation durch T-Zell-Rezeptoren oder Chemokinrezeptoren und ist daher für die Migration und Adhäsion von T-Zellen entscheidend. Es wurde auch berichtet, dass ADAP an die bekannten Aktinregulatoren Ena/VASP und Nck bindet. In dieser Arbeit zeigen wir, dass ADAP direkt mit Aktin interagiert und *in vitro* zur Polymerisation von Aktin führt. Die Region, die für die Polymerisationsaktivität verantwortlich ist, wurde auf die ungeordneten N-terminalen 381 Aminosäuren von ADAP eingegrenzt. ADAP induziert auch die Bündelung von Aktinfilamenten in einem *in vitro* Co-Sedimentationstest. Die Fragmente von ADAP, die in Polymerisationstests Aktivität zeigten, waren auch bei der Bündelung von Aktinfilamenten aktiv. Die Bildung von Filamenten und Aktinfasern durch ADAP und verschiedene ADAP-Fragmente wurde durch Negativ-Stain-Elektronenmikroskopie bestätigt, die beim Vergleich von ADAP_1-381, ADAP in voller Länge und dem ADAP/SKAP55-Komplex Bündel unterschiedlicher Größe und Muster zeigte. Die Beteiligung des N-Terminus von ADAP am Aktin-Remodeling wurde ferner in Jurkat-T-Zellen bestätigt, bei denen eine Beeinträchtigung der Adhäsion und Migration festgestellt wurde und der Gesamt-F-Aktin-Gehalt nach Stimulation in Zellen, die ADAP ohne N-Terminus exprimieren, signifikant reduziert war. NMR-Untersuchungen bestätigten auch die Bindung von ADAP an monomeres und filamentöses Aktin und lieferten Informationen über mehrere Epitope in den N-terminalen 200 Aminosäureresten von ADAP, die an dieser direkten Interaktion beteiligt sind. Eine weitere Bestätigung dieser Epitope lieferte die Crosslinking-Massenspektrometrie, bei der festgestellt wurde, dass kurze ADAP-Motive, die häufig mit Lysin-Prolin-Dipeptiden angereichert sind, an allen vier Subdomänen von monomerem Aktin binden, was auf einen multivalenten Interaktionsmodus schließen lässt. Im Gegensatz dazu wurde festgestellt, dass dieselben ADAP-Motive entlang der Achse des F-Aktinfilaments an der Schnittstelle der Aktin-Dimere konvergieren. Die verstärkte Aktinpolymerisationsaktivität von ADAP in Gegenwart von Aktinbindungsproteinen wie Profilin (ein Aktinverlängerer) und CapZ (ein Kappenprotein) deutet darauf hin, dass ADAP über das minus-Ende des Aktinfilaments polymerisiert. Die Zugabe von Cofilin führt jedoch zunächst zu einer verstärkten Polymerisationsaktivität von ADAP, gefolgt von einer starken Depolymerisation. Dies deutet darauf hin, dass Cofilin eine überlappende Bindungsstelle mit ADAP auf dem Filament hat, wie auch unsere Docking-Modelle nahelegen. Insgesamt deuten diese Ergebnisse auf einen neuartigen Mechanismus der Aktinpolymerisation durch den intrinsisch ungeordneten Bereich von ADAP hin, der die lokale Aktinkonzentration

durch einen schwammartigen, multivalenten Interaktionsmodus erhöht, der zu sofortiger Polymerisation, Bildung von Filamenten und Aktinbündeln führt.

Abbreviations

AA	amino acid
ACN	acetonitril
ADAP	adhesion and degranulation promoting adaptor protein
Ala	alanine
AP1	activator protein 1
APC	antigen presenting cell
ARP2/3	actin related protein 2/3
ATP	adenosine triphosphate
Bcl 10	B-cell lymphoma 10
BSA	bovine serum albumin
CaM	calmodulin
CARMA1	CARD-containing MAGUK protein 1
CBM	CARMA-1(Bcl10/MALT1
CD	cluster of differentiation
cDNA	complementary DNA
CDR	complementarity-determining region
Cdk2	cyclin-dependent kinase 2
cSMAC	central supramolecular activation cluster
DAG	diacylglycerol
DC	dendritic cells
DM	dimerization domain
DN	double negative
DNA	deoxyribonucleic acid
dNTP	deoxynucleotide
DP	double positive
dSMAC	distal supramolecular activation cluster
DTT	dithiothreitol
EDTA	ethylenediaminetetraacetic acid

EGTA	ethylene glycol-bis(beta-aminoethyl ether)
ER	endoplasmic reticulum
ERK	extracellular signal-regulated kinase
ESI	electrospray ionization
EVH1	ena/vasp homology domain1
EVL	ena/vasp-like protein
FA	formic acid
FAK-1	focal adhesion kinase 1
FERM	four-point-one/ezrin/radixin/moesin
FYB	fyn-binding protein
FYN	feline yes-related protein
GADS	grb2-related adaptor downstream of shc
GDP	guanosine diphosphate
GEF	GTP exchange factor
GPCR	G protein-coupled receptor
Grb2	growth factor receptor bound protein 2
GST	glutathione S-transferase
GTP	guanosine triphosphate
HEPES	4-(2-hydroxyethyl)-1-piperazineethanesulfonic acid
HEVs	high endothelial venules
HPK-1	hematopoietic progenitor kinase1
hSH3	helical extended src homology 3 domain
ICAM	intercellular adhesion molecule
IFNγ	interferon gamma
IkB	inhibitor of kappa B
IL	interleukin
IMAC	immobilized metal ion affinity chromatography
IP3	inositol-1,4,5-triphosphate
ITAM	immunoreceptor tyrosine-based activation motifs

ITK	interleukin T cell-kinase
kDa	kilo dalton
LAT	linker of activated t cells
LCK	lymphocyte-specific protein tyrosine kinase
LFA-1	lymphocyte function-associated antigen-1
MALT1	mucosa-associated lymphoid tissue lymphoma translocation protein 1
MAPK	mitogen-activated protein kinase
MHC	major histocompatibility complex
mRNA	messenger RNA
MS	mass spectrometry
Mst1	mammalian sterile20-like kinase 1
NCK	non-catalytic region of tyrosine kinase
Ndr	nuclear Dbf2-related kinase
NFAT	nuclear activated T cells
NFkB	nuclear factor kappa light chain enhancer of activated B cells
Ni-NTA	nickel nitrilotriacetic acid
NK	natural killer cell
NLS	nuclear localization signal
NMR	nuclear magnetic resonance
nTregs	natural regulatory T cells
P	proline
PAMPs	pathogen associated molecular patterns
PBS	phosphate buffer saline
PCR	polymerase chain reaction
PH	pleckstrin homology
PI3K	phosphoinositide 3 kinase
PIP2	phosphoinositol-4,5-bisphosphate
PLCγ1	phospholipase C gamma 1
PM	plasma membrane

pMHC	peptide bound major histocompatibility complex
pSMAC	peripheral supramolecular activation cluster
pY	phosphorylated tyrosine
Rap1	Ras proximity 1
RapL	regulator for cell adhesion and polarization enriched in lymphoid tissues
Ras	rat sarcoma
RasGAP	ras GTPase-activating protein
RIAM	Rap1 GTP-interacting adaptor molecule
Rpm	rounds per minute
RT	room temperature
S	serine
SDS-PAGE	sodium dodecyl sulfate polyacrylamide gel electrophoresis
SEC	size exclusion chromatography
Ser	serine
SH2	src homology 2
SH3	src homology 3
shADAP	suppress endogenous ADAP
shRNA	small hairpin RNA
SKAP55	src kinase associated phosphoprotein of 55 kDa
SKAP-HOM	SKAP55 homolog
SLAP130	SLP-76 associated phosphoprotein of 130kDa
SLP76	SH2 domain-containing leukocyte of 76 kDa
SOS	son of sevenless
Syk	spleen tyrosine kinase
TBS-T	tris-buffered saline with tween 20
TCR	T cell receptor
TFA	trifluoroacetic acid
TGF	transforming growth factor
Th	T helper
Thr	threonine
Tyr	tyrosine

VASP	vasodilator-stimulated phosphoprotein
VCAM	vascular cell adhesion molecule
VLA-4	very-late antigen-4
WASP	Wiskott-Aldrich syndrome protein
WB	western blot
Y	tyrosine
ZAP70	zeta-chain-associated protein kinase 70 kDa

Bibliography

1. Martinez, R.M., et al., *Molecular analysis and clinical significance of Lactobacillus spp. recovered from clinical specimens presumptively associated with disease.* J Clin Microbiol, 2014. **52**(1): p. 30-6.
2. Ramachandran, G., *Gram-positive and gram-negative bacterial toxins in sepsis: a brief review.* Virulence, 2014. **5**(1): p. 213-8.
3. Linares, D.M., P. Ross, and C. Stanton, *Beneficial Microbes: The pharmacy in the gut.* Bioengineered, 2016. **7**(1): p. 11-20.
4. Chaplin, D.D., *Overview of the human immune response.* J Allergy Clin Immunol, 2006. **117**(2 Suppl Mini-Primer): p. S430-5.
5. Janeway C., et al., *Immunobiology _ 5th_Edition* 2001.
6. Kirman, J.R., K.M. Quinn, and R.A. Seder, *Immunological memory.* Immunol Cell Biol, 2019. **97**(7): p. 615-616.
7. Shah, D.K., *T-cell development in the thymus.* Immune Development.
8. Starr, T.K., S.C. Jameson, and K.A. Hogquist, *Positive and negative selection of T cells.* Annu Rev Immunol, 2003. **21**: p. 139-76.
9. Villa, A. and L.D. Notarangelo, *RAG gene defects at the verge of immunodeficiency and immune dysregulation.* Immunol Rev, 2019. **287**(1): p. 73-90.
10. Germain, R.N., *T-cell development and the CD4-CD8 lineage decision.* Nat Rev Immunol, 2002. **2**(5): p. 309-22.
11. Koch, U. and F. Radtke, *Mechanisms of T cell development and transformation.* Annu Rev Cell Dev Biol, 2011. **27**: p. 539-62.
12. Kumar, B.V., T.J. Connors, and D.L. Farber, *Human T Cell Development, Localization, and Function throughout Life.* Immunity, 2018. **48**(2): p. 202-213.
13. Xing, Y. and K.A. Hogquist, *T-cell tolerance: central and peripheral.* Cold Spring Harb Perspect Biol, 2012. **4**(6).
14. Zhu, J., H. Yamane, and W.E. Paul, *Differentiation of effector CD4 T cell populations.* Annu Rev Immunol, 2010. **28**: p. 445-89.
15. Seder, R.A. and R. Ahmed, *Similarities and differences in CD4+ and CD8+ effector and memory T cell generation.* Nature immunology 2003. **4**.
16. Martin, M.D. and V.P. Badovinac, *Defining Memory CD8 T Cell.* Front Immunol, 2018. **9**: p. 2692.
17. Bromley, S.K., et al., *The immunological synapse.* Annu. Rev. Immunol. , 2001: p. 375–96.
18. Tittarelli, A., et al., *Connexin-Mediated Signaling at the Immunological Synapse.* Int J Mol Sci, 2020. **21**(10).
19. Springer, T.A. and M.L. Dustin, *Integrin inside-out signaling and the immunological synapse.* Curr Opin Cell Biol, 2012. **24**(1): p. 107-15.
20. Kumari, S., et al., *Cytoskeletal tension actively sustains the migratory T-cell synaptic contact.* EMBO J, 2020. **39**(5): p. e102783.
21. Michael L. Dustin and J.A. Cooper, *The immunological synapse and the actin cytoskeleton.* nature immunology, 2000. **1**.
22. Burkhardt, J.K., E. Carrizosa, and M.H. Shaffer, *The actin cytoskeleton in T cell activation.* Annu Rev Immunol, 2008. **26**: p. 233-59.
23. Roy, N.H. and J.K. Burkhardt, *The Actin Cytoskeleton: A Mechanical Intermediate for Signal Integration at the Immunological Synapse.* Front Cell Dev Biol, 2018. **6**: p. 116.
24. Rudd, C.E., A. Taylor, and H. Schneider, *CD28 and CTLA-4 coreceptor expression and signal transduction.* Immunol Rev, 2009. **229**(1): p. 12-26.
25. Smith-Garvin, J.E., G.A. Koretzky, and M.S. Jordan, *T cell activation.* Annu Rev Immunol, 2009. **27**: p. 591-619.

26. Patrussi, L. and C.T. Baldari, *Intracellular mediators of CXCR4-dependent signaling in T cells.* Immunol Lett, 2008. **115**(2): p. 75-82.
27. Witte, A., *Emerging Roles of ADAP, SKAP55, and SKAP-HOM for Integrin and NF-κB Signaling in T cells.* Journal of Clinical & Cellular Immunology, 2013. **01**(S12).
28. Su, X., et al., *Phase separation of signaling molecules promotes T cell receptor signal transduction.* Science, 2016. **352**(6285): p. 595-9.
29. Rangarajan, S., et al., *Peptide-MHC (pMHC) binding to a human antiviral T cell receptor induces long-range allosteric communication between pMHC- and CD3-binding sites.* J Biol Chem, 2018. **293**(41): p. 15991-16005.
30. Dadwal, N., et al., *The Multiple Roles of the Cytosolic Adapter Proteins ADAP, SKAP1 and SKAP2 for TCR/CD3 -Mediated Signaling Events.* Frontiers in Immunology, 2021. **12**.
31. Downey-Biechler, C., et al., *Inside-out signaling through FAK-integrin axis may regulate circulating cancer cell metastatic adhesion.* Proc Natl Acad Sci U S A, 2019. **116**(40): p. 19795-19796.
32. Kuropka, B., et al., *Tyrosine-phosphorylation of the scaffold protein ADAP and its role in T cell signaling.* Expert Rev Proteomics, 2016. **13**(6): p. 545-54.
33. Wang, D., et al., *CD3/CD28 costimulation-induced NF-kappaB activation is mediated by recruitment of protein kinase C-theta, Bcl10, and IkappaB kinase beta to the immunological synapse through CARMA1.* Mol Cell Biol, 2004. **24**(1): p. 164-71.
34. Kosco, K.A., et al., *SKAP55 modulates T cell antigen receptor-induced activation of the Ras-Erk-AP1 pathway by binding RasGRP1.* Mol Immunol, 2008. **45**(2): p. 510-22.
35. Springer, T.A., *Traffic Signals for Lymphocyte Recirculation and Leukocyte Emigration: The Multistep Paradigm.* Cell, Vol. 76, 301-314,, 1994.
36. Shimizu, Y., D.M. Rose, and M.H. Ginsberg, *Integrins in the Immune System*. 1999. p. 325-380.
37. Emily K Griffiths and J.M. Penninger, *Communication between the TCR and integrins: role of the molecular adapter ADAP/Fyb/Slap.* Current Opinion in Immunology, 2002. **14**: p. 317–322.
38. Hogg, N., et al., *T-cell integrins: more than just sticking points.* J Cell Sci, 2003. **116**(Pt 23): p. 4695-705.
39. Millar, R.P. and A.J. Pawson, *Outside-in and inside-out signaling: the new concept that selectivity of ligand binding at the gonadotropin-releasing hormone receptor is modulated by the intracellular environment.* Endocrinology, 2004. **145**(8): p. 3590-3.
40. Kinashi, T., *Intracellular signalling controlling integrin activation in lymphocytes.* Nat Rev Immunol, 2005. **5**(7): p. 546-59.
41. Harburger, D.S. and D.A. Calderwood, *Integrin signalling at a glance.* J Cell Sci, 2009. **122**(Pt 2): p. 159-63.
42. Hogg, N., I. Patzak, and F. Willenbrock, *The insider's guide to leukocyte integrin signalling and function.* Nat Rev Immunol, 2011. **11**(6): p. 416-26.
43. Shen, B., M.K. Delaney, and X. Du, *Inside-out, outside-in, and inside-outside-in: G protein signaling in integrin-mediated cell adhesion, spreading, and retraction.* Curr Opin Cell Biol, 2012. **24**(5): p. 600-6.
44. Zhang, Y. and H. Wang, *Integrin signalling and function in immune cells.* Immunology, 2012. **135**(4): p. 268-75.
45. Nordenfelt, P., H.L. Elliott, and T.A. Springer, *Coordinated integrin activation by actin-dependent force during T-cell migration.* Nat Commun, 2016. **7**: p. 13119.
46. Thiere, M., et al., *Integrin Activation Through the Hematopoietic Adapter Molecule ADAP Regulates Dendritic Development of Hippocampal Neurons.* Front Mol Neurosci, 2016. **9**: p. 91.
47. Gang Niu and X. Chen, *Why Integrin as a Primary Target for Imaging and Therapy.* Theranostics, 2011. **1**: p. 30-47.

48. Bridget A. LolloS, K.W.H.C., Elaine M. Hanson, Vincent T. Moy, and Adrienne A. Brian, *Direct evidence for two affinity states for lymphocyte function-associated antigen 1 on activated T cells. J. Biol. Chem. (1993)..pdf.* 1993.
49. Kliche, S., et al., *The ADAP/SKAP55 signaling module regulates T-cell receptor-mediated integrin activation through plasma membrane targeting of Rap1.* Mol Cell Biol, 2006. **26**(19): p. 7130-44.
50. Forster, R. and S. Sozzani, *Emerging aspects of leukocyte migration.* Eur J Immunol, 2013. **43**(6): p. 1404-6.
51. Hanna, S. and A. Etzioni, *Leukocyte adhesion deficiencies.* Ann N Y Acad Sci, 2012. **1250**: p. 50-5.
52. Steven, D.M., et al., *Lfa-1 immunodeficiency disease.* J. Exp. MED, 1986. **164**: p. 855-867.
53. Gael Menasche, et al., *Regulation of T-cell antigen receptormediated inside-out signaling by cytosolic adapter proteins and Rap1 effector molecules.* Immunological Reviews, 2007. **218**: p. 82-91.
54. Sanchez-Lockhart, M., M. Kim, and J. Miller, *Cutting edge: A role for inside-out signaling in TCR regulation of CD28 ligand binding.* J Immunol, 2011. **187**(11): p. 5515-9.
55. Michie, K.A., et al., *Two Sides of the Coin: Ezrin/Radixin/Moesin and Merlin Control Membrane Structure and Contact Inhibition.* Int J Mol Sci, 2019. **20**(8).
56. Waldt, N., et al., *Filamin A Phosphorylation at Serine 2152 by the Serine/Threonine Kinase Ndr2 Controls TCR-Induced LFA-1 Activation in T Cells.* Frontiers in Immunology, 2018. **9**.
57. Su, W., et al., *Rap1 and its effector RIAM are required for lymphocyte trafficking.* Blood, 2015. **126**(25): p. 2695-703.
58. Lim, D., Y. Lu, and C.E. Rudd, *Non-cleavable talin rescues defect in the T-cell conjugation of T-cells deficient in the immune adaptor SKAP1.* Immunol Lett, 2016. **172**: p. 40-6.
59. Jo, E.K., H. Wang, and C.E. Rudd, *An essential role for SKAP-55 in LFA-1 clustering on T cells that cannot be substituted by SKAP-55R.* J Exp Med, 2005. **201**(11): p. 1733-9.
60. Kliche, S., et al., *CCR7-mediated LFA-1 functions in T cells are regulated by 2 independent ADAP/SKAP55 modules.* Blood, 2012. **119**(3): p. 777-85.
61. Huang, Y., et al., *Deficiency of ADAP/Fyb/SLAP-130 destabilizes SKAP55 in Jurkat T cells.* J Biol Chem, 2005. **280**(25): p. 23576-83.
62. Raab, M., et al., *SKAP1 protein PH domain determines RapL membrane localization and Rap1 protein complex formation for T cell receptor (TCR) activation of LFA-1.* J Biol Chem, 2011. **286**(34): p. 29663-70.
63. Raab, M., et al., *LFA-1 activates focal adhesion kinases FAK1/PYK2 to generate LAT-GRB2-SKAP1 complexes that terminate T-cell conjugate formation.* Nat Commun, 2017. **8**: p. 16001.
64. Jung, S.H., et al., *ARAP, a Novel Adaptor Protein, Is Required for TCR Signaling and Integrin-Mediated Adhesion.* J Immunol, 2016. **197**(3): p. 942-52.
65. Reversat, A., et al., *Cellular locomotion using environmental topography.* Nature, 2020.
66. Flynn, D.C., *Adaptor proteins.* Oncogene 2001. **20**: p. 6270 - 6272.
67. Togni, M., et al., *The role of adaptor proteins in lymphocyte activation.* Mol Immunol, 2004. **41**(6-7): p. 615-30.
68. Wang, H., et al., *SKAP-55 regulates integrin adhesion and formation of T cell-APC conjugates.* Nat Immunol, 2003. **4**(4): p. 366-74.
69. Da Silva, A.J., et al., *Cloning of a novel T-cell protein FYB that binds FYN and SH2-domain-containing leukocyte protein 76 and modulates interleukin 2 production.* Proc. Natl. Acad. Sci., 1997. **Vol. 94, pp. 7493–7498**.

70. Musci, M.A., et al., *Molecular cloning of SLAP-130, an SLP-76-associated substrate of the T cell antigen receptor-stimulated protein tyrosine kinases.* J Biol Chem, 1997. **272**(18): p. 11674-7.
71. Veale, M., et al., *Novel isoform of lymphoid adaptor FYN-T-binding protein (FYB-130) interacts with SLP-76 and up-regulates interleukin 2 production.* J Biol Chem, 1999. **274**(40): p. 28427-35.
72. Boning, M.A.L., et al., *ADAP Promotes Degranulation and Migration of NK Cells Primed During in vivo Listeria monocytogenes Infection in Mice.* Front Immunol, 2019. **10**: p. 3144.
73. Rudolph, J., et al., *Immune Cell-Type Specific Ablation of Adapter Protein ADAP Differentially Modulates EAE.* Front Immunol, 2019. **10**: p. 2343.
74. Swen Engelmann, et al., *The Adhesion- and Degranulation-Promoting Adaptor Protein and Its Role in the Modulation of Experimental Autoimmune Encephalomyelitis.* Critical Reviews in Immunology, 2015. **35(1):1–14**
75. Junke Liu, H.K., Monika Raab, Antonio J. Da Silva, Stine-Kathrein Kraeft, And Christopher E. Rudd, *FYB (FYN binding protein) serves as a binding partner for lymphoid protein and FYN kinase substrate SKAP55 and a SKAP55-related protein in T cells.* PNAS, 1998.
76. Lewis, J.B., et al., *ADAP is an upstream regulator that precedes SLP-76 at sites of TCR engagement and stabilizes signaling microclusters.* J Cell Sci, 2018. **131**(21).
77. Dyson, H.J. and P.E. Wright, *Intrinsically unstructured proteins and their functions.* Nat Rev Mol Cell Biol, 2005. **6**(3): p. 197-208.
78. Wright, P.E. and H.J. Dyson, *Intrinsically disordered proteins in cellular signalling and regulation.* Nat Rev Mol Cell Biol, 2015. **16**(1): p. 18-29.
79. Anne Marie-Cardine, L.R.H.-T., Nancy J. Boerth, Haoran Zhao, Burkhart Schraven, and Gary A. Koretzky, *Molecular Interaction between the Fyn-associated Protein SKAP55 and the SLP-76-associated Phosphoprotein SLAP-130.* THE JOURNAL OF BIOLOGICAL CHEMISTRY, 1998.
80. Menasche, G., et al., *RIAM links the ADAP/SKAP-55 signaling module to Rap1, facilitating T-cell-receptor-mediated integrin activation.* Mol Cell Biol, 2007. **27**(11): p. 4070-81.
81. Heuer, K., et al., *Structure of a helically extended SH3 domain of the T cell adapter protein ADAP.* Structure, 2004. **12**(4): p. 603-10.
82. Heuer, K., et al., *The helically extended SH3 domain of the T cell adaptor protein ADAP is a novel lipid interaction domain.* J Mol Biol, 2005. **348**(4): p. 1025-35.
83. Heuer, K., et al., *Lipid-binding hSH3 domains in immune cell adapter proteins.* J Mol Biol, 2006. **361**(1): p. 94-104.
84. Ju¨rgen Zimmermann, et al., *Redox-Regulated Conformational Changes in an SH3 Domain.* Biochemistry 2007. **46**: p. 6971-6977.
85. Krause, M., et al., *Fyn-binding Protein (Fyb)/SLP-76–associated Protein (SLAP), Ena/Vasodilator-stimulated Phosphoprotein (VASP) Proteins and the Arp2/3 Complex Link T Cell Receptor (TCR) Signaling to the Actin Cytoskeleton.* The Journal of Cell Biology, 2000. **Volume 149**: p. 181–194.
86. Degen_Janine, *The ADAP/SKAP55-Module Regulates F-Actin Cytoskeleton Reorganization Through the Interaction with Ena/VASP Proteins in T cells.* PhD Dissertation, 2020.
87. Estin, M.L., et al., *Ena/VASP proteins regulate activated T-cell trafficking by promoting diapedesis during transendothelial migration.* Proc Natl Acad Sci U S A, 2017. **114**(14): p. E2901-E2910.
88. Bear, J.E. and F.B. Gertler, *Ena/VASP: towards resolving a pointed controversy at the barbed end.* J Cell Sci, 2009. **122**(Pt 12): p. 1947-53.
89. Mueller, K.L., et al., *Adhesion and degranulation-promoting adapter protein (ADAP) positively regulates T cell sensitivity to antigen and T cell survival.* J Immunol, 2007. **179**(6): p. 3559-69.

90. Sylvester, M., et al., *Adhesion and degranulation promoting adapter protein (ADAP) is a central hub for phosphotyrosine-mediated interactions in T cells.* PLoS One, 2010. **5**(7): p. e11708.
91. Kuropka, B., et al., *Analysis of Phosphorylation-dependent Protein Interactions of Adhesion and Degranulation Promoting Adaptor Protein (ADAP) Reveals Novel Interaction Partners Required for Chemokine-directed T cell Migration.* Mol Cell Proteomics, 2015. **14**(11): p. 2961-72.
92. Pauker, M.H., et al., *Functional cooperation between the proteins Nck and ADAP is fundamental for actin reorganization.* Mol Cell Biol, 2011. **31**(13): p. 2653-66.
93. Lettau, M., et al., *The adapter proteins ADAP and Nck cooperate in T cell adhesion.* Mol Immunol, 2014. **60**(1): p. 72-9.
94. Lettau, M., J. Pieper, and O. Janssen, *Nck adapter proteins: functional versatility in T cells.* Cell Commun Signal, 2009. **7**: p. 1.
95. Parzmair, G.P., et al., *ADAP plays a pivotal role in CD4+ T cell activation but is only marginally involved in CD8+ T cell activation, differentiation, and immunity to pathogens.* J Leukoc Biol, 2017. **101**(2): p. 407-419.
96. Engelmann, S., et al., *T cell-independent modulation of experimental autoimmune encephalomyelitis in ADAP-deficient mice.* J Immunol, 2013. **191**(10): p. 4950-9.
97. al, W.e., *Immune adaptor ADAP in T cells regulates HIV-1 transcription and cell-cell viral spread via different co-receptors.* Retrovirology, 2013.
98. Li, C., et al., *ADAP and SKAP55 deficiency suppresses PD-1 expression in CD8+ cytotoxic T lymphocytes for enhanced anti-tumor immunotherapy.* EMBO Mol Med, 2015. **7**(6): p. 754-69.
99. Levin, C., et al., *Deleterious mutation in the FYB gene is associated with congenital autosomal recessive small-platelet thrombocytopenia.* J Thromb Haemost, 2015. **13**(7): p. 1285-92.
100. Hanan Hamamy, et al., *Recessive thrombocytopenia likely due to a homozygous pathogenic variant in the FYB gene: case report.* BMC Medical Genetics, 2014. **15:135**.
101. Wang, H., Y. Lu, and C.E. Rudd, *SKAP1 is dispensable for chemokine-induced migration of primary T-cells.* Immunol Lett, 2010. **128**(2): p. 148-53.
102. Togni, M., et al., *Regulation of in vitro and in vivo immune functions by the cytosolic adaptor protein SKAP-HOM.* Mol Cell Biol, 2005. **25**(18): p. 8052-63.
103. Anne Marie-Cardine, E.B., Christoph Eckerskorn, Henning Kirchgessner, Stefan C. Meuer, and Burkhart Schraven, *Molecular Cloning of SKAP55, a Novel Protein That Associates with the Protein Tyrosine Kinase p59fyn in Human T-lymphocytes.* THE JOURNAL OF BIOLOGICAL CHEMISTRY, 1997.
104. Hyun Kang, C.F., Jonathan S.Duke-Cohan, Andrea Musacchio4, Gerhard Wagner and Christopher E.Rudd, *SH3 domain recognition of a proline-independent tyrosine-based RKxxYxxY motif in immune cell adaptor SKAP55.* The EMBO Journal, 2000.
105. Ophir, M.J., B.C. Liu, and S.C. Bunnell, *The N terminus of SKAP55 enables T cell adhesion to TCR and integrin ligands via distinct mechanisms.* J Cell Biol, 2013. **203**(6): p. 1021-41.
106. Witte, A., et al., *D120 and K152 within the PH Domain of T Cell Adapter SKAP55 Regulate Plasma Membrane Targeting of SKAP55 and LFA-1 Affinity Modulation in Human T Lymphocytes.* Mol Cell Biol, 2017. **37**(7).
107. Raab, M., K. Strebhardt, and C.E. Rudd, *Immune adaptor protein SKAP1 (SKAP-55) forms homodimers as mediated by the N-terminal region.* BMC Res Notes, 2018. **11**(1): p. 869.
108. Libo Yao, P.J., Luciano G. Frigeri¶, Wei Han‡, Jun Fujita, Yuko Kawakami, John R. Apgar, and Toshiaki Kawakami, *Pleckstrin Homology Domains Interact with Filamentous Actin.pdf.* THE JOURNAL OF BIOLOGICAL CHEMISTRY, 1999.
109. Dedden, D., et al., *The Architecture of Talin1 Reveals an Autoinhibition Mechanism.* Cell, 2019. **179**(1): p. 120-131 e13.

110. Swanson, K.D., et al., *The Skap-hom Dimerization and PH Domains Comprise a 3'-Phosphoinositide-Gated Molecular Switch.* Molecular Cell, 2008. **32**(4): p. 564-575.
111. Zhou, L., et al., *SKAP2, a novel target of HSF4b, associates with NCK2/F-actin at membrane ruffles and regulates actin reorganization in lens cell.* J Cell Mol Med, 2011. **15**(4): p. 783-95.
112. Durocher, M., et al., *Inflammatory, regulatory, and autophagy co-expression modules and hub genes underlie the peripheral immune response to human intracerebral hemorrhage.* J Neuroinflammation, 2019. **16**(1): p. 56.
113. Zeng, H., et al., *HPV infection related immune infiltration gene associated therapeutic strategy and clinical outcome in HNSCC.* BMC Cancer, 2020. **20**(1): p. 796.
114. Claudio Agostinelli, H.R., Jennifer Paterson, and A.U.A. Vishvesh Shende, Elena Agostini, Fabio Fuligni, Simona Righi, Sebastiano Spagnolo, Pier Paolo Piccaluga, Edward A. Clark, Stefano A. Pileri, Teresa Marafioti,, *Intracellular TCR-signaling Pathway: Novel Markers for Lymphoma Diagnosis and Potential Therapeutic Targets.* 2014. **Am J Surg Pathol ;38:1349–1359**.
115. Smith, X., A. Taylor, and C.E. Rudd, *T-cell immune adaptor SKAP1 regulates the induction of collagen-induced arthritis in mice.* Immunol Lett, 2016. **176**: p. 122-7.
116. Raab, M., K. Strebhardt, and C.E. Rudd, *Immune adaptor SKAP1 acts a scaffold for Polo-like kinase 1 (PLK1) for the optimal cell cycling of T-cells.* Sci Rep, 2019. **9**(1): p. 10462.
117. Samstag, Y., et al., *Actin cytoskeletal dynamics in T lymphocyte activation and migration.* J Leukoc Biol, 2003. **73**(1): p. 30-48.
118. Raab, M., et al., *T cell receptor "inside-out" pathway via signaling module SKAP1-RapL regulates T cell motility and interactions in lymph nodes.* Immunity, 2010. **32**(4): p. 541-56.
119. Beemiller, P. and M.F. Krummel, *Regulation of T-cell receptor signaling by the actin cytoskeleton and poroelastic cytoplasm.* Immunol Rev, 2013. **256**(1): p. 148-59.
120. Yu, Y., A.A. Smoligovets, and J.T. Groves, *Modulation of T cell signaling by the actin cytoskeleton.* J Cell Sci, 2013. **126**(Pt 5): p. 1049-58.
121. Blanchoin, L., et al., *Actin dynamics, architecture, and mechanics in cell motility.* Physiol Rev, 2014. **94**(1): p. 235-63.
122. Kumari, S., et al., *T cell antigen receptor activation and actin cytoskeleton remodeling.* Biochim Biophys Acta, 2014. **1838**(2): p. 546-56.
123. Dupre, L., et al., *T Lymphocyte Migration: An Action Movie Starring the Actin and Associated Actors.* Front Immunol, 2015. **6**: p. 586.
124. Comrie, W.A. and J.K. Burkhardt, *Action and Traction: Cytoskeletal Control of Receptor Triggering at the Immunological Synapse.* Front Immunol, 2016. **7**: p. 68.
125. Huranova, M. and O. Stepanek, *Role of actin cytoskeleton at multiple levels of T cell activation.* AIMS Molecular Science, 2016. **3**(4): p. 585-596.
126. Pollard, T.D., *Actin and Actin-Binding Proteins.* Cold Spring Harb Perspect Biol, 2016. **8**(8).
127. N. Tsopoulidis, et al., *T cell receptor–triggered nuclear actin network formation drives CD4+ T cell effector functions.* SCIENCE IMMUNOLOGY, 2019. **4**.
128. Dupre, L., K. Boztug, and L. Pfajfer, *Actin Dynamics at the T Cell Synapse as Revealed by Immune-Related Actinopathies.* Front Cell Dev Biol, 2021. **9**: p. 665519.
129. Alon, R. and Z. Shulman, *Chemokine triggered integrin activation and actin remodeling events guiding lymphocyte migration across vascular barriers.* Exp Cell Res, 2011. **317**(5): p. 632-41.
130. Paavilainen, V.O., et al., *Structure of the actin-depolymerizing factor homology domain in complex with actin.* J Cell Biol, 2008. **182**(1): p. 51-9.
131. Wolfgang Kabsch, et al., *Atomic structure of the actin: DNase I complex.* NATURE, 1990. **VOL 347**.

132. Sofia Y. KHAITLINA , Joanna MORACZEWSKA , and H. STRZELECKA-GOLASZEWSKA, *The actin/actin interactions involving the N- terminus of the DNase-I-binding loop are crucial for stabilization of the actin filament.* Eur. J. Biochem, 1993. **218, 911 -920**.
133. Wang, H., R.C. Robinson, and L.D. Burtnick, *The structure of native G-actin.* Cytoskeleton (Hoboken), 2010. **67**(7): p. 456-65.
134. Oosawa, F. and M. Kasal, *A Theory of Linear and Helical Aggregations of Macromolecules.* J. Mol. Biol., 1962: p. 4, 10-21.
135. Qu, Z., et al., *Distinct actin oligomers modulate differently the activity of actin nucleators.* FEBS J, 2015. **282**(19): p. 3824-40.
136. Uruno, T., et al., *Activation of Arp2/3 complexmediated actin polymerization by cortactin.* Nature Cell Biology, 2001. **4**.
137. Michelot, A., et al., *The formin homology 1 domain modulates the actin nucleation and bundling activity of Arabidopsis FORMIN1.* Plant Cell, 2005. **17**(8): p. 2296-313.
138. Margot E. Quinlan, J.E.H., Eugen Kerkhoff, R. Dyche Mullins, *Drosophila Spire is an actin nucleation factor.* NATURE, 2005. **VOL 433**.
139. Firat-Karalar, E.N. and M.D. Welch, *New mechanisms and functions of actin nucleation.* Curr Opin Cell Biol, 2011. **23**(1): p. 4-13.
140. Katkar, H.H., et al., *Insights into the Cooperative Nature of ATP Hydrolysis in Actin Filaments.* Biophys J, 2018. **115**(8): p. 1589-1602.
141. McCullagh, M., M.G. Saunders, and G.A. Voth, *Unraveling the mystery of ATP hydrolysis in actin filaments.* J Am Chem Soc, 2014. **136**(37): p. 13053-8.
142. Pavlov, D., et al., *Actin filament severing by cofilin.* J Mol Biol, 2007. **365**(5): p. 1350-8.
143. L. CARLSSON, et al., *Actin Polymerizability is Influenced by Profilin, a Low Molecular Weight Protein in Non-muscle Cells.* J. Mol. Biol., 1977. **115**: p. 465-483.
144. Namgoong, S., et al., *Mechanism of actin filament nucleation by Vibrio VopL and implications for tandem W domain nucleation.* Nat Struct Mol Biol, 2011. **18**(9): p. 1060-7.
145. Rubenstein, P.E., *The functional importance of multiple actin isoforms.* BioEssays, 1990. **12**.
146. Bosch, M., et al., *Analysis of the function of Spire in actin assembly and its synergy with formin and profilin.* Mol Cell, 2007. **28**(4): p. 555-68.
147. Ducka, A.M., et al., *Structures of actin-bound Wiskott-Aldrich syndrome protein homology 2 (WH2) domains of Spire and the implication for filament nucleation.* Proc Natl Acad Sci U S A, 2010. **107**(26): p. 11757-62.
148. Eisuke Nishida, Shohei Maekawa, and H. Sakai, *Cofilin, a Protein in Porcine Brain That Binds to Actin Filaments and Inhibits Their Interactions with Myosin and Tropomyosin.* Biochemistry, 1984. **23,** : p. 5307-5313.
149. Rudolf K. Meyer and U. Aebi, *Bundling of Actin Filaments by ct-Actinin Depends on Its Molecular Length.* 1990 **110**: p. 2013-2024.
150. Galkin, V.E., et al., *Remodeling of actin filaments by ADF/cofilin proteins.* Proc Natl Acad Sci U S A, 2011. **108**(51): p. 20568-72.
151. Winkelman, J.D., et al., *Fascin- and alpha-Actinin-Bundled Networks Contain Intrinsic Structural Features that Drive Protein Sorting.* Curr Biol, 2016. **26**(20): p. 2697-2706.
152. Tanaka, K., et al., *Structural basis for cofilin binding and actin filament disassembly.* Nat Commun, 2018. **9**(1): p. 1860.
153. Kotila, T., et al., *Mechanism of synergistic actin filament pointed end depolymerization by cyclase-associated protein and cofilin.* Nat Commun, 2019. **10**(1): p. 5320.
154. Huehn, A.R., et al., *Structures of cofilin-induced structural changes reveal local and asymmetric perturbations of actin filaments.* Proc Natl Acad Sci U S A, 2020. **117**(3): p. 1478-1484.

155. Dennis M. Mwangangi, Edward Manser, and R.C. Robinson, *The structure of the actin filament uncapping complex mediated by twinfilin.* Sci. Adv. , 2021. **7 : eabd5271**.
156. Andrianantoandro, E. and T.D. Pollard, *Mechanism of actin filament turnover by severing and nucleation at different concentrations of ADF/cofilin.* Mol Cell, 2006. **24**(1): p. 13-23.
157. Zimmerle, C.T. and C. Frieden, *Effect of pH on the mechanism of actin polymerization.* Biochemistry, 1988: p. 7766-7772.
158. Vedula, P., et al., *Diverse functions of homologous actin isoforms are defined by their nucleotide, rather than their amino acid sequence.* Elife, 2017. **6**.
159. Herman, h.M., *Actin isoforms.* Current opinion in cell biology, 1999. **5**: p. 48-55.
160. Nowakowski, A.B., W.J. Wobig, and D.H. Petering, *Native SDS-PAGE: high resolution electrophoretic separation of proteins with retention of native properties including bound metal ions.* Metallomics, 2014. **6**(5): p. 1068-78.
161. Laboratories, B.-R., *A Guide to Polyacrylamide Gel Electrophoresis and Detection.* Bulletin 6040
162. Doolittle L.K., M.K.R., Shae B. Padrick, *Measurement and analysis of in vitro actin polymerization.* Methods Mol Biol, 2013. **1046**: p. 273-93.
163. O'Reilly, F.J. and J. Rappsilber, *Cross-linking mass spectrometry: methods and applications in structural, molecular and systems biology.* Nat Struct Mol Biol, 2018. **25**(11): p. 1000-1008.
164. Gong, Z., S.X. Ye, and C. Tang, *Tightening the Crosslinking Distance Restraints for Better Resolution of Protein Structure and Dynamics.* Structure, 2020. **28**(10): p. 1160-1167 e3.
165. Gotze, M., et al., *A Simple Cross-Linking/Mass Spectrometry Workflow for Studying System-wide Protein Interactions.* Anal Chem, 2019. **91**(15): p. 10236-10244.
166. Rappsilber, J., M. Mann, and Y. Ishihama, *Protocol for micro-purification, enrichment, pre-fractionation and storage of peptides for proteomics using StageTips.* Nat Protoc, 2007. **2**(8): p. 1896-906.
167. Gallagher, J.R., et al., *Negative-Stain Transmission Electron Microscopy of Molecular Complexes for Image Analysis by 2D Class Averaging.* Curr Protoc Microbiol, 2019. **54**(1): p. e90.
168. Meineke, B.M., *Molekulare Eigenschaften des Integrin-regulierenden ADAP-SKAP55-Signalkomplexes.* PhD dissertation, 2012.
169. Vranken, W.F., et al., *The CCPN data model for NMR spectroscopy: development of a software pipeline.* Proteins, 2005. **59**(4): p. 687-96.
170. Kurcinski, M., et al., *CABS-dock web server for the flexible docking of peptides to proteins without prior knowledge of the binding site.* Nucleic Acids Res, 2015. **43**(W1): p. W419-24.
171. Kurcinski, M., et al., *A protocol for CABS-dock protein-peptide docking driven by side-chain contact information.* Biomed Eng Online, 2017. **16**(Suppl 1): p. 73.
172. Dass, R., F.A.A. Mulder, and J.T. Nielsen, *ODiNPred: comprehensive prediction of protein order and disorder.* Sci Rep, 2020. **10**(1): p. 14780.
173. Merino, F., et al., *Structural transitions of F-actin upon ATP hydrolysis at near-atomic resolution revealed by cryo-EM.* Nat Struct Mol Biol, 2018. **25**(6): p. 528-537.
174. Yamashita, A., K. Maeda, and Y. MaeÂda, *Crystal structure of CapZ: structural basis for actin filament barbed end capping.* The EMBO Journal, 2003. **Vol. 22 No.7 pp. 1529±1538**.
175. Huang, S., et al., *Utilization of paramagnetic relaxation enhancements for structural analysis of actin-binding proteins in complex with actin.* Sci Rep, 2016. **6**: p. 33690.
176. Jones, D.T., *Protein Secondary Structure Prediction Based on Position-specific Scoring Matrices.* J. Mol. Biol., 1999. **292**: p. 195-202.
177. Buchan, D.W.A. and D.T. Jones, *The PSIPRED Protein Analysis Workbench: 20 years on.* Nucleic Acids Res, 2019. **47**(W1): p. W402-W407.

178. Liu, F., et al., *Optimized fragmentation schemes and data analysis strategies for proteome-wide cross-link identification.* Nat Commun, 2017. **8**: p. 15473.
179. Baker, R.G., et al., *The adapter protein SLP-76 mediates "outside-in" integrin signaling and function in T cells.* Mol Cell Biol, 2009. **29**(20): p. 5578-89.
180. Cabrales Fontela, Y., et al., *Multivalent cross-linking of actin filaments and microtubules through the microtubule-associated protein Tau.* Nat Commun, 2017. **8**(1): p. 1981.
181. Weirich, K.L., et al., *Liquid behavior of cross-linked actin bundles.* Proc Natl Acad Sci U S A, 2017. **114**(9): p. 2131-2136.
182. Rossi, J.J., *Expression strategies for short hairpin RNA interference triggers.* Hum Gene Ther, 2008. **19**(4): p. 313-7.
183. Papa, R., et al., *Actin Remodeling Defects Leading to Autoinflammation and Immune Dysregulation.* Front Immunol, 2020. **11**: p. 604206.
184. Dale A. Moulding, et al., *Actin cytoskeletal defects in immunodeficiency.* Immunological Reviews, 2013. **Vol. 256:** : p. 282–299.
185. Kasirer-Friede, A., et al., *ADAP is required for normal alphaIIbbeta3 activation by VWF/GP Ib-IX-V and other agonists.* Blood, 2007. **109**(3): p. 1018-25.
186. Kasirer-Friede, A., Z.M. Ruggeri, and S.J. Shattil, *Role for ADAP in shear flow-induced platelet mechanotransduction.* Blood, 2010. **115**(11): p. 2274-82.
187. Courtemanche, N. and T.D. Pollard, *Interaction of profilin with the barbed end of actin filaments.* Biochemistry, 2013. **52**(37): p. 6456-66.
188. Narita, A., et al., *Structural basis of actin filament capping at the barbed-end: a cryo-electron microscopy study.* EMBO J, 2006. **25**(23): p. 5626-33.
189. Carlier, M.F., *A new twist in actin filament nucleation.* Nat Struct Mol Biol, 2011. **18**(9): p. 967-9.
190. Borgia, A., et al., *Extreme disorder in an ultrahigh-affinity protein complex.* Nature, 2018. **555**(7694): p. 61-66.
191. Tae Hun Kim, et al., *Phospho-dependent phase separation ofFMRP and CAPRIN1 recapitulates regulation of translation and deadenylation.* Science, 2019. **365**: p. 825–829.
192. Kanaan, N.M., et al., *Liquid-liquid phase separation induces pathogenic tau conformations in vitro.* Nat Commun, 2020. **11**(1): p. 2809.
193. Clore, G.M. and J. Iwahara, *Theory, practice, and applications of paramagnetic relaxation enhancement for the characterization of transient low-population states of biological macromolecules and their complexes.* Chem Rev, 2009. **109**(9): p. 4108-39.
194. Xiaowen Yang, et al., *Structural basis for protein–protein interactions in the 14-3-3 protein family.* PNAS, 2006. **vol. 103** p. 17237–17242.
195. Guri Tzivion, Ying H Shen, and J. Zhu, *14-3-3 proteins; bringing new definitions to scafolding.* Nature Publishing Group, 2001. **20,** : p. 6331 - 6338.
196. Boudreau, A., et al., *14-3-3sigma stabilizes a complex of soluble actin and intermediate filament to enable breast tumor invasion.* Proc Natl Acad Sci U S A, 2013. **110**(41): p. E3937-44.
197. Nurmi, S.M., C.G. Gahmberg, and S.C. Fagerholm, *14-3-3 proteins bind both filamin and alphaLbeta2 integrin in activated T cells.* Ann N Y Acad Sci, 2006. **1090**: p. 318-25.
198. Pennington, K.L., et al., *The dynamic and stress-adaptive signaling hub of 14-3-3: emerging mechanisms of regulation and context-dependent protein-protein interactions.* Oncogene, 2018. **37**(42): p. 5587-5604.

List of figures

Appendix

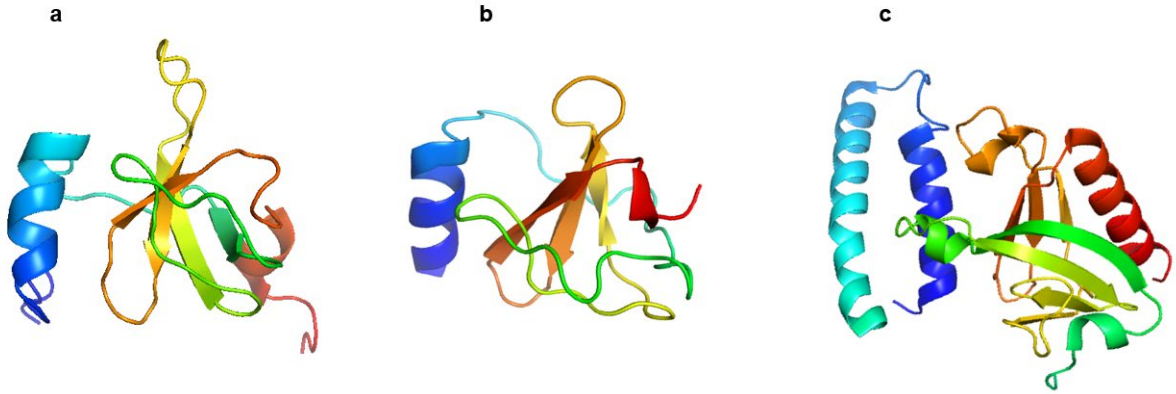

Appendix figure 1: (a) Structure of hSH3_N domain of ADAP (PDB: 2GTO) [84]. (b) Structure of hSH3_C domain of ADAP (PDB: 1RI9) [81]. (c) Structure of DM-PH domain of SKAP-HOM (PDB: 2OTX) [110]

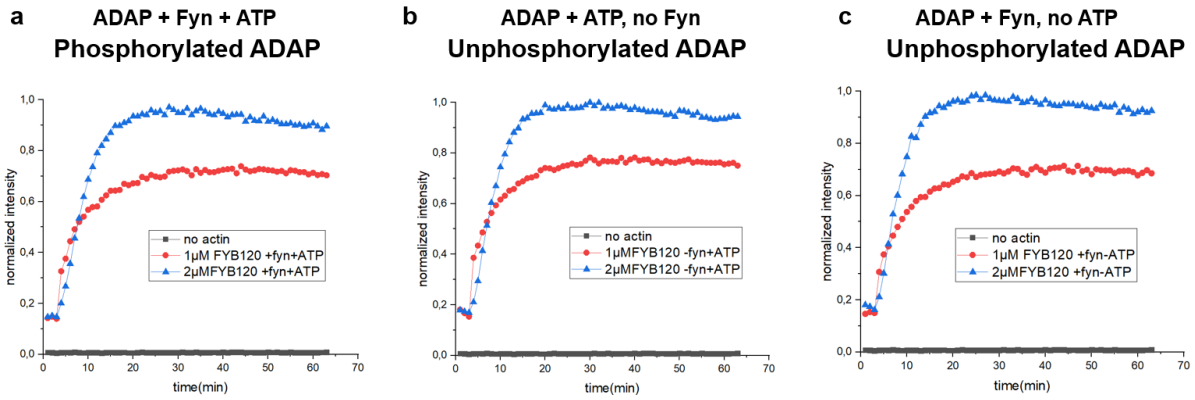

Appendix figure 2: In vitro polymerization assay with phosphorylated and unphosphorylated ADAP showed no major differences. (a) Different concentrations of phosphorylated ADAP (incubated with Fyn and ATP) were added to 5µM of pyrene actin. (b-c) two different controls of unphosphorylated ADAP (b) Different concentrations of unphosphorylated ADAP (incubated with ATP but no Fyn) (c) unphosphorylated ADAP (incubated with Fyn but no ATP) were added to 5µM of pyrene actin. (Note: These samples were measured on old plate reader)

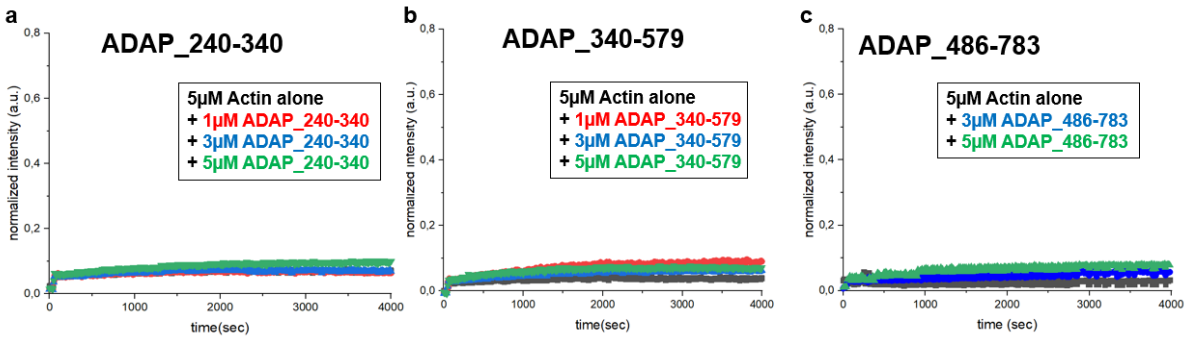

Appendix figure 3: Polymerization curves of different fragments of ADAP. (a) Different ADAP fragments (shown in Fig 3.5) were checked for polymerization activity. The N-terminal fragments 240-340, 340-579 (construct containing the SKAP55 binding region) and 486-783 (the C-terminus of ADAP) do not induce actin polymerization.

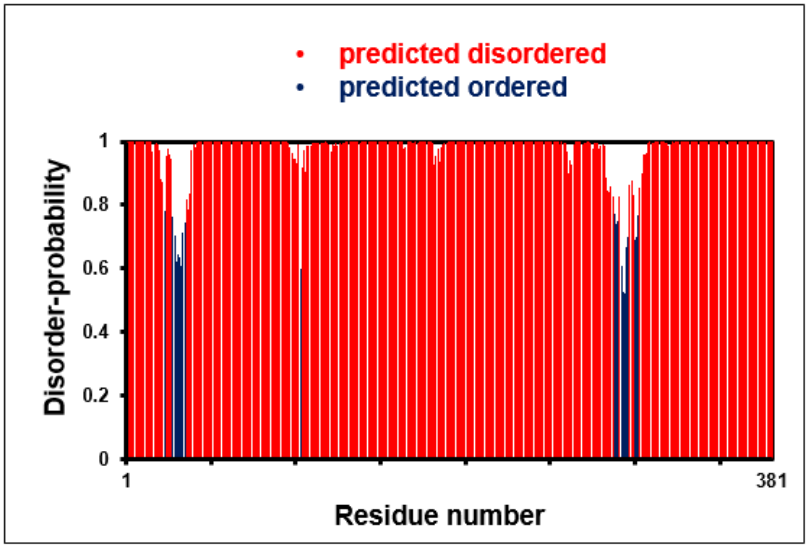

Appendix figure 4: Theoretical prediction of structure of ADAP1-381 using (https://st-protein.chem.au.dk/odinpred) (Dass et al. 2020), suggests that the N-terminus of ADAP is predicted to be mostly disordered (regions highlighted in red) with only two regions showing reduced disorder probability (highlighted in blue).

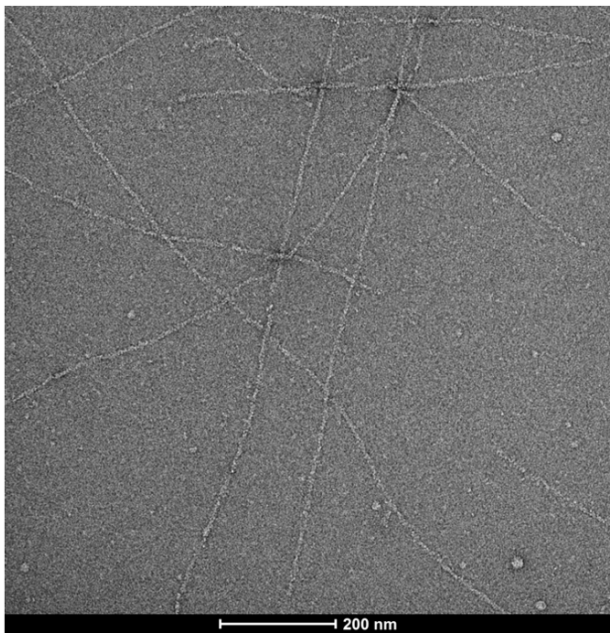

Appendix figure 5: Negative stain electron microscopy image of filamentous actin formed by actin polymerizing buffer containing 10mM ATP. The long filaments formed by the buffer look different compared to the ones formed by ADAP full length, ADAP/SKAP55 complex or ADAP_1-381 proteins (Fig. 3.11 to 3.13).

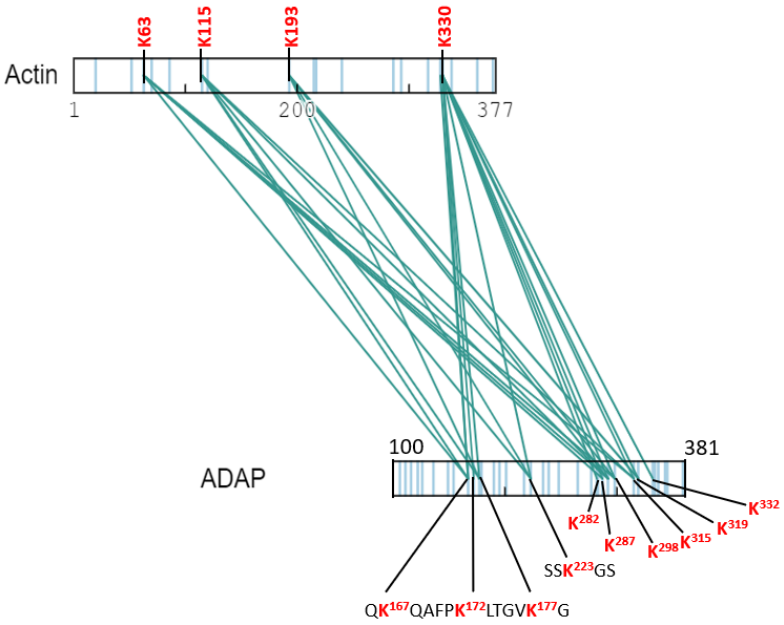

Appendix figure 6: Crosslinking MS of truncated ADAP with non-polymerizing (NP) actin. Cross-links between ADAP_100-381 and NP-actin are shown as green lines while the cross-linked lysine residues are marked in red on both proteins. (The marked residues on are indicated on actin monomer structure in Fig. 3.24

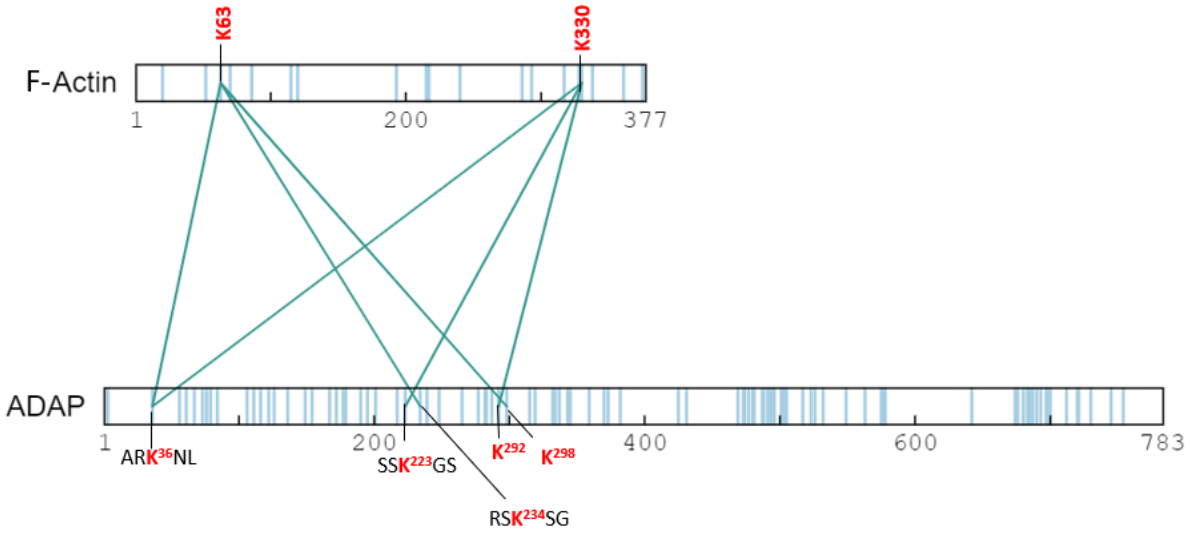

Appendix figure 7: Crosslinking MS of ADAP full length with pre-polymerized F-actin. Cross-links between ADAP full length (1-783) and F-actin are shown as green lines while the cross-linked lysine residues are marked in red on both proteins. This result confirms that it's the N-terminus of ADAP involved in interaction with actin. The marked residues on actin are indicated on actin dimer structure in Fig. 3.25

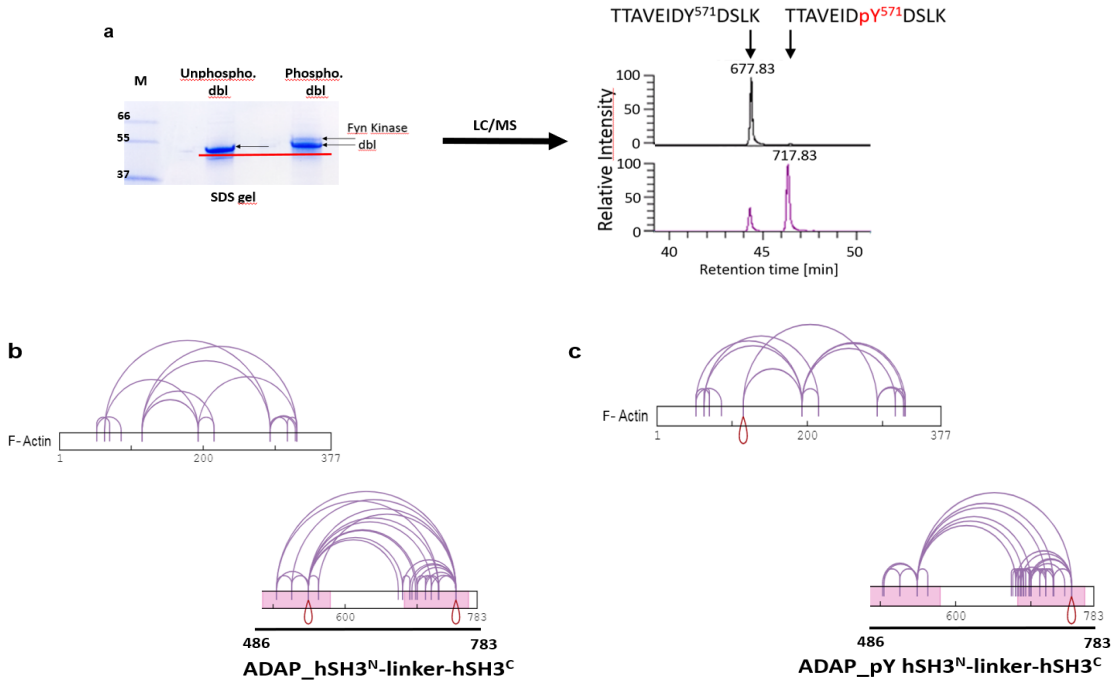

Appendix figure 8: (a) The C-terminus of ADAP (486-783) was phosphorylated in vitro with Fyn kinase and analyzed on SDS PAGE. The bands were further cut and digested with trypsin and analyzed by mass spectrometry (specifically the tyrosine at position 571) to check the efficiency of tyrosine phosphorylation. (Interestingly if the protein is phosphorylated it runs a little higher than the actual size). (b-c) Crosslinking mass spectrometry of (b) un-phosphorylated ADAP (c) phosphorylated ADAP with pre-polymerized filamentous actin (F-actin). The intra-crosslinks are shown as pink lines and no inter-crosslinks were observed between the two proteins. This confirms that ADAP do not interact with actin through the c-terminus.

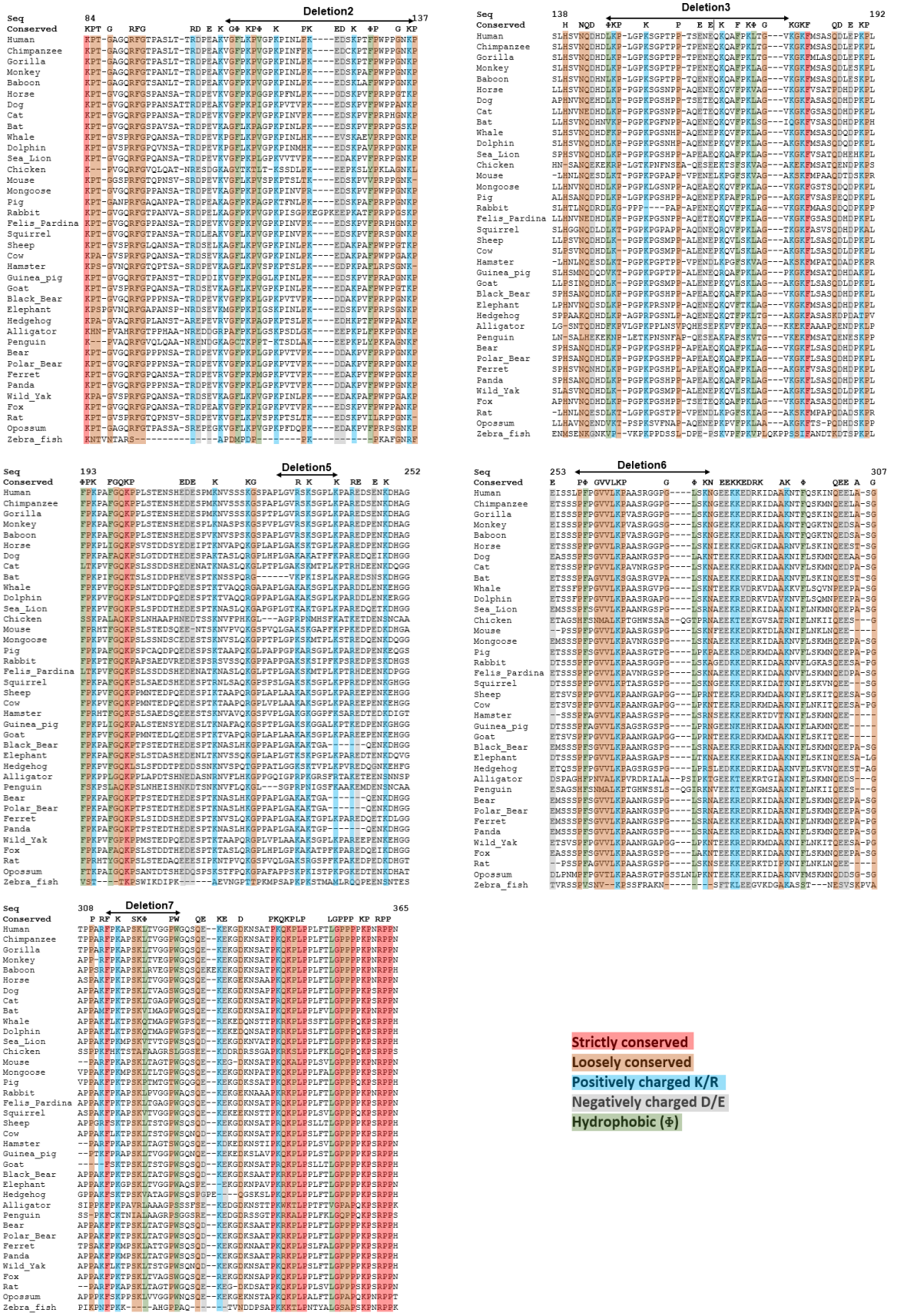

Appendix figure 9: conserved motifs in N-terminus of ADAP among different species. The N-terminal 1-381 residues of ADAP were matched with the sequence in different species and scanned for conserved motifs. The motifs used in deletion mutants are indicated similar to **Fig. 4.1**

Acknowledgement

I would like to thank my supervisor Prof. Christian Freund for giving me the opportunity to work on such an interesting project and for arranging the funding. Our discussions and your ideas concerning the project have continuously guided me through the PhD time and are surely irreplaceable. It wouldn't have been possible without your steady support.

I would also like to thank Dr. Jana Sticht for your help during this time. Your immense knowledge in the field of NMR and easy way of explaining such complex concepts. You helped me to learn and perform NMR experiments. Your comments on this thesis were really helpful.

I also want to thank Dr. Stefanie Kliche for all your help regarding the cellular experiments without which this thesis would have been incomplete. You also gave me a chance to work on the review published in the context of this project. Thanks to Charlie (PhD student of Stefanie) who was my poster-partner and presentation-partner during the MGK-PhD retreats or SFB 854 retreats.

A big thanks goes to the entire AG Freund, especially Steffen, Miri and Miguel for all the discussions during our coffee breaks (I mean a lot of coffee breaks!!). Steffen, thanks a lot for ordering reagents and materials on time after a lot of negotiations. I am thankful to Huan and Tatjana, we three joined the lab together which was a good thing happened to me because we could talk about all the difficulties occurring specially during the initial phase of the PhD. Our discussions together and attitude to look for solutions were really helpful for the completion of this work. We three also went for glue wine together on the very first week of Christmas markets every year. A big thanks to Benno for our discussions on the project and all your inputs. Also, for measuring and analyzing all the mass spec samples. Then thanks to all the present and past members of AG Freund, I got a chance to learn things from: Jakob, Eliot, Esam, Fabian, Lisa, Marek and Zeina. I also want to thank Almudena, Chris and Frank for all your help, chit-chats, and specializations for the completion of this work. Thanks to Fan Liu and Heike (from FMP) for measuring and analyzing all the crosslinking mass spec samples. I would also like to thank AG Bottanelli for all the beer evenings.

Thanks to my friends Ravi, Ankush, Abhishek, Sanjib, Sanket, Arpita, and Nipin for your support, continuous entertainment and all the weekend parties. I am also thankful to my family, especially my siblings Shivali, Shilauni and Ayush for your motivation to do a PhD at very first place. Finally, thanks to Freie University and SFB 854.